2013

Multimodal analysis in normal aging, mild cognitive impairment, and Alzheimer's disease: group differentiation, baseline cognition, and prediction of future cognitive decline

BOSTON UNIVERSITY

SCHOOL OF MEDICINE

Dissertation

MULTIMODAL ANALYSIS IN NORMAL AGING, MILD COGNITIVE IMPAIRMENT, AND ALZHEIMER'S DISEASE: GROUP DIFFERENTIATION, BASELINE COGNITION, AND PREDICTION OF FUTURE COGNITIVE DECLINE

by

CORINNA MAE BAUER

B.Mus., B.Sc., University of Western Ontario, 2007

M.A., Boston University School of Medicine, 2008

Submitted in partial fulfillment of the

requirements for the degree of

Doctor of Philosophy

2013

Approved by

First Reader [redacted]

Ronald Killiany, Ph.D.
Associate Professor of Anatomy Neurobiology

Second Reader [redacted]

Douglas Rosene, Ph.D.
Professor of Anatomy Neurobiology

ACKNOWLEDGEMENTS

I would like to particularly thank the Alzheimer's Disease Neuroimaging Initiative (ADNI) volunteer participants, without whom none of this research would have been possible. Data collection and sharing for this project was funded by the ADNI (National Institutes of Health Grant U01 AG024904). ADNI is funded by the National Institute on Aging, the National Institute of Biomedical Imaging and Bioengineering, and through generous contributions from the following: Abbott; Alzheimer's Association; Alzheimer's Drug Discovery Foundation; Amorfix Life Sciences Ltd.; AstraZeneca; Bayer HealthCare; BioClinica, Inc.; Biogen Idec Inc.; Bristol-Myers Squibb Company; Eisai Inc.; Elan Pharmaceuticals Inc.; Eli Lilly and Company; F. Hoffmann-La Roche Ltd and its affiliated company Genentech, Inc.; GE Healthcare; Innogenetics, N.V.; IXICO Ltd.; Janssen Alzheimer Immunotherapy Research & Development, LLC.; Johnson & Johnson Pharmaceutical Research & Development LLC.; Medpace, Inc.; Merck & Co., Inc.; Meso Scale Diagnostics, LLC.; Novartis Pharmaceuticals Corporation; Pfizer Inc.; Servier; Synarc Inc.; and Takeda Pharmaceutical Company. The Canadian Institutes of Health Research is providing funds to support ADNI clinical sites in Canada. Private sector contributions are facilitated by the Foundation for the National Institutes of Health (www.fnih.org). The grantee organization is the Northern California Institute for Research and Education, and the study is coordinated by the Alzheimer's Disease Cooperative Study at the University of California, San Diego. ADNI data are disseminated by the

Laboratory for NeuroImaging at the University of California, Los Angeles. This research was also supported by NIH grants P30 AG010129 and K01 AG030514.

MULTIMODAL ANALYSIS IN NORMAL AGING, MILD COGNITIVE IMPAIRMENT, AND ALZHEIMER'S DISEASE: GROUP DIFFERENTIATION, BASELINE COGNITION, AND PREDICTION OF FUTURE COGNITIVE DECLINE

(Order No.)

CORINNA MAE BAUER

Boston University School of Medicine, 2013

Major Professor: Ronald Killiany, Ph.D., Associate Professor of Anatomy and Neurobiology

ABSTRACT

Alzheimer's disease (AD) is a progressive neurodegenerative disease with an insidious onset that makes it difficult to distinguish from normal aging. It begins with an impairment of memory that develops into amnestic mild cognitive impairment (aMCI) and later to dementia as deficits become apparent in other cognitive domains. Effective biomarkers that differentiate normal aging, MCI, and AD and predict future cognitive decline are needed. Potential biomarkers have been studied in isolation, but their impact when combined is not understood. The goal of this project is to determine the optimal combination of CSF biomarkers, MRI morphometry, FDG PET metabolism, and neuropsychological test scores to differentiate between normal aging subjects and those with MCI and AD. This study addresses: 1) the optimal normalization region and partial volume correction method to quantify FDG PET analysis, 2) the effects of adjusting MRI-

based cortical thickness measures for differences in gray/white matter tissue contrast in normal aging and disease, 3) whether multimodal multivariate stepwise logistic regression models can predict group membership, and 4) whether multimodal multivariate stepwise linear regression models can determine which imaging and CSF biomarker variables best predict future cognitive decline. The results indicate that normalizing FDG PET to the cerebellum along with using a gray matter mask for partial volume correction provides optimal prediction. In contrast, age-associated changes in gray/white matter intensity ratio did not differentiate between the groups and only slightly improved the efficacy of cortical thickness as a biomarker. MRI morphometry of the gray matter and neuropsychological test scores were better able to discriminate between the groups than FDG PET or CSF biomarker concentrations. Combining all modalities significantly improved the index of discrimination, especially at the earliest stages of the disease. MRI gray matter morphometry variables were more highly associated with baseline cognitive function and best predicted future cognitive decline compared to other variables. Overall these findings demonstrate that a multimodal approach using MRI morphometry, FDG PET metabolism, neuropsychological test scores, and CSF biomarkers provides significantly better discrimination than any modality alone. Hence, the variables important for discriminating between the groups may be candidates for biomarkers in human clinical interventional trials.

TABLE OF CONTENTS

LIST OF TABLES

LIST OF FIGURES

ABBREVIATIONS

Aβ-42	ABeta 1-42
AD	Alzheimer's disease
Adj.	adjusted
ADNI	Alzheimer's Disease Neuroimaging Initiative
AIC	Akaike's information criteria
aMCI	amnestic mild cognitive impairment
ANOVA	analysis of variance
APC	annualized percent change
CDR	clinical dementia rating
CSF	cerebrospinal fluid
FDG	^{18}F-flurodeoxyglucose
GE	General Electric
GM	gray matter
GMM	gray matter mask
GWIR	gray/white matter intensity ratio
MCI	mild cognitive impairment
MMSE	Mini-mental status examination
MRI	magnetic resonance imaging
NFT	neurofibrillary tangle
Param. Est.	parameter estimate
PET	positron emission tomography

pTau	phosphorylated tau
PVC	partial volume correction
RAVLT	Rey auditory verbal learning test
ROC	receiver operating characteristic
ROI	region of interest
Sd	standard deviation
Std dev	standard deviation
Std. Est.	standardized estimate
STS	superior temporal sulcus
tTau	total tau
WM	White matter

Chapter 1 - General introduction

INTRODUCTION

Alzheimer's disease (AD) is the most common form of dementia. At the present time it is affecting approximately 5.4 million Americans and the incidence is expected to nearly double within the next few decades as the population ages (Anon 2012). The rate of development of AD is heightened in individuals with amnestic mild cognitive impairment (MCI). Amnestic MCI is characterized by cognitive deficits primarily affecting memory, preserved overall cognitive and functional abilities, and the absence of dementia (R. C. Petersen 2001). Individuals with MCI convert to AD at a rate of 10 to 15% per year in comparison to approximately 1% per year in "normal aging" individuals (R. C. Petersen 2001), making it imperative to generate effective methods for identifying the early signs in individuals with MCI who go on to develop AD. The clinical presentation of MCI is heterogeneous, making it difficult to determine at what stage in the normal aging, MCI, AD spectrum an individual may be in. There are a number of factors that may contribute to diagnosis, including performance on neuropsychological tests, brain morphometric measurements, brain glucose uptake, and concentrations of biomarkers in cerebrospinal fluid (CSF).

Pathologically, AD and MCI are characterized by the presence of intracellular neurofibrillary tangles (NFTs) and extracellular amyloid plaques. The NFTs are composed of insoluble hyperphosphorylated tau protein. Normal tau protein, the non-hyperphosphorylated type, is involved in microtubule stabilization of the axonal cytoskeleton. In the presence of NFTs, however, the

integrity of the cytoskeleton is impaired, such that neurons are dysfunctional and there is synaptic and neuronal loss (Gómez-Isla et al. 1997; Mosconi 2005). In AD and MCI, NFTs accumulate in the hippocampus, entorhinal cortex, amygdala, and other limbic areas that are important memory structures. As the disease progresses, the NFTs affect more neocortical areas, resulting in a deficit in other cognitive domains (Mosconi 2005) . While NFTs have a predilection for medial temporal lobe and limbic structures, amyloid plaques tend to accumulate more in the association cortices and, as the disease progresses, affect more hippocampal structures (H Braak & E. Braak 1991; D. R. Thal et al. 2002). The extent of amyloid distribution is less closely related to the severity of impairment on cognition than the NFTs (Mosconi 2005). Amyloid plaques are extracellular, are composed of insoluble fibrils of amyloid-beta (Aβ), and may be related to the hypometabolism that is observed using FDG PET (Mosconi 2005). The underlying pathology is difficult to monitor *in vivo*, however, using imaging techniques, CSF sampling, and neuropsychological testing, it is possible to monitor the state of the disease progression. But, which method provides the best differentiation between normal aging, MCI, and AD? CSF levels of ABeta 1-42 (Aβ-42), total tau, and phosphorylated tau, structural brain changes as measured with MRI morphometry, and functional brain changes as measured with FDG PET may all be useful.

There is evidence that there is free exchange of molecules between the brain and CSF (Reiber & Peter 2001), which makes CSF a likely candidate for

biomarker for MCI and AD. There are three major markers of AD that are present in CSF, namely total tau (tTau), hyperphosphorylated tau (pTau), and Aβ-42 (Zetterberg et al. 2003). It has been suggested that these markers are able to identify AD in its early stages with fairly high accuracy (Hansson et al. 2006), with increases in pTau and tTau have been observed in AD compared to normal aging (K Blennow et al. 1995; M. Ewers et al. 2007). However, there is overlap between AD and other forms of dementia in this measure, making it potentially difficult to rule out differential diagnoses. CSF of both MCI and AD subjects shows decreased concentrations of Aβ-42 (M. Ewers et al. 2007), which may reflect an increased deposition of Aβ in aggregated plaques in the brain (Cedazo-Minguez & Winblad 2010). Although the increase in Aβ-42 and decreases in both pTau and tTau in CSF have been observed in MCI and AD, to what extent they can differentiate between normal aging, MCI, and AD and to what degree this can be improved upon by the addition of imaging data is not fully understood.

Once of the consequences of AD pathology is a disruption of synaptic function. This may be indirectly measured via changes in glucose metabolism. FDG PET, a glucose analogue, is typically used as a marker of synaptic function, as metabolic changes are closely tied to glucose consumption. There is a relatively consistent pattern of decreased metabolism that occurs in AD. The regions that tend to show hypometabolism are the posterior cingulate/retrosplenial cortex and the cortical structures in the parieto-temporal junction, such as the angular gyrus and the precuneus. Some studies also

indicate a decrease in hippocampal metabolism (De Santi S. et al. 2001; Y. Li et al. 2008; Mosconi et al. 2009), although this is not consistently observed (Kawachi et al. 2006; Matsunari et al. 2007; K. Ishii et al. 2005). There is not a consistent pattern for MCI (Mosconi et al. 2008). Glucose metabolism changes mirror the Braak and Braak staging of NFTs (Mosconi et al. 2009), thus FDG PET may be able to differentiate between normal aging, MCI, and AD groups with a high degree of discrimination.

As previously mentioned, one of the consequences of AD pathology is neuronal loss. This loss is indirectly visible *in vivo* through imaging techniques, such as MRI. MRI is particularly useful for this, as it is a 3-dimensional imaging method. This enables researchers to examine the various ways in which atrophy can present itself, namely through changes in cortical surface area, thickness, or volume, of the cortical structures. Cortical thickness has been shown to be a particularly useful metric for tracking disease progression; however, cortical surface area has not been examined to its full extent. Volumetric and cortical thickness changes have been observed consistently in MCI and AD, with the earliest detectable changes occurring in the entorhinal cortex and hippocampus, spreading outward to other cortical and subcortical structures (Michael Ewers et al. 2011; R J Killiany et al. 2002; P. M. Thompson et al. 2003). The combination of structures that best differentiates normal aging, MCI, and AD from one another has not been fully examined in a ROI-based data-driven approach. Many studies have limited their search to only cortical thickness in a set of ten or so

predetermined ROIs. This may be detrimental to the ability to identify the MRI features that best characterize and differentiate between groups.

Ultimately the accumulation of NFTS and Aβ, and the resultant changes in synaptic function and neuronal loss, manifests as cognitive deficits. The first round of testing when a patient presents with a memory complaint to the clinic is typically a battery of neuropsychological tests. Each of the tests in the battery is meant to measure performance on different types of cognitive skills (e.g. executive function, visuospatial abilities, etc.) or forms of memory (e.g. long-term memory, recall, recognition). The Mini-mental status examination (MMSE) is often used as a metric of dementia severity, but because it covers a range of general cognitive abilities, it is often insensitive to early stage AD (Devanand et al. 1997; Galasko et al. 1990; Herlitz et al. 1997), in which memory is the primary complaint. The clinical dementia rating (CDR) is another commonly utilized metric for determining dementia severity. Using the CDR, normal aging would be a score of 0, MCI receives a value of 0.5, and once the scores run above 1, the individual likely has dementia. The test examines six domains: memory, orientation, judgment and problem solving, function in community affairs, home and hobbies, and personal care. The difficulty is that the test scoring is geared more for determining the more severe stages of dementia. Thus, the question arises, is there a better set of tests for examining changes in cognition that occur between normal aging and MCI, and then between MCI and AD and differentiate between these groups?

Each of the four modalities we discussed above has been implicated to be useful for discriminating normal aging, MCI, and AD. There is evidence that a combination of these methods may be better than the individual methods on their own (Kawachi et al. 2006). However, there are some additional factors that may attribute to the efficacy of FDG PET or cortical thickness measures for differentiating between subject groups.

PET imaging has innately poor spatial resolution, which can pose problems when it is used in neurodegenerative diseases where progressive atrophy is a defining feature of the disease, such as AD. What happens is that in atrophic regions, signal from neighboring tissues, such as CSF in which there is no metabolism, the metabolic values can be artificially low. This is particularly a problem in structures that are already small. Thus, in regions such as the medial temporal lobes, the already small volume combined with atrophy can easily result in artificially low metabolic values. To eliminate this problem, partial volume correction (PVC) strategies in post-processing can be used. This is not done consistently and few studies directly compare the ability of different PVC methods to differentiate accurately between normal aging, MCI, and AD. Thus, this study will address the issue of partial volume correction across the AD spectrum.

FDG PET data utilized in this study is non-quantitative because venous blood was not sampled during the data acquisition. Thus, in order to directly compare the FDG metabolism between subjects, we need to normalize the data

to a reference region that does not change with the disease. The best region to normalize with for differentiating between normal aging, MCI, and AD is under contention. Thus, the second chapter will address the choice of reference region for normalization of FDG PET data.

Cortical thickness values are determined in part by the gray/white matter boundary. This boundary is often elusive, as the tissue contrast is often subtle, particularly when the tissue is affected by pathology. Thus, it has been suggested that adjusting cortical thickness for changes in gray/white matter intensity ratio (GWIR) may improve cortical thickness accuracy (Grydeland et al. 2012; D H Salat et al. 2009), which may in turn result in its being a better predictor of MCI and AD (Grydeland et al. 2012). In this light, the third chapter will address the issues of GWIR in normal aging, the ability of GWIR to predict group membership on its own and as an adjustment factor for cortical thickness, and finally the potential change in cortical thickness effect size after adjusting for GWIR will be examined.

The third study addresses the ability to differentiate between normal aging, MCI, and AD with different modalities, namely MRI morphometry (e.g. cortical thickness, surface area, and volume), FDG metabolism, CSF biomarker concentration, and neuropsychological test scores. The discriminability of each modality on its own was determined, followed by an examination of the change in discriminability after combining modalities.

The fourth study addresses the use of CSF biomarkers, MRI morphometry, and FDG PET to predict baseline cognitive performance on a number of tasks and also to predict future cognitive decline in these tasks. We chose the tasks that had been shown in the third study to best differentiate between all three subject groups, namely clock draw, Trails A and B, digit span forward and backward, and 30 minute recall, recognition, and number of recognition errors. Stepwise linear regression models were used to predict baseline and follow-up change from baseline MRI morphometric and FDG metabolic data. Both imaging modalities were first tested on their own and then together, for those tests in which both modalities contributed.

There are a number of statistical techniques that are common to all four studies, including residuals and regression. The regression used in the fourth study is stepwise linear, whereas the type used for the first three studies is stepwise logistic. I will briefly describe these techniques here and the importance of them for what information they can divulge. Residuals are used to control for the effects of a nuisance variable on a variable(s) of interest. Another common way to do this is to use ratios and divide the variable of interest by the nuisance variable. The problem with ratios is that it is unclear whether the resulting value is mostly driven by the numerator or denominator, and there are also no units. This can cause problems when we want to know how the variable of interest on its own, independent of the nuisance variable, affects MCI or AD because when we use a ratio, the final value is still influenced by the nuisance variable. Residuals

remove the variance of the nuisance variable from the variable of interest while maintaining the units.

Stepwise logistic regression is used consistently throughout the first three studies to determine the ability of a set of variables to discriminate between diagnostic groups. In almost all cases, with the exception of when examining all three groups together, the outcome variable (e.g. the diagnostic group) is dichotomous (e.g. normal aging or MCI). Thus, the models assess which variables are indicative of normal aging, MCI, or AD. Whether or not a variable is determined to be a predictor of disease group is determined based on the odds ratio, which is a measure of the amount of influence a variable has on the outcome variable (e.g. how much the odds of MCI increases or decreases based on hippocampal volume). The odds ratio is calculated for each variable and if the odds ratio meets a predetermined cutoff value, it is entered as a variable in the model. For every variable that is entered into the model, each variable already present in the model is reassessed and if it no longer meets the cutoff value, it leaves the model. Thus, the end result is a set of variables that contribute independent variance to the determination of diagnostic group. The ability of the overall model to differentiate between groups is determined with the c-statistic, which is a measure of discrimination with values between 0.5 and 1, whereby 1 is perfect discrimination and 0.5 is random discrimination.

Stepwise linear regression is similar to stepwise logistic regression, with the exception that the outcome variable is not categorical, but is linear. Thus,

goal is to determine the set of variables that best fits the slope of the outcome variable (e.g. digit span backward score). The variables that contribute variance to the model is determined in a stepwise manner, although rather than an odds ratio, the variance is measures by standardized betas. The ability of the overall model to predict the outcome variable is determined with the adjusted R-square, which is a measure of the total variance in the outcome variable that the model accounts for. It ranges from 0 to 1, with 1 representing 100% of the variation in the outcome variable.

Using these statistical techniques, the overall goal of this dissertation is to use a data-driven approach to examine the relationships between imaging measures, CSF biomarkers, and neuropsychological tests in normal aging, MCI, and AD in depth in order to identify the factors that are most associated with each stage of the disease as well as predictive of future decline.

REFERENCES

Anon, 2012. 2012 Alzheimer's disease facts and figures. *Alzheimer's and Dementia*, 8(2), pp.131–168.

Blennow, K et al., 1995. Tau protein in cerebrospinal fluid: a biochemical marker for axonal degeneration in Alzheimer disease? *Molecular and chemical neuropathology / sponsored by the International Society for Neurochemistry and the World Federation of Neurology and research groups on neurochemistry and cerebrospinal fluid*, 26(3), pp.231–245.

Braak, H & Braak, E., 1991. Neuropathological stageing of Alzheimer-related changes. *Acta neuropathologica*, 82(4), pp.239–259.

Cedazo-Minguez, A. & Winblad, B., 2010. Biomarkers for Alzheimer's disease and other forms of dementia: Clinical needs, limitations and future aspects. *Experimental Gerontology*, 45(1), pp.5–14.

Devanand, D.P. et al., 1997. Questionable dementia: clinical course and predictors of outcome. *Journal of the American Geriatrics Society*, 45(3), pp.321–328.

Ewers, M. et al., 2007. Multicenter assessment of CSF-phosphorylated tau for the prediction of conversion of MCI. *Neurology*, 69(24), pp.2205–2212.

Ewers, Michael et al., 2011. Staging Alzheimer's disease progression with multimodality neuroimaging. *Progress in Neurobiology*, 95(4), pp.535–546.

Galasko, D. et al., 1990. The Mini-Mental State Examination in the early diagnosis of Alzheimer's disease. *Archives of neurology*, 47(1), pp.49–52.

Gómez-Isla, T. et al., 1997. Neuronal loss correlates with but exceeds neurofibrillary tangles in Alzheimer's disease. *Annals of Neurology*, 41(1), pp.17–24.

Grydeland, H. et al., 2012. Improved prediction of Alzheimer's disease with longitudinal white matter/gray matter contrast changes. *Human brain mapping*. Available at: http://www.ncbi.nlm.nih.gov/pubmed/22674625 [Accessed August 2, 2012].

Hansson, O. et al., 2006. Association between CSF biomarkers and incipient Alzheimer's disease in patients with mild cognitive impairment: a follow-up study. *Lancet neurology*, 5(3), pp.228–234.

Herlitz, A. et al., 1997. Detection of mild dementia in community surveys. Is it possible to increase the accuracy of our diagnostic instruments? *Archives of neurology*, 54(3), pp.319–324.

Ishii, K. et al., 2005. Comparison of gray matter and metabolic reduction in mild Alzheimer's disease using FDG-PET and voxel-based morphometric MR studies. *European Journal of Nuclear Medicine and Molecular Imaging*, 32(8), pp.959–963.

Kawachi, T. et al., 2006. Comparison of the diagnostic performance of FDG-PET and VBM-MRI in very mild Alzheimer's disease. *European Journal of Nuclear Medicine and Molecular Imaging*, 33(7), pp.801–809.

Killiany, R.J. et al., 2002. MRI measures of entorhinal cortex vs hippocampus in preclinical AD. *Neurology*, 58(8), pp.1188–1196.

Li, Y. et al., 2008. Regional analysis of FDG and PIB-PET images in normal aging, mild cognitive impairment, and Alzheimer's disease. *European Journal of Nuclear Medicine and Molecular Imaging*, 35(12), pp.2169–2181.

Matsunari, I. et al., 2007. Comparison of 18F-FDG PET and optimized voxel-based morphometry for detection of Alzheimer's disease: aging effect on diagnostic performance. *Journal of Nuclear Medicine: Official Publication, Society of Nuclear Medicine*, 48(12), pp.1961–1970.

Mosconi, L., 2005. Brain glucose metabolism in the early and specific diagnosis of Alzheimer's disease. *European Journal of Nuclear Medicine and Molecular Imaging*, 32(4), pp.486–510.

Mosconi, L. et al., 2009. FDG-PET changes in brain glucose metabolism from normal cognition to pathologically verified Alzheimer's disease. *European Journal of Nuclear Medicine and Molecular Imaging*, 36(5), pp.811–822.

Mosconi, L., Pupi, A. & De Leon, M.J., 2008. Brain glucose hypometabolism and oxidative stress in preclinical Alzheimer's disease. *Annals of the New York Academy of Sciences*, 1147, pp.180–195.

Petersen, R. C., 2001. Current Concepts in Mild Cognitive Impairment. *Archives of Neurology*, 58(12), pp.1985–1992.

Reiber, H. & Peter, J.B., 2001. Cerebrospinal fluid analysis: disease-related data patterns and evaluation programs. *Journal of the neurological sciences*, 184(2), pp.101–122.

Salat, D.H. et al., 2009. Age-associated alterations in cortical gray and white matter signal intensity and gray to white matter contrast. *NeuroImage*, 48(1), pp.21–28.

De Santi S. et al., 2001. Hippocampal formation glucose metabolism and volume losses in MCI and AD. *Neurobiology of Aging*, 22(4), pp.529–539.

Thal, D.R. et al., 2002. Phases of Aβ-deposition in the human brain and its relevance for the development of AD. *Neurology*, 58(12), pp.1791–1800.

Thompson, P.M. et al., 2003. Dynamics of Gray Matter Loss in Alzheimer's Disease. *The Journal of Neuroscience*, 23(3), pp.994–1005.

Zetterberg, H., Wahlund, L.-O. & Blennow, Kaj, 2003. Cerebrospinal fluid markers for prediction of Alzheimer's disease. *Neuroscience letters*, 352(1), pp.67–69.

Chapter 2 - Differentiating between normal aging, mild cognitive impairment, and Alzheimer's disease with FDG PET: Effects of normalization region and partial volume correction method

INTRODUCTION

Individuals with mild cognitive impairment (MCI) and Alzheimer's disease (AD) show disease-related decreases in 18F-flurodeoxyglucose (FDG) PET metabolism, which correlate with changes in memory function (Desgranges et al. 2002). This hypometabolism tends to follow the pattern of pathology observed in AD, first affecting the medial temporal lobes and spreading outwards to involve the temporal, parietal, and frontal cortices while sparing the primary sensory areas. These changes are less severe in MCI, as it is a precursor of AD and individuals tend to not have the same degree of clinical impairments. Despite many studies outlining FDG uptake in MCI and AD, there is a lack of consistency in two key components to PET data processing; namely, choice of reference region for normalization and partial volume correction.

Normalization allows for the direct comparison of non-quantitative PET data between subjects and may decrease variance within the dataset. In order to qualify for a candidate reference region for normalization, the brain region must fulfill a number of criteria: it must not be affected by the disease or condition being studied, it must be easily and reliably identifiable, and it ought to provide the most accurate differentiation of subject groups (Dukart et al. 2010; Yakushev et al. 2008). The optimal choice of reference region for normalization has been debated in the field, with the pons (Minoshima et al. 1995), cerebellum (Dukart et al. 2010), and primary somatosensory cortices (Yakushev et al. 2008) all being suggested to be the best region. In addition, many studies utilize the whole brain

and a proportional mean scaling factor (Dukart et al. 2010; Samuraki et al. 2007), which, in the case of AD, likely does not fulfill the first criteria for a reference region, as widespread global changes in metabolism are often observed. Studies that compare normalization regions tend to be relatively small and utilize only one research site, thus the results may not be applicable to other studies. Large-scale studies, such as the Alzheimer's disease neuroimaging initiative (ADNI) are prime candidates for examining which reference region is optimal for differentiating normal aging, MCI, and AD from one another, as the sample size is large and multiple research sites are used.

The other critical PET image analysis step often ignored in MCI and AD research is partial volume correction. When it is used, there are numerous methods, few of which address the region-of-interest (ROI) based analysis. PET images have innately limited spatial resolution. This becomes a problem when the disease of interest is characterized by regional atrophy, such as hippocampal and entorhinal atrophy in AD and MCI. Because of the progressive AD-related atrophy, small brain regions, which are more sensitive to partial volume effects, tend to display artificially low FDG uptake values, thereby falsely enhancing difference between the disease and control groups (Rousset & H. Zaidi 2006). Essentially then, if partial volume correction is not used, then the disease-related hypometabolism may not be true changes in metabolism, but are likely metabolism changes contaminated by tissue atrophy. To eliminate this problem, some FDG PET studies use partial volume correction (PVC) that is based on

voxel-wise analysis (Meltzer et al. 1999; Meltzer et al. 1996; Park et al. 2006; Rousset et al. 1998; Rousset & H. Zaidi 2006; Samuraki et al. 2007; Daisuke Yanase et al. 2005). One group has also published a study using a region of interest (ROI)-based FDG PET partial volume correction (K B Walhovd, A M Fjell, A M Dale, et al. 2010). The present study will examine the effects of partial volume correction on FDG uptake in MCI and AD using two methods: the use of gray matter mask (GMM) (Daisuke Yanase et al. 2005; Matsuda et al. 2003), typically a voxel-based approach, to remove non-gray matter voxels adapted for use with FreeSurfer, a semi-automated image analysis software program, and the statistical approach of Walhovd and colleagues (K B Walhovd, A M Fjell, A M Dale, et al. 2010). In the second approach, cortical thickness and subcortical volume residuals are used to correct for partial volume effects.

The main aims of this study were to first examine which ROI provides the most sensitive normalization when differentiating between normal aging, MCI, and AD in a large sample collected at multiple research centers. The second aim of this study was to examine the effects of PVC on normal aging, MCI, and AD using two techniques: 1) applying a grey matter mask (GMM) (Matsuda et al. 2003; Daisuke Yanase et al. 2005), and 2) taking residuals of uptake after removing the effects of cortical thickness plus subcortical volume (K B Walhovd, A M Fjell, A M Dale, et al. 2010). These aims were tested by building statistical models of discrimination to identify the best set of anatomically-based FDG PET measures to differentiate between normal aging, MCI, and AD.

MATERIALS AND METHODS

Subjects

The data for use in this study were chosen from the larger pool of data that has been made publically available by the Alzheimer's Disease Neuroimaging Initiative. Data was screened to include all subjects who had both PET and MRI scans available for use on the ADNI/LONI website (www.loni.ucla.edu/ADNI) at the time this study began. From this screened dataset, PET data from 21 subjects was of poor contrast and quality and had to be omitted from the analyses for this study. Three subjects were omitted due to missing information. This left us with data from 403 subjects. They had an age range of 55-89 years with an overall average age of 75.47 years. Of this group, 146 were female and 257 were male. In terms of subgroups, 105 were identified as health control subjects, 204 fell into the category of MCI and 94 fell into the category of having AD as determined by the ADNI (Table 2.1).

All subjects completed a battery of neuropsychological tests, including the mini-mental state examination (MMSE) (M. F. Folstein et al. 1975), the CDR-Sum of Boxes(J C Morris 1993), and the Global dementia scale (Auer & B Reisberg 1997; B Reisberg et al. 1988). On the basis of their cognitive status the subjects were classified by the ADNI clinical core as: (a) normal controls with normal cognition and memory, CDR 0, and MMSE between 24-30; (b) amnestic MCI with memory complaint verified by a study partner, memory loss measured by education-adjusted performance on the Logical Memory II subscale of the

Wechsler Memory Scale-Revised (Wechsler 1987), preserved activities of daily living, CDR 0.5, MMSE between 24 and 30, and absence of dementia at time of baseline MRI scan; or (c) probable AD with memory complaint validated by an informant, abnormal memory function for age and education level, absence of depression, impaired activities of daily living, diminished cognition, CDR > 0.5, and MMSE between 20 - 26.

Alzheimer's Disease Neuroimaging Initiative

The ADNI was a 5-year non-randomized natural history non-treatment study utilizing data from multiple study centers across the United States and Canada. One of the main goals of the ADNI was to develop optimized methods and uniform standards for the acquisition of multicenter MRI and PET data on normal control subjects and patients with MCI and AD in drug/treatment trials. For more information about the ADNI please refer to http://www.adni-info.org.

MRI scans

For this study, we chose MRI scans from those acquired by the ADNI on 1.5T scanners from General Electric (GE), Philips Medical Systems (Philips), and Siemens Medical Solutions (Siemens). Specific pulse sequence guidelines can be found at http://www.loni.ucla.edu/ADNI/Research/Cores/index.shtml. In this study we used the two MPRAGE scan acquired at baseline for each participant. The data from the LONI website was downloaded for use in it's original format since the Freesurfer processing pipeline has its own normalizing procedures.

FDG PET scans

For this study, we chose FDG PET scans from those acquired by the ADNI on GE, Philips, or Siemens scanners. Specific protocols for each scanner are available from the ADNI website (http://adni.loni.ucla.edu/research/protocols/pet-protocols/). These data were corrected for radiation attenuation and scatter using scanner-specific algorithms and each image was visually assessed for potential artifacts by the ADNI PET core at the University of Michigan. For this study we used the original PET data that was not pre-processed by the ADNI PET core so that we could have local control of all the processing steps as with the MRI scans.

Freesurfer Analysis

All MRI and PET scans were processed with the Freesurfer 4.4.1 image analysis suite, which is documented and freely available for download from http://surfer.nmr.mgh.harvard.edu/. The FDG PET scans were re-processed in version 5.1.0 in order to do GMM partial volume correction. For each subject, the 2 DICOM T1-weighted MRI datasets were motion corrected, averaged, segmented into gray matter, white matter, and cerebral spinal fluid (CSF), and intensity normalized. The cortex was parcellated into regions of interest based on gyral and sulcal structure. For each of the cortical regions volume, surface area, and cortical thickness were determined. Volume was calculated for each of the subcortical structures. Please refer to the FreeSurfer wiki page for more detailed information (http://surfer.nmr.mgh.harvard.edu/fswiki).

PET Processing

Once the T1-weighted MRI images were processed, the PET images were affine spatial transformed into "anatomical space" 1x1x1, 256x256x256, which was the same resolution as the transformed MRI images. The PET and MRI images were then co-registered using an automated Freesurfer boundary based application using 6 degrees of freedom, such that no skewing or twisting of the data occurred (Figure 2.1). The resulting coregistration was visually assessed for accuracy and adjusted if necessary (approximately 25% of the datasets). After the two datasets were co-registered, the PET data was applied as a mask to the MRI images and analyses performed. FDG uptake was measured in specific ROIs according to the cerebral cortex parcellations generated on the representative MRI images (Desikan et al. 2006). A total of 41 cortical and subcortical areas were examined for changes in MRI morphometry and FDG uptake related to MCI and AD relative to normal aging (Figures 2 and 3).

PET reference region for normalization

To control for individual global variations and to increase sensitivity of the method for differentiating between subject groups (Yakushev et al. 2008), a number of reference regions for normalization were tested, namely the brainstem, precentral gyrus, postcentral gyrus, cerebellum, and thalamus. These regions were chosen because they have been reported by others to be good candidates for normalization (Minoshima et al. 1995; Dukart et al. 2010). The

reference regions were first tested for disease effects before and after PVC and if there were no disease-related differences found using ANOVA, they were assessed as normalization regions. Normalization was done using residuals.

PET Gray matter mask partial volume correction

Each participant's MRI was segmented into gray matter (GM), white matter (WM) and cerebrospinal fluid space (CSF). The MRI WM segment was made binary and, after registration, served as a WM mask for the PET images. The WM PET mask was then made binary and multiplied by the original PET image to obtain a WM-only PET image. The GM PET image with partial volume correction (PVC) was obtained by subtracting the WM PET image from the original PET image and then multiplying this image by a binary GM MRI mask. The Freesurfer parcellations were then applied to the GM PET.

PET residuals partial volume correction

The second PVC method was a statistical-based approach in which the effects of cortical thickness and subcortical volume were removed from the FDG PET metabolic values via residuals. This approach has been used in the past with FDG PET data processed in FreeSurfer (K B Walhovd, A M Fjell, A M Dale, et al. 2010).

Statistical Analysis

In order to assess the equity of the male-female distribution in the three diagnostic groups, χ^2 tests were performed. ANOVA was used in order to assess

the age distribution in the three diagnostic groups. T-tests showed no significant left/right differences, thus the data from the two hemispheres was averaged.

Logistic regression Analyses

For each candidate normalization region we created a logistic stepwise regression model for diagnostic group, controlling for age, gender, and education by forcing them into the model. This was accomplished by running linear regressions for MCI vs. normal, AD vs. MCI, and all three groups together with each FDG PET regional uptake variable individually in order to identify their predictor values. If the point estimate was below 0.75 or above 1.25 the FDG PET regional uptake variable was determined to be an adequate predictor on its own and was entered as a variable in the overall model.

Separate models were created for differentiating between AD and MCI, MCI and normal aging, and all three groups together based upon data normalized to each of the candidate normalization regions. The c-statistic and AIC for each model were used to assess its utility. Hosmer-Lemeshow goodness of fit Chi square tests were used to assess the models' calibration.

RESULTS

Chi-square tests revealed no significant differences for distribution of males and females between groups (df=2, p=0.3517). Age was not significantly different between control, MCI, and AD groups, as indicated with ANOVA (p=0.6684).

Normalization region

We tested the pre- and post-central gyri, thalamus, brainstem (as a surrogate for the pons), and cerebellum both before and after partial volume correction for significant differences between groups in order to assess if disease state has an effect on them. After these initial tests, only uptake in the brainstem and cerebellum was preserved as normalization candidates. ANOVA indicated that in the non-partial volume corrected PET data, the pre- and post-central gyri showed significantly decreased FDG uptake ($p < 0.05$) with disease progression eliminating them as potential normalization candidates. After partial volume correction, the thalamus showed significantly decreased uptake with disease ($p < 0.05$) and was eliminated as a potential candidate for normalization. Conversely, the brainstem and cerebellum did not show significant disease-related differences ($p > 0.05$) making them good candidates for normalizing the FDG PET uptake data. To determine which region was better, we created logistic regression models for differentiating between all three subject groups normalizing to brainstem and cerebellum individually and in combination, which resulted in three separate models. To compare the models directly we took only the common regions to all three models and forced them into separate final models. These final models showed that the cerebellum slightly outperformed the brainstem, with c-statistics of 0.826 and 0.823, respectively. Thus, for the remainder of the study, the cerebellum was used as the normalization region.

Partial Volume Correction

ANOVAs for the effects of partial volume correction

To assess the effects of PVC, we examined the differences in between-group relationships as determined by Tukey's post-hoc ANOVA tests. Prior to PVC, the majority of regions showed significant differences between normal aging, MCI, and AD (Table 2.2), with the exception of some cingulate, frontal, visual, and mid-brain regions. The highest degrees of change were observed in the medial temporal lobe, frontal, temporal, and parietal regions. After PVC using residuals, nearly all previously significant regions of hypometabolism were no longer significant, with the exception of the postcentral gyrus. Three regions showed an increase in significance, namely the amygdala, thalamus, and temporal pole. After PVC using the GMM method, there were again mixed effects, with some regions decreasing in significance and other regions increasing in significance. Table 2.2 outlines the specific details.

Stepwise logistic regression models

To examine the effects of partial volume correction, we created a series of models that differentiated normal aging from MCI, normal aging from AD, MCI from AD, and all three groups from one another before partial volume correction, after correction using a statistically-based residuals approach, and after correction using the GMM. Here we present the results from differentiating normal aging from MCI and normal aging from AD. In all models, age, gender,

and education were forced in to control for the variance they may have had on the model. Similar results were found for all four model conditions, thus the other two groups of models for differentiating AD from MCI and all three groups are presented in the supplementary material.

Models normal aging from MCI

Partial volume correction significantly decreased the ability to predict group membership using FDG PET data, regardless of which method of PVC was used. The GMM method provided a better model than cortical thickness residuals, both in terms of c-statistic (ROC) and AIC. Prior to partial volume correction, models differentiating between normal aging and MCI provided a c-statistic of 0.810 and AIC of 310 (Table 2.3). Hosmer-Lemeshow goodness of fit shows that this model is well calibrated (chi-square = 11.82, p = 0.16). The regions that contributed significant amounts of variance to the model included the entorhinal cortex and the hippocampus. Age was the only other significant predictor. Banks of the superior temporal sulcus, caudal middle frontal, inferior temporal, and superior temporal all contributed variance to the model, but these failed to reach statistical significance.

After correcting using cortical thickness and subcortical volume residuals, the c-statistic was 0.678 and AIC was 361. Hosmer-Lemeshow goodness of fit shows that this model is well calibrated (chi-square = 7.33, p = 0.50). The difference in c-statistics between non-PVC and residuals-PVC models was statistically significant (p = 0.0008). The regions that were significant predictors

were the amygdala and temporal pole. The paracentral gyrus contributed but failed to reach statistical significance.

After correcting using the GMM method, the c-statistic was 0.688 and AIC was 355. Hosmer-Lemeshow goodness of fit shows that this model is well calibrated (chi-square = 4.29, p = 0.83). The difference in c-statistics between non-PVC and GMM-PVC models was also statistically significant (p = 0.0015). The regions that contributed significantly to the model were the entorhinal, fusiform, inferior temporal, and the isthmus of the cingulate. The c-statistic and AIC both indicate that the GMM method of PVC provides the best model for discriminating MCI from normal aging.

Models differentiating normal aging from AD

Again, partial volume correction significantly decreased the ability to discriminate group and the GMM method provided a better model, both in terms of c-statistic and AIC, than the residuals method of PVC (Table 2.4). Prior to PVC, differentiating between normal aging and AD subject groups provided a model with a c-statistic of 0.972 and AIC of 110. However, Hosmer-Lemeshow goodness of fit test shows that this model is not well calibrated and may not provide consistent results (chi-square = 50.86, p < 0.0001). The variables that contributed significantly to the model include precuneus,, rostral anterior cingulate, isthmus of the cingulate, insula, parahippocampal gyrus, hippocampus, and superior parietal. Age was also a significant predictor.

After correcting using cortical thickness and subcortical volume residuals, the c-statistic was 0.864 and AIC was 195. Hosmer-Lemeshow goodness of fit shows that this model is well calibrated (chi-square = 6.57, p = 0.58). The regions that contributed significantly to the model were the entorhinal, amygdala, parahippocampus, thalamus, paracentral gyrus, and the inferior temporal lobe. Education was a significant predictor, as well.

After correcting using GMM, the c-statistic was 0.879 and AIC was 185. Hosmer-Lemeshow goodness of fit shows that this model is well calibrated (chi-square = 3.89, p = 0.87). The regions that contributed significantly to the model were the entorhinal, parahippocampus, middle temporal, temporal pole, and the paracentral and post-central gyri. Education was also a significant predictor. Other regions that contributed, although not significantly, to the model were the isthmus of the cingulate and the precuneus.

Direct comparison of models

Because different regions, only some of which are previously attributed to MCI and AD, contributed to each of the models of different correction types, we wanted to verify the efficacy of one correction method over another by allowing only specific brain regions that are consistently affected in MCI and AD into the models. Thus, we re-created models using only the measures of the entorhinal cortex, age, gender, and education in order to directly compare the non-partial volume corrected model and the two PVC models. When comparing MCI and

normal aging, c = 0.726 for non-PVC, c = 0.655 for GMM, and c = 0.594 for cortical thickness residuals. When comparing AD and normal aging, c = 0.865 for non-PVC, c = 0.713 for GMM, and c = 0.653 for cortical thickness residuals. Similar results were found for comparing MCI and AD and for differentiating all three groups. The results of these analyses confirm that GMM provides higher c-statistics than cortical thickness residuals, but lower than non-PVC values.

Correlations with Age

Correlations between FDG uptake and age were only tested on the normal aging subjects to avoid contamination from AD-related effects, thus n_{age}= 105 and $n_{FDG\ uptake}$= 98. GMM-type PVC removed most of the age-related changes in FDG uptake compared to both non-PVC uptake and residual-PVC uptake (data not shown). Prior to partial volume correction, there were significant negative correlations between age and FDG uptake in a number of regions. After PVC using cortical thickness and subcortical volume residuals, a number of significant negative correlations between age and FDG uptake remained. There was also a significant positive correlation in the caudate. After PVC using the GMM method, there was a significant positive correlation between age and FDG uptake in the pallidum (R = 0.24613, p = 0.0146). No other regions showed significant age-related correlations.

DISCUSSION

FDG PET can provide vital information in the study of degenerative diseases such as Alzheimer's disease. In the raw, unprocessed form, FDG PET data is difficult to interpret quantitatively particularly when making comparisons between groups. In order to make these comparisons more meaningful, the uptake in each scan must be normalized to a control region within the scan and corrected for the influence of factors that could adversely impact the data. In this study we first examined which anatomically based ROI could serve as an appropriate region for normalizing FDG uptake across subjects ranging from normal aging, MCI and Alzheimer's disease. Next we looked into a means for addressing partial volume effects, a morphometric feature which can become more pronounced with atrophy in disease states such as Alzheimer's disease. We assessed two methods, one using a gray matter mask to remove the potential confounding effects of the white matter, and the second using a statistical correction based upon using the residuals derived from cortical thickness or subcortical volume depending upon the structure. Specifically we sought to identify the best correction factors for partial volume errors and normalization to obtain the statistical model which best differentiates between FDG uptake in normal aging, MCI, and AD. The influence of partial volume correction on age-related effects was also examined in healthy control subjects.

Normalization region ANOVA

Our results suggest that the cerebellum is the best region to use for normalizing scans when using FDG PET data to differentiate between normal aging, MCI, and early stage AD. Of the other regions that we assess, the pre- and post-central gyri showed significant hypometabolism in the AD group which is consistent with previous studies (Minoshima et al. 1995), thereby affirming that they are not appropriate normalization regions when AD subjects are being used. Interestingly, others have found that the somatosensory cortex (the pre- and post-central gyri combined) provided the best normalized data for discriminating between normal aging and MCI subject groups (Yakushev et al. 2008) though since they did not use partial volume correction their data and findings may be based on a mixture of metabolic and morphometric changes.

We also found that after PVC the thalamus showed significant hypometabolism in the AD group. Similarly, Minoshima et al. (1995) found significant disease-related differences in the thalamus; however, this was without any partial volume correction making it difficult to discern whether this was due to changes in metabolism, volume, or both. In this study we only found thalamus differences after correcting for partial volume effects suggesting that this difference is the result of a true reduction in metabolism and not a change in volume.

Taken together, our findings on the pre- and post-central gyrus and thalamus affirm the importance of correcting for partial volume effects. It also

underscores the importance of testing the reference region for disease-related effects in the subject sample to ensure its validity as a reference region.

Partial Volume Correction

Many studies that have looked at choosing a normalization region have not corrected for partial volume effects and those which have looked at PVC have not examined which brain region was best for normalization in their sample. Since these two factors can interact, it was important to look at both factors simultaneously in a sample that included not only normal aging and AD subjects, but also MCI subjects, which have been neglected in these types of study.

We found that the adapted GMM method, which corrects the data at the image level, provided a higher index of discriminability in all group comparisons than using a statistical correction with cortical thickness or subcortical volume residuals. In addition, the regions that were chosen by the analysis for inclusion into the final models with the GMM method also are more consistent with those typically impacted by Alzheimer's disease.

The changes in Tukey's post-hoc analysis indicate that there is an interaction between partial volume correction and FDG metabolism amongst the three groups. The decrease in significance observed throughout the cortex would indicate that the FDG data prior to correcting for partial volume was likely contaminated by atrophy, particularly in the AD group, as reflected by the low uptake values. We would like to point out that in a number of instances, regions

typically associated with AD, (e.g. the hippocampus) were in the non-PVC model, but not in the PVC model. This does not necessarily imply that the regions no longer showed significant hypometabolism with disease. The logistic models indicate which variables contribute unique amounts of variance to the discrimination of two or more subject groups. Thus, there can still be significant disease-associated hypometabolism in a region that is not in the logistic model. Thus, the hippocampus may contribute variance to differentiating normal aging from MCI, but if the variance overlaps with a region that contributes more variance, such as the entorhinal cortex, then the hippocampus would not be included in the model, but the entorhinal cortex would be.

Correlations with age

We examined age-related correlations with FDG uptake before and after partial volume correction with the GMM and residual methods. We found that the efficacy for removing age-related changes in FDG uptake varied depending on which PVC method was used. Residuals failed to remove most of the correlations, while the GMM-PVC method removed most of the age-related changes. Previous studies on FDG changes in normal aging have shown reductions in the frontal and temporal lobes, particularly the dorsolateral frontal cortex (S De Santi et al. 1995); superior frontal cortex(Kuhl et al. 1982); and in the cingulate, parahippocampal, superior temporal, medial frontal, and posterior parietal cortices (Martin et al. 1991). On the contrary, a number of studies have observed no correlations between age and FDG uptake (M J de Leon, Ferris,

George, Christman, et al. 1983; M J de Leon, Ferris, George, B Reisberg, et al. 1983; M J de Leon et al. 1984; Rapoport 1986). There are limited studies specifically looking at the change in age correlations with FDG uptake after correcting for partial volume effects (Cidis Meltzer et al. 2000). Consistent with their results, we found that correcting PET values for partial volume removes the majority of age-related effects, but only when using the GMM method. For instance, after PVC, the medial orbitofrontal cortex still showed age correlations in their study, while in ours the age-related decline in the medial orbitofrontal cortex remained after cortical thickness residual PVC, but was removed with GMM-PVC. Along the same lines, cortical thickness residuals actually increased the significance of many of the age/FDG uptake correlations. GMM PVC removed all age-related decline with the exception of the pallidum.

CONCLUSION

We sought to determine which choice of reference region for normalization provided the best model for discriminating between normal aging, MCI, and AD subject groups and also to determine the effects of partial volume correction on the statistical models. Partial volume correction is necessary for identifying which brain regions show true changes in FDG uptake with disease progression independent of any changes in MRI morphometry. Our results indicate that for this study sample, the cerebellum was the best region for normalization. The best models were those in which there was no partial volume correction, but by correcting for partial volume effects we can be certain that the FDG changes are

from decreased metabolism and not influenced by atrophy. Out of the two PVC methods tested (cortical thickness and subcortical volume residuals and GMM), we found that the GMM provides a higher index of discriminability, as measured with the c-statistic. Not only that, but the regions that were predictors in the GMM model better concurred with the literature on which regions are involved at the MCI and early AD disease stages. In addition, we can conclude that partial volume correction with the GMM diminished the age-related changes observed in the normal aging population. These results together suggest that perhaps the GMM is better than using residuals for FDG PET data processed in Freesurfer.

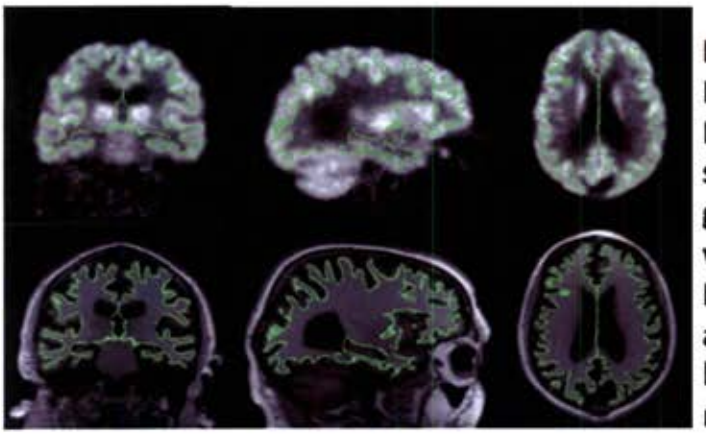

Figure 1. Coregistration of FDG PET and T1-weighted MPRAGE MRI scans shown in coronal, sagittal, and axial sections. The green line indicates the gray/ white matter boundary. The FDG PET scans are on the top and the MRI scans are on the bottom . The images are from a normal aging 83 year old male.

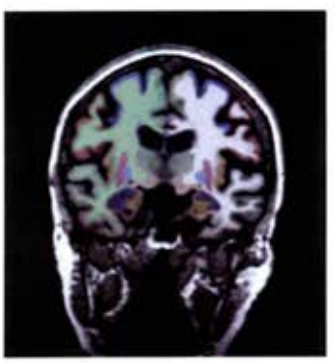

Figure 2. Coronal view of parcellated cortical and subcortical regions. Female MCI subject age 79

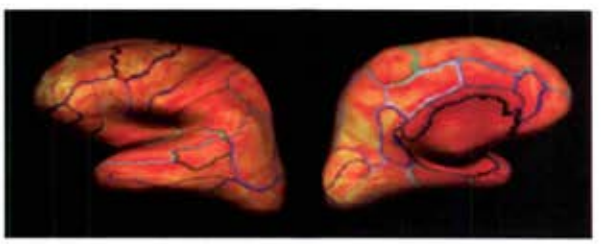

Figure 3. Lateral and medial views of raw FDG uptake mapped onto inflated brain. Parcellated cortical regions are outlined.

Table 2.1 Demographic information

	Subjects (male/female)	**Age mean years (std dev)**	**Education Mean (std dev)**	**MMSE**
Normal Aging	105 (64/41)	75.81 (4.75)	15.90 (3.12)	28.98 (1.12)
MCI	204 (137/67)	75.44 (7.22)	15.80 (2.88)	27.15 (1.71)[a]
AD	94 (56/38)	74.91 (7.37)	14.61 (3.21)[a,b]	23.48 (2.14)[a,b]

[a] significant difference from normal aging ($p < 0.05$), [b] significant difference from MCI ($p < 0.05$).

Table 2.2 ANOVA results for FDG uptake changes between normal aging, MCI, and AD subject groups. The first three columns show p-values from ANOVAs comparing uptake in normal aging, MCI, and AD before partial volume correction (PVC) and after PVC using residuals and gray matter mask (GMM) methods. The MCI vs. normal, AD, vs. MCI, and AD vs. normal columns show the specific relationships between groups, whereby '<' indicates a decrease in MCI compared to normal in the first column, AD < MCI, and AD < normal in the three columns, respectively ($p > 0.05$). Similarly, '>' indicates a sgnificant increase in one group compared to the other, i.e. MCI > normal, AD > MCI, and AD > normal. '=' indicates no significant change in uptake between groups.

	P-value non-PVC	P-value residuals	P-value GMM	MCI vs. normal	AD vs. MCI	AD vs. normal
banks sts	<.0001	0.63	0.001	<, =, =	=, =, =	<, =, <
caudal anterior cingulate	0.60	0.33	0.42	=, =, =	=, =, =	=, =, =
caudal middle frontal	0.73	0.32	0.05	=, =, =	=, =, =	=, =, =
cuneus	<.0001	0.40	0.25	<, =, =	=, =, =	<, =, =
entorhinal	0.0007	0.07	<.0001	=, =, <	=, =, =	<, <, <
frontal pole	<.0001	0.12	0.28	<, =, =	<, =, =	<, =, =
fusiform	<.0001	0.18	0.03	<, =, <	<, =, =	<, =, =
inferior parietal	<.0001	0.07	0.0006	<, =, <	<, =, =	<, <, <
inferior temporal	0.04	0.007	<.0001	=, =, <	=, <, =	<, <, <
insula	0.007	0.72	0.24	=, =, =	=, =, =	<, =, =
isthmus of the cingulate	0.09	0.07	<.0001	=, =, <	=, =, =	=, <, <
lateral occipital	0.14	0.05	0.29	=, =, =	=, =, =	=, =, =
lateral orbitofrontal	0.007	0.39	0.11	=, =, =,	=, =, =	<, =, =
lingual	0.001	0.20	0.28	=, =, =,	=, =, =	<, =, =
medial orbitofrontal	<.0001	0.83	0.11	=, =, =,	<, =, =	<, =, =
middle temporal	0.0009	0.21	<.0001	=, =, <	<, =, =	<, =, <
paracentral	0.0001	0.02	0.02	=, >, =	<, =, >	<, >, >
parahippocampal gyrus	0.03	0.008	0.005	=, =, <	=, =, =	<, <, <
pars opercularis	0.003	0.34	0.17	=, =, =	<, =, =	<, =, =
pars orbitalis	0.002	0.39	0.25	=, =, =	<, =, =	<, =, =
pars triangularis	<.0001	0.52	0.28	<, =, =	<, =, =	<, =, =
pericalcarine	0.82	0.14	0.13	=, =, =	=, =, =	=, =, =
postcentral gyrus	<.0001	0.04	0.0004	<, =, =	<, =, >	<, =, >
posterior cingulate	0.13	0.11	0.06	=, =, =	=, =, =	=, =, <
precentral gyrus	0.007	0.61	0.005	=, =, =	=, =, >	<, =, =
precuneus	0.03	0.08	0.008	=, =, <	=, =, =	<, =, <
rostral anterior cingulate	<.0001	0.31	0.24	=, =, =	<, =, =	<, =, =
rostral middle frontal	<.0001	0.29	0.17	=, =, =	<, =, =	<, =, =
superior frontal	0.001	0.58	0.06	=, =, =	<, =, =	<, =, =
superior parietal	<.0001	0.77	0.13	<, =, =	<, =, =	<, =, =
superior temporal	0.04	0.36	0.03	=, =, <	=, =, =	>, =, =
supramarginal	<.0001	0.25	0.13	<, =, =	<, =, =	<, =, =
temporal pole	0.37	0.003	0.01	=, >, <	=, =, =	=, =, =
transverse temporal	<.0001	0.24	0.41	<, =, =	<, =, =	<, =, =
amygdala	0.47	<.0001	0.004	=, <, <	=, <, =	=, <, <
caudate	0.50	0.44	0.07	=, =, =	=, =, =	=, =, =
hippocampus	0.002	0.16	0.002	=, =, <	<, =, =	<, =, <
pallidum	0.01	0.74	0.03	=, =, =	=, =, =	<, =, >
putamen	0.13	0.89	0.002	=, =, <	=, =, =	=, =, =
thalamus	0.04	0.001	0.19	=, =, =	=, =, =	<, <, =

Table 2.3 Stepwise logistic regression models for differentiating between MCI and normal aging groups before and after partial volume correction. The top model shows the non-pvc model (c = 0.810), followed by the cortical thickness + subcortical volume residuals (c = 0.678), and the GMM on the bottom (c = 0.688).

MCI versus normal aging	Unit	Odds Ratio (95%CI)	p-value
Non-PVC model			
gender	1	1.855 (0.995 - 3.462)	0.05
education	2.9586	0.881 (0.655 - 1.185)	0.40
age	6.5536	0.597 (0.439 - 0.812)	0.001
entorhinal	337.3	0.681 (0.478 - 0.970)	0.03
banks STS	341.8	0.773 (0.558 - 1.071)	0.12
caudal middle frontal	876.3	0.742 (0.538 - 1.023)	0.07
inferior temporal	1279	0.744 (0.520 - 1.064)	0.11
superior temporal	1166.3	1.418 (0.948 - 2.122)	0.09
hippocampus	532.6	0.345 (0.222 - 0.537)	<0.0001
Cortical thickness + subcortical volume residuals			
gender	1	1.131 (0.645 - 1.985)	0.67
education	2.9586	0.907 (0.703 - 1.171)	0.45
age	6.5536	0.815 (0.625 - 1.064)	0.13
paracentral gyrus	371.1	1.261 (0.949 - 1.674)	0.11
temporal pole	225.5	1.478 (1.134 - 1.927)	0.004
amygdala	21.0682	0.667 (0.499 - 0.890)	0.006
Gray matter mask			
gender	1	1.507 (0.869 - 2.612)	0.14
education	2.9574	0.857 (0.658 - 1.117)	0.25
age	6.4782	0.798 (0.611 - 1.041)	0.10
entorhinal	1349.3	0.549 (0.361 - 0.835)	0.005
fusiform	1235.9	2.439 (1.342 - 4.434)	0.004
inferior temporal	1301	0.576 (0.341 - 0.975)	0.04
isthmus of the cingulate	2007.9	0.588 (0.386 - 0.895)	0.01

Table 2.4 Stepwise logistic regression models for differentiating between AD and normal aging groups before and after partial volume correction. The top model shows the non-pvc model (c = 0.972), followed by the cortical thickness + subcortical volume residuals (c = 0.864), and the GMM on the bottom (c = 0.879).

AD versus normal aging	Unit	Odds Ratio (95%CI)	p-value
Non-PVC model			
gender	1	2.395 (0.664 - 8.639)	0.18
education	3.2426	0.561 (0.295 - 1.068)	0.08
age	6.0469	0.203 (0.079 - 0.523)	0.001
frontal pole	131.3	0.621 (0.321 - 1.201)	0.16
fusiform	1171.9	0.483 (0.229 - 1.019)	0.06
precuneus	1003.1	0.132 (0.044 - 0.393)	0.0003
rostral anterior cingulate	276.6	2.040 (1.002 - 4.156)	0.05
isthmus of the cingulate	272.3	2.725 (1.090 - 6.808)	0.03
insula	660.4	2.997 (1.271 - 7.067)	0.01
parahippocampal gyrus	305.3	0.441 (0.214 - 0.909)	0.03
superior parietal	1458.7	3.218 (1.245 - 8.318)	0.02
hippocampus	621.4	0.012 (0.002 - 0.067)	<0.0001
Cortical thickness + subcortical volume residuals			
gender	1	1.408 (0.575 - 3.45)	0.45
education	3.2426	0.526 (0.344 - 0.802)	0.003
age	6.0469	0.703 (0.470 - 1.051)	0.09
entorhinal	246.9	0.597 (0.391 - 0.912)	0.02
inferior temporal	1297.9	0.595 (0.368 - 0.961)	0.03
paracentral gyrus	328.2	2.671 (1.640 - 4.351)	<0.0001
parahippocampal gyrus	183.3	0.505 (0.307 - 0.833)	0.007
amygdala	23.6388	0.322 (0.195 - 0.530)	<0.0001
thalamus	52.2657	0.612 (0.411 - 0.911)	0.02
Gray matter mask			
gender	1	1.072 (0.450 - 2.551)	0.88
education	3.2507	0.574 (0.379 - 0.869)	0.009
age	5.9331	1.051 (0.705 - 1.567)	0.81
entorhinal	1508.9	0.103 (0.033 - 0.325)	0.0001
isthmus of the cingulate	2183.6	0.423 (0.120 - 1.495)	0.18
middle temporal	1686	0.231 (0.106 - 0.501)	0.0002
paracentral gyrus	2075.2	2.471 (1.020 - 5.987)	0.05
parahippocampal gyrus	1576.2	4.218 (1.220 - 14.579)	0.02
postcentral gyrus	1575.6	3.685 (1.463 - 9.279)	0.006
precuneus	2083.1	0.333 (0.102 - 1.087)	0.07
temporal pole	1264.5	3.130 (1.132 - 8.655)	0.03

Table 2.5 Stepwise logistic regression models for differentiating between all three groups before and after partial volume correction. The top model shows the non-pvc model (c = 0.831), followed by the cortical thickness + subcortical volume residuals (c = 0.693), and the GMM on the bottom (c = 0.735).

All three groups	**Unit**	**Odds Ratio (95%CI)**	**p-value**
Non-PVC model			
gender	1	0.738 (0.466 - 1.170)	0.20
education	3.0693	0.768 (0.615 - 0.960)	0.02
age	6.6897	0.656 (0.520 - 0.827)	0.0004
entorhinal	363.1	0.660 (0.493 - 0.882)	0.005
caudal middle frontal	865.2	0.712 (0.539 - 0.939)	0.02
frontal pole	132.3	0.772 (0.600 - 0.994)	0.04
inferior temporal	1387.9	0.532 (0.395 - 0.716)	<0.0001
medial orbitofrontal	405.5	1.266 (0.969 - 1.656)	0.08
precuneus	921.5	0.714 (0.539 - 0.944)	0.02
superior frontal	1986.8	1.691 (1.217 - 2.348)	0.002
temporal pole	307.2	1.449 (1.126 - 1.866)	0.004
hippocampus	575.6	0.336 (0.242 - 0.466)	<0.0001
caudate	562.4	1.337 (1.069 - 1.672)	0.01
Cortical thickness + subcortical volume residuals			
gender	1	1.196 (0.763 - 1.874)	0.43
education	3.0693	0.729 (0.595 - 0.893)	0.002
age	6.6897	0.781 (0.638 - 0.959)	0.02
inferior temporal	1299.2	0.657 (0.525 - 0.822)	0.0002
amygdala	23.057	0.561 (0.453 - 0.695)	<0.0001
thalamus	51.4717	0.741 (0.604 - 0.909)	0.004
Gray matter mask			
gender	1	1.047 (0.690 - 1.589)	0.830
education	3.0711	0.687 (0.558 - 0.845)	0.0004
age	6.586	0.998 (0.808 - 1.232)	0.98
entorhinal	1405.3	0.718 (0.566 - 0.912)	0.007
inferior parietal	1761.9	0.599 (0.436 - 0.822)	0.002
isthmus of the cingulate	1974.2	0.588 (0.431 - 0.803)	0.0008
postcentral gyrus	1517.7	2.675 (1.988 - 3.601)	<0.0001
pallidum	710.9	1.231 (0.989 - 1.531)	0.06

Table 2.6 Stepwise logistic regression models for differentiating between AD and MCI groups before and after partial volume correction. The top model shows the non-pvc model (c = 0.774), followed by the cortical thickness + subcortical volume residuals (c = 0.714), and the GMM on the bottom (c = 0.726).

AD versus MCI	Unit	Odds Ratio (95%CI)	p-value
Non-PVC model			
gender	1	0.904 (0.501 - 1.632)	0.74
education	3.0409	0.664 (0.503 - 0.877)	0.004
age	7.2123	0.908 (0.672 - 1.228)	0.53
inferior temporal	1366.6	0.628 (0.436 - 0.906)	0.01
precuneus	927	0.691 (0.486 - 0.982)	0.04
rostral middle frontal	1573.9	1.267 (0.896 - 1.793)	0.18
hippocampus	552.8	0.49 (0.351 - 0.684)	<0.0001
Cortical thickness + subcortical volume residuals			
gender	0.902	0.902 (0.476 - 1.711)	0.75
education	0.63	0.63 (0.476 - 0.834)	0.001
age	0.899	0.899 (0.675 - 1.196)	0.46
inferior temporal	0.787	0.787 (0.564 - 1.099)	0.16
parahippocampal gyrus	0.75	0.75 (0.537 - 1.049)	0.09
amygdala	0.616	0.616 (0.460 - 0.824)	0.001
thalamus	0.75	0.75 (0.567 - 0.992)	0.04
Gray matter mask			
gender	1	0.716 (0.406 - 1.265)	0.25
education	3.0423	0.61 (0.461 - 0.808)	0.0006
age	7.0892	1.085 (0.811 - 1.452)	0.58
inferior temporal	1337.9	0.552 (0.407 - 0.749)	0.0001
postcentral gyrus	1564	1.779 (1.285 - 2.463)	0.0005
putamen	2407.4	1.425 (1.043 - 1.946)	0.03

References

Auer, S. & Reisberg, B., 1997. The GDS/FAST staging system. *International Psychogeriatrics / IPA*, 9 Suppl 1, pp.167–171.

Cidis Meltzer, C. et al., 2000. Does Cerebral Blood Flow Decline in Healthy Aging? A PET Study with Partial-Volume Correction. *Journal of Nuclear Medicine*, 41(11), pp.1842 –1848.

Desgranges, B. et al., 2002. The neural substrates of episodic memory impairment in Alzheimer's disease as revealed by FDG–PET: relationship to degree of deterioration. *Brain*, 125(5), pp.1116–1124.

Desikan, R.S. et al., 2006. An automated labeling system for subdividing the human cerebral cortex on MRI scans into gyral based regions of interest. *NeuroImage*, 31(3), pp.968–980.

Dukart, J. et al., 2010. Differential effects of global and cerebellar normalization on detection and differentiation of dementia in FDG-PET studies. *NeuroImage*, 49(2), pp.1490–1495.

Folstein, M.F., Folstein, S.E. & McHugh, P.R., 1975. "Mini-mental state". *Journal of Psychiatric Research*, 12(3), pp.189–198.

Kuhl, D.E. et al., 1982. Effects of human aging on patterns of local cerebral glucose utilization determined by the [18F]fluorodeoxyglucose method. *Journal of Cerebral Blood Flow and Metabolism: Official Journal of the International Society of Cerebral Blood Flow and Metabolism*, 2(2), pp.163–171.

De Leon, M.J., Ferris, S.H., George, A.E., Reisberg, B., et al., 1983. Computed tomography and positron emission transaxial tomography evaluations of normal aging and Alzheimer's disease. *Journal of Cerebral Blood Flow and Metabolism: Official Journal of the International Society of Cerebral Blood Flow and Metabolism*, 3(3), pp.391–394.

De Leon, M.J., Ferris, S.H., George, A.E., Christman, D.R., et al., 1983. Positron emission tomographic studies of aging and Alzheimer disease. *AJNR. American Journal of Neuroradiology*, 4(3), pp.568–571.

De Leon, M.J. et al., 1984. Positron emission tomography and computed tomography assessments of the aging human brain. *Journal of Computer Assisted Tomography*, 8(1), pp.88–94.

Martin, A.J. et al., 1991. Decreases in regional cerebral blood flow with normal aging. *Journal of Cerebral Blood Flow and Metabolism: Official Journal of the International Society of Cerebral Blood Flow and Metabolism*, 11(4), pp.684–689.

Matsuda, H. et al., 2003. Correction for partial-volume effects on brain perfusion SPECT in healthy men. *Journal of Nuclear Medicine: Official Publication, Society of Nuclear Medicine*, 44(8), pp.1243–1252.

Meltzer, C.C. et al., 1999. Comparative evaluation of MR-based partial-volume correction schemes for PET. *Journal of Nuclear Medicine: Official Publication, Society of Nuclear Medicine*, 40(12), pp.2053–2065.

Meltzer, C.C. et al., 1996. Regional hypometabolism in Alzheimer's disease as measured by positron emission tomography after correction for effects of partial volume averaging. *Neurology*, 47(2), pp.454–461.

Minoshima, S. et al., 1995. Preserved pontine glucose metabolism in Alzheimer disease: a reference region for functional brain image (PET) analysis. *Journal of Computer Assisted Tomography*, 19(4), pp.541–547.

Morris, J.C., 1993. The Clinical Dementia Rating (CDR): current version and scoring rules. *Neurology*, 43(11), pp.2412–2414.

Park, H.-J. et al., 2006. Cortical surface-based analysis of 18F-FDG PET: measured metabolic abnormalities in schizophrenia are affected by cortical structural abnormalities. *NeuroImage*, 31(4), pp.1434–1444.

Rapoport, S.I., 1986. Positron emission tomography in normal aging and Alzheimer's disease. *Gerontology*, 32 Suppl 1, pp.6–13.

Reisberg, B. et al., 1988. Global Deterioration Scale (GDS). *Psychopharmacology Bulletin*, 24(4), pp.661–663.

Rousset, O.G., Ma, Y. & Evans, A.C., 1998. Correction for partial volume effects in PET: principle and validation. *Journal of Nuclear Medicine: Official Publication, Society of Nuclear Medicine*, 39(5), pp.904–911.

Rousset, O.G. & Zaidi, H., 2006. Correction for Partial Volume Effects in Emission Tomography. In Habib Zaidi, ed. *Quantitative Analysis in Nuclear Medicine Imaging*. Boston: Kluwer Academic Publishers, pp. 236–271. Available at: http://www.springerlink.com/content/t250737450351613/ [Accessed August 31, 2011].

Samuraki, M. et al., 2007. Partial volume effect-corrected FDG PET and grey matter volume loss in patients with mild Alzheimer's disease. *European Journal of Nuclear Medicine and Molecular Imaging*, 34(10), pp.1658–1669.

De Santi, S. et al., 1995. Age-related changes in brain: II. Positron emission tomography of frontal and temporal lobe glucose metabolism in normal subjects. *The Psychiatric Quarterly*, 66(4), pp.357–370.

Walhovd, K.B. et al., 2010. Multi-modal imaging predicts memory performance in normal aging and cognitive decline. *Neurobiology of Aging*, 31(7), pp.1107–1121.

Wechsler, D., 1987. *WMS-R: Wechsler Memory Scale--Revised manual*, Psychological Corp., Harcourt Brace Jovanovich.

Yakushev, I. et al., 2008. Choice of reference area in studies of Alzheimer's disease using positron emission tomography with fluorodeoxyglucose-F18. *Psychiatry Research*, 164(2), pp.143–153.

Yanase, D. et al., 2005. Brain FDG PET study of normal aging in Japanese: effect of atrophy correction. *European Journal of Nuclear Medicine and Molecular Imaging*, 32(7), pp.794–805.

Chapter 3 - Does the gray/white intensity ratio matter when discriminating between normal aging, mild cognitive impairment, and Alzheimer's disease?

INTRODUCTION

Alzheimer's disease (AD) is the leading form of dementia today. It is characterized by an insidious onset of progressive decline in cognition associated with the accumulation of amyloid plaques and neurofibrillary tangles throughout the cortex. Mild cognitive impairment (MCI), particularly the amnestic form, is thought to be a precursor to AD and is characterized by the same pathology, though in lesser amounts. The accumulation of neurofibrillary tangles in the cortex has been associated with neuronal loss and atrophy (Gómez-Isla et al. 1997; Grignon et al. 1998). This atrophy can be visualized using MRI measures, such as cortical thickness.

With MRI, two boundaries can be identified that are critical for calculating cortical thickness: the gray matter-pial surface and the gray/white matter boundary. The accurate identification of both these boundaries is critical for calculating cortical thickness (Bruce Fischl & Anders M. Dale 2000). Alterations in the brain due to processes such as aging or disease may impact the MRI signal, such that the gray/white matter boundary becomes blurred. Indeed, age- (D H Salat et al. 2009; Westlye et al. 2009) and AD-related (Grydeland et al. 2012; D H Salat et al. 2011; Westlye et al. 2009) changes in gray/white matter intensity ratio (GWIR)s have been observed. Adjusting cortical thickness values for the age-related gray/white matter intensity changes may improve the ability to observe age-related cortical thickness changes (D H Salat et al. 2009). Similarly adjusting for changes in the GWIR in AD may add to the ability to differentiate

between normal aging and AD subjects (Grydeland et al. 2012); however, this has yet to be tested in an independent sample in subjects diagnosed with MCI and AD.

The main goal of this study is to examine the effects of GWIR on cortical thickness in normal aging, MCI, and AD subjects using data from the Alzheimer's Disease Neuroimaging Initiative (ADNI). Specifically, we tested the following hypotheses: 1) GWIR correlates positively with age in normal aging subjects, 2) GWIR decreases progressively between normal aging, MCI, and AD subject groups, 3) adjusting cortical thickness measurements for GWIR improves the ability to differentiate between normal aging, MCI, and AD subjects using statistical models, and 4) the effect size of cortical thickness increases after adjusting for GWIR.

METHODS

Subjects

The data for use in this study were obtained from the Alzheimer's Disease Neuroimaging Initiative. Data were screened to include all subjects who had both PET and MRI scans available for use on the ADNI/LONI website at the time this study began because this project evolved off of a larger project looking at both PET and MRI. Demographic information can be found in Table 3.1.

As part of the ADNI, all subjects completed a battery of neuropsychological tests. On the basis of their cognitive status the subjects were

classified by the ADNI clinical core as: (a) normal controls with normal cognition and memory, (b) amnestic MCI with memory complaint verified by a study partner, or (c) probable AD with memory complaint validated by an informant.

Alzheimer's Disease Neuroimaging Initiative

The ADNI was a 5-year non-randomized natural history non-treatment study utilizing data from multiple study centers across the United States and Canada. One of the main goals of the ADNI was to develop optimized methods and uniform standards for the acquisition of multicenter MRI and PET data on normal control subjects and patients with MCI and AD in drug/treatment trials. For more information about the ADNI please refer to http://www.adni-info.org.

MRI acquisition and analysis

For this study, we analyzed the baseline T1-weighted MPRAGE MRI scans from those acquired by the ADNI on 1.5T scanners from General Electric, Philips Medical Systems, and Siemens Medical Solutions. Specific pulse sequence guidelines can be found at http://www.loni.ucla.edu/ADNI/Research/Cores/index.shtml. All MRI scans were processed with the Freesurfer 5.1.0 (Dale A.M. et al. 1999; B. Fischl et al. 1999), which is documented and freely available. The processing pipeline has been described in detail elsewhere (Dale A.M. et al. 1999; B. Fischl et al. 1999; Bruce Fischl et al. 2002; Bruce Fischl, André van der Kouwe, et al. 2004; Bruce Fischl, David H Salat, et al. 2004; Bruce Fischl & Anders M. Dale 2000). Briefly, for each

subject, the 2 DICOM T1-weighted MRI datasets were motion corrected, averaged, segmented into gray matter, white matter, and cerebral spinal fluid, and intensity normalized. As outlined in Salat (D H Salat et al. 2009), gray matter tissue intensities were measured 35% through the thickness of the cortical ribbon. White matter tissue intensities were measured 1mm below the gray/white matter boundary, into the white matter. The GWIR was calculated by dividing the white matter by the gray matter intensity values. The ratios were then projected onto the cortical surface and smoothed with a Gaussian kernel with a full width at half maximum of 30mm. The cortex was parcellated into ROIs based on gyral and sulcal structure using the Desikan/Killiany atlas (Desikan et al. 2006). Cortical thickness and GWIR were calculated for each of the 68 cortical parcellations.

Statistical Analysis

Equality of the male-female distribution in the three diagnostic groups was examined with χ^2 tests. Age, education, and MMSE distributions in the three diagnostic groups were examined with ANOVA.

Residuals were used to adjust for GWIR on cortical thickness values within each parcellated brain region. Paired t-tests showed significant left/right differences, thus the data from the two hemispheres were not averaged.

To examine whether adjusting cortical thickness for GWIR improved predictability we created logistic stepwise regression models. To identify the most salient brain regions for differentiating our three subject groups, each cortical

thickness (adjusted and non-adjusted) variable and each GWIR variable was entered into a separate logistic regression. The variables with a point estimate below 0.75 or above 1.25 cutoff values were entered into stepwise logistic regressions to differentiate AD vs. normal aging, MCI vs. normal aging, AD vs. MCI, and all three groups. Age, gender, and education were forced into the models, effectively controlling for any influence they may have on the variables on interest. The entry and exit criteria for the stepwise models were based on a significance level of 0.20. The c-statistic for each model was used to compare goodness-of-fit between models. C-statistics of the raw and GWIR adjusted models were compared using the DeLong test (E. R. DeLong et al. 1988). The efficacy of the adjustment factor was examined based on changes in the c-statistic of the final logistic regression model.

The estimated effect sizes of the adjustment factor on cortical thickness were calculated, whereby F-ratio = (F-adjusted thickness/F-non-adjusted thickness)^2. Pearson correlation was used to examine the relationship between aging and GWIR and the relationship between raw cortical thickness and GWIR adjusted cortical thickness values.

RESULTS

Chi-square tests revealed no significant differences for distribution of males and females between groups (df=2, p=0.35). Age was not significantly different between control, MCI, and AD groups, as indicated by ANOVA (p=0.52).

The AD subject group had on average a year less education than normal and AD groups ($p < 0.05$). MMSE also showed significant decreases in both the MCI and AD subject groups ($p < 0.05$) (Table 3.1).

Age-related changes in GWIR:

We examined the correlations between age and GWIR and found only two regions that were significantly correlated: left pars orbitalis ($r = 0.10$, $p = 0.04$) and the right temporal pole ($r = 0.14$, $p = 0.004$). We did not correct for multiple comparisons, but it is not likely that the left pars orbitalis would remain significant after adjusting for multiple correlations. None of the other regions showed significant age-related changes ($p > 0.05$) (Data not shown).

Gray/white intensity ratio does not differ between diagnostic groups:

Differences in GWIR between normal aging, MCI, and AD for each of the cortical brain regions was examined using ANOVA followed by Tukey's honestly significant difference test. None of the brain regions showed significant differences in GWIR between any of the groups ($p > 0.05$) (Data not shown).

Gray/white matter intensity ratio is not effective at discriminating between *normal aging*, MCI, and AD

The ability of GWIR to discriminate between normal aging, MCI, and AD was examined with stepwise logistic regression. None of the cortical regions tested made the initial cutoff for comparing AD vs. MCI or for comparing all three groups. Three regions made the initial cutoff for comparing MCI vs. normal aging

and one region made the initial cutoff for AD vs. normal aging. The final model for MCI vs. normal aging had a c-statistic of 0.601 and aside from age, gender, and education, included only the right lateral orbitofrontal gyrus. The final model for AD vs. normal aging had a c-statistic of 0.638 and included only the right parahippocampal gyrus (Data not shown).

Improved discrimination of diagnostic groups after adjusting cortical thickness for gray/white intensity ratio

We examined if adjusting for GWIR could increase the ability of cortical thickness to differentiate between the three diagnostic groups. Small differences in the c-statistic after adjusting for GWIR were observed. After adjustment, the c-statistic increased across all diagnostic groupings except for AD vs. normal aging, in which the c-statistic decreased. None of the changes in c-statistic reached statistical significance. For differentiating between normal aging and AD, cortical thickness provided a c-statistic of 0.978 (confidence interval = 0.963, 0.993) and GWIR adjusted cortical thickness provided a c-statistic of 0.965 (confidence interval = 0.945, 0.986) (Tables 3.2a, 3.2b). The difference between the c-statistics was not statistically significant ($p = 0.10$). The cortical thickness models before and after adjustment for differentiating MCI vs. normal aging provided c-statistics of 0.796 (confidence interval = 0.739, 0.839) and 0.810 (confidence interval = 0.747, 0.846), respectively (Tables 3.3a, 3.3b). The difference between the c-statistics was not statistically significant ($p = 0.39$). The models for differentiating AD vs. MCI before and after adjustment provided c

statistics of 0.834 (confidence interval = 0.778, 0.873) and 0.837 (confidence interval = 0.784, 0.878), respectively (Tables 3.4a, 3.4b). The difference between the c-statistics was not statistically significant (p = 0.40). The non-adjusted and adjusted cortical thickness models for differentiating between all three groups provided c statistics of 0.829 and 0.830, respectively (Tables 3.5a, 3.5b). Because the outcome variable had three levels, the c-statistics could not be directly compared. These results indicate that although the GWIR on its own does not show diagnostic changes, adjusting for GWIR slightly improves discriminability between most diagnostic groups.

Effects of adjusting cortical thickness for GWIR:

We next examined the relationship between groups in cortical thickness before and after GWIR adjustment. After adjusting the cortical thickness measures for GWIR, the difference between diagnostic groups changed in only six regions, namely the left isthmus of the cingulate, left pericalcarine, left postcentral, right pericalcarine, right postcentral, and right posterior cingulate (Tables 3.6a and 3.6b). The squared F-ratios indicate that there was an increase in power in of 34 of 68 regions throughout the frontal, temporal and cingulate cortices after adjusting cortical thickness for GWIR, as indicated by F-ratios greater than 1 (Table 3.2a and 3.2b). The highest effects were observed in the left posterior cingulate (F-ratio = 1.59), left temporal pole (F = 1.16), left pericalcarine (F-ratio = 6.24), right cuneus (F-ratio = 1.13), right insula (F-ratio = 1.12), and the right pericalcarine (F-ratio = 42.76). Correlations between adjusted

and unadjusted cortical thickness measures were significant in all regions ($r > 0.99$, $p < 0.0001$) (data not shown).

DISCUSSION

Recent studies indicate that there is an age-related change in the gray/white matter intensity ratio, which changes disproportionately in Alzheimer's subjects (D H Salat et al. 2009; D.H. Salat et al. 2011; Westlye et al. 2009). The Alzheimer's-related changes have only been tested in one sample thus far. We expanded these studies by applying them to the ADNI sample and including MCI subjects. By including MCI subjects we apply the results to a wider spectrum of the disease progression.

Age-associated changes in GWIR

In this study we found isolated positive correlations with age only in the left pars orbitalis and the right temporal pole. This indicates an increase in GWIR with age and a reduction in tissue contrast in these regions with increasing age. Previous studies have indicated a widespread reduction in gray/white matter contrast with age (D H Salat et al. 2009; Westlye et al. 2009); however, the age range in both of these other studies was larger, encompassing more young subjects than are included in the ADNI dataset. It is plausible that the limited age-related changes we observed may have been a product of the age range included in our study.

GWIR in MCI and AD

The GWIR did not differ between normal aging, MCI, and AD in any of the cortical brain regions. This was rather surprising as we were expecting to observe increases in the ratio in temporal regions, as has previously been observed (D.H. Salat et al. 2011). While it is not entirely clear why this discrepancy exists, there are a number of factors that will need further investigation in future studies. These include differences in the scanners used, differences in pulse sequence, and differences in subject sampling. The data analyzed in this study was drawn from General Electric, Philips and Siemens 1.5T scanners located at multiple research sites, rather than the one scanner and site used in previous works (D.H. Salat et al. 2011; D H Salat et al. 2009). Also, since the ADNI worked to develop pulse sequence parameters that could be used to produce equivalent T1 weighted images at all sites (Jack Jr. et al. 2008) it should come as no surprise that the OASIS and ADNI study sequences differ in a number of ways which could impact the signal obtained from the different tissue types. Our finding of no significant differences in GWIR between normal aging, MCI, and AD suggest that for this measurement to be a good candidate biomarker for MCI or AD, MRI sequence optimalization would need to take place to ensure differences can be found in the marker in the dataset of interest.

GWIR is not able to differentiate between normal aging, MCI, and AD

Stepwise logistic models for differentiating between normal aging, MCI, and AD using only the GWIR values did not provide good indices of

discrimination. This provides further evidence that although gray/white matter intensity has previously been shown to differ between AD and normal aging (Westlye et al. 2009), it cannot differentiate between these two groups meaningfully as an independent measure in the ADNI dataset.

Adjusting cortical thickness for GWIR increased the ability to differentiate between normal aging, MCI, and AD

We examined if adjusting cortical thickness for GWIR increased the overall ability to differentiate between normal aging, MCI, and AD. We observed that in nearly all cases, with the exception of AD vs. normal aging, the c-statistic increased after adjustment, albeit not significantly, indicating that adjusting cortical thickness for GWIR can improve the ability to predict MCI and AD. In general the finding of improved discrimination is in agreement with the results found in a recent study in which GWIR was added to a logistic regression model predicting disease group (Grydeland et al. 2012).

It appears that our results, obtained with data from ADNI, differ in a number of ways from those obtained from studies using OASIS data. First, we did not observe widespread age-related correlations, as was found in Salat's study (D H Salat et al. 2009). Second, we did not observe significant changes in GWIR between normal aging, MCI, and AD. This is contrary to the results found by Salat and Westyle (D H Salat et al. 2009; D.H. Salat et al. 2011; Westlye et al. 2009). Third, we did not find as widespread increase in power in cortical thickness after adjusting for GWIR as Westyle did (Westlye et al. 2009). And

finally, we did not find the same increase in predictability of AD compared to normal aging after adjustment as Grydeland found (Grydeland et al. 2012). This suggests that when using GWIR in MCI and AD subjects, it must be done with caution, as results have yet to be consistently obtained across samples that use different parameters for acquiring T1-weighted MPRAGE scans.

Effects of GWIR adjustment on cortical thickness

Although there were no significant differences in GWIR between the normal aging, MCI, and AD groups, we did observe an increase in effect size based on the square ratios of the F-values after adjustment, although these did not reach statistical significance. In addition, we observed more pronounced cortical thickness changes in the AD group in a few regions. The majority of these regions have not typically been reported to be impacted by disease pathology in the early stages of the disease. Less pronounced AD-related differences in cortical thickness were also observed throughout the cortex. Taken together, this suggests that adjusting for GWIR does influence the cortical thickness measurements to some degree, which is in agreement with a previous study that found an increase in power after adjusting cortical thickness for intensity ratio when comparing AD to normal aging (Westlye et al. 2009). We have extended these findings to include MCI, indicating that adjusting cortical thickness for GWIR may increase the effect sizes between MCI and normal aging or AD groups. Further work needs to be done to better understand if this adjustment factor is truly working to remove a disease-related artifact or if the

process of adjusting the data is simply reducing the variance in the data with a mathematical function.

CONCLUSIONS

Overall our results provide weak support for adjusting cortical thickness for gray/white intensity ratio based on improvements in c-statistics for differentiating normal aging, MCI, and AD. We were unable to use GWIR as an independent predictor of MCI or AD as it was not able to differentiate between subject groups, nor did it show any significant differences between normal aging, MCI, or AD throughout the cortex.

Cortical thickness is becoming an important biomarker for potentially identifying those at risk for, or in the earliest stages of, Alzheimer's disease. For this tool to become optimized, it is critical that sources of errant variance in this measure be identified and removed. However, the present study reminds us that it is vital to confirm that the errant source of variance is actually present in the data before trying to remove it. This will become more important as imaging studies embrace higher field strengths and more sophisticated coils.

Table 3.1 Demographic information				
	Subjects (male/female)	**Age mean years (std dev)**	**Education Mean (std dev)**	**MMSE**
Normal Aging	105 (64/41)	75.81 (4.75)	15.90 (3.12)	28.98 (1.12)
MCI	204 (137/67)	75.44 (7.22)	15.80 (2.88)	27.15 (1.71)[a]
AD	94 (56/38)	74.91 (7.37)	14.61 (3.21)[a,b]	23.48 (2.14)[a,b]
[a] significant difference from normal aging ($p < 0.05$), [b] significant difference from MCI ($p < 0.05$).				

Table 3.2a Cortical thickness model for predicting AD vs. normal aging. The c-statistic indicates the ability of the model to discriminate between the subject groups. Point estimates with 95% confidence intervals are presented. STS = superior temporal sulcus.

	unit	Point Estimate (C.I)	p-value
Age	6.11	0.26 (0.09 - 0.72)	0.01
Gender	1.00	2.68 (0.59 - 12.16)	0.2
Education	3.22	0.40 (0.21 - 0.78)	0.007
Right frontal pole	0.28	1.82 (0.89 - 3.72)	0.1
Left rostral middle frontal	0.19	0.09 (0.02 - 0.49)	0.005
Left medial orbitofrontal	0.21	0.18 (0.05 - 0.59)	0.005
Left pars triangularis	0.20	2.66 (0.85 - 8.33)	0.09
Left superior frontal	0.21	90.96 (9.70 - 852.65)	<.0001
Right caudal anterior cingulate	0.29	4.18 (1.59 - 10.99)	0.004
Left middle temporal	0.26	0.02 (0.002 - 0.15)	0.0003
Left banks STS	0.25	0.43 (0.15 - 1.25)	0.12
Right entorhinal	0.55	0.02 (0.002 - 0.11)	<.0001
Left parahippocampus	0.39	0.13 (0.04 - 0.46)	0.001
Right superior parietal	0.20	4.48 (1.00 - 20.05)	0.05
Right precuneus	0.19	0.05 (0.007 - 0.31)	0.002
Right cuneus	0.14	0.45 (0.19 - 1.10)	0.08
Right lingual	0.13	2.39 (0.88 - 6.51)	0.09
Left insula	0.23	3.70 (1.30 - 10.53)	0.01
c = 0.978			

Table 3.2b GWIR-corrected cortical thickness models for predicting AD vs. normal aging. The c-statistics indicate the ability of the model to discriminate between the subject groups. Point estimates with 95% confidence intervals are presented. STS = superior temporal sulcus.

	unit	Point Estimate (C.I)	p-value
Age	6.11	0.84 (0.41 - 1.69)	0.62
Gender	1.00	0.75 (0.22 - 2.56)	0.65
Education	3.22	0.36 (0.19 - 0.66)	0.001
Left rostral middle frontal	0.19	0.16 (0.05 - 0.49)	0.001
Left pars opercularis	0.20	2.6 (1.02 - 6.65)	0.05
Left precentral gyrus	0.23	4.86 (1.87 - 12.63)	0.001
Left posterior cingulate	0.20	2.64 (1.08 - 6.45)	0.03
Left middle temporal	0.26	0.23 (0.06 - 0.83)	0.03
Left inferior temporal	0.26	0.38 (0.12 - 1.21)	0.1
Left temporal pole	0.43	1.75 (0.77 - 3.99)	0.18
Left banks STS	0.25	0.30 (0.11 - 0.79)	0.01
Right entorhinal	0.55	0.15 (0.06 - 0.36)	<.0001
Left parahippocampus	0.39	0.22 (0.10 - 0.47)	<.0001
Right precuneus	0.19	0.33 (0.14 - 0.80)	0.01
Left insula	0.23	2.58 (1.12 - 5.95)	0.03
c = 0.965			

Table 3.3a Cortical thickness model for predicting MCI vs. normal aging. The c-statistic indicates the ability of the model to discriminate between the subject groups. Point estimates with 95% confidence intervals are presented.

	unit	Point Estimate (C.I)	p-value
Age	6.49	0.58 (0.42 - 0.78)	0.0004
Gender	1.00	1.76 (0.98 - 3.18)	0.06
Education	2.96	0.86 (0.65 - 1.13)	0.28
Left rostral middle frontal	0.17	0.69 (0.41 - 1.15)	0.15
Left caudal middle frontal	0.21	0.64 (0.39 - 1.07)	0.09
Left medial orbitofrontal	0.21	0.77 (0.55 - 1.06)	0.11
Left superior frontal	0.20	2.11 (1.18 - 3.76)	0.01
Left middle temporal	0.22	0.39 (0.23 - 0.64)	0.0002
Right entorhinal	0.49	0.54 (0.38 - 0.78)	0.0008
Left parahippocampus	0.38	0.70 (0.52 - 0.94)	0.02
Left inferior parietal	0.19	1.87 (1.11 - 3.16)	0.02
Right fusiform	0.21	1.51 (1.02 - 2.24)	0.04
Right precuneus	0.17	0.67 (0.42 - 1.06)	0.09
c = 0.791			

Table 3.3b GWIR-corrected cortical thickness models for predicting MCI vs. normal aging. The c-statistics indicate the ability of the model to discriminate between the subject groups. Point estimates with 95% confidence intervals are presented. STS = superior temporal sulcus.

	unit	Point Estimate (C.I)	p-value
Age	6.50	0.61 (0.45 - 0.83)	0.001
Gender	1.00	1.58 (0.86 - 2.88)	0.14
Education	2.96	0.88 (0.66 - 1.17)	0.38
Left rostral middle frontal	0.17	0.62 (0.37 - 1.05)	0.08
Left caudal middle frontal	0.21	0.57 (0.34 - 0.95)	0.03
Left medial orbitofrontal	0.21	0.75 (0.54 - 1.04)	0.09
Left pars opercularis	0.20	1.54 (1.00 - 2.36)	0.05
Left superior frontal	0.20	2.16 (1.20 - 3.89)	0.01
Left middle temporal	0.22	0.37 (0.22 - 0.63)	0.0002
Right banks STS	0.22	0.78 (0.54 - 1.13)	0.19
Right entorhinal	0.49	0.60 (0.42 - 0.86)	0.006
Left parahippocampus	0.38	0.70 (0.51 - 0.95)	0.02
Left inferior parietal	0.19	2.15 (1.25 - 3.70)	0.006
Right fusiform	0.21	1.40 (0.92 - 2.12)	0.12
Right precuneus	0.17	0.64 (0.40 - 1.03)	0.07
c = 0.797			

Table 3.4a Cortical thickness model for predicting AD vs. MCI. The c-statistic indicates the ability of the model to discriminate between the subject groups. Point estimates with 95% confidence intervals are presented. STS = superior temporal sulcus.

	unit	Point Estimate (C.I)	p-value
Age	7.26	0.84 (0.60 - 1.16)	0.28
Gender	1.00	0.75 (0.40 - 1.49)	0.0004
Education	3.03	0.57 (0.42 - 0.78)	0.37
Left isthmus of the cingulate	0.26	0.53 (0.34 - 0.82)	0.005
Left posterior cingulate	0.19	1.47 (0.96 - 2.25)	0.08
Left inferior temporal	0.24	0.41 (0.26 - 0.66)	0.0003
Left temporal pole	0.44	1.51 (1.01 - 2.25)	0.04
Right banks STS	0.23	0.61 (0.41 - 0.92)	0.02
Right entorhinal	0.54	0.49 (0.34 - 0.71)	0.0001
Left parahippocampus	0.39	0.78 (0.55 - 1.11)	0.17
Right supramarginal	0.20	1.38 (0.89 - 2.15)	0.15
Left insula	0.22	1.38 (0.92 - 1.07)	0.12
c= 0.822			

Table 3.4b GWIR-corrected cortical thickness models for predicting AD vs. MCI. The c-statistics indicate the ability of the model to discriminate between the subject groups. Point estimates with 95% confidence intervals are presented. STS = superior temporal sulcus.

	unit	Point Estimate (C.I)	p-value
Age	7.27	0.82 (0.59 - 1.14)	0.23
Gender	1.00	0.84 (0.44 - 1.60_	0.6
Education	3.04	0.55 (0.40 - 0.76)	0.0002
Left isthmus of the cingulate	0.26	0.48 (0.31 - 0.76)	0.002
Left posterior cingulate	0.19	1.54 (1.00 - 2.39)	0.05
Right middle temporal	0.23	0.59 (0.34 - 1.03)	0.07
Left inferior temporal	0.24	0.44 (0.27 - 0.72)	0.001
Left temporal pole	0.43	1.52 (1.01 - 2.28)	0.04
Right banks STS	0.23	0.69 (0.45 - 1.07)	0.09
Right entorhinal	0.53	0.50 (0.33 - 0.75)	0.001
Left parahippocampus	0.39	0.74 (0.52 - 1.06)	0.1
Right supramarginal	0.20	1.38 (0.85 - 2.24)	0.2
Right fusiform	0.22	1.52 (0.94 - 2.47)	0.09
Left insula	0.22	1.42 (0.94 - 2.15)	0.09
c= 0.831			

Table 3.5a Cortical thickness model for predicting all three groups. The c-statistic indicates the ability of the model to discriminate between the subject groups. Point estimates with 95% confidence intervals are presented. STS = superior temporal sulcus.

	unit	Point Estimate (C.I)	p-value
Age	6.70	0.67 (0.53 - 0.84)	0.0005
Gender	1.00	1.39 (0.88 - 2.21)	0.16
Education	3.06	0.65 (0.52 - 0.81)	<.0001
Left rostral middle frontal	0.18	0.60 (0.40 - 0.89)	0.01
Left caudal middle frontal	0.22	0.75 (0.50 - 1.14)	0.18
Left medial orbitofrontal	0.21	0.75 (0.57 - 0.98)	0.03
Left pars opercularis	0.20	1.45 (1.04 - 2.03)	0.03
Left pars orbitalis	0.28	1.23 (0.92 - 1.64)	0.16
Left superior frontal	0.20	1.61 (1.03 - 2.53)	0.04
Right Isthmus of the cingulate	0.26	1.24 (0.95 - 1.63)	0.12
Left middle temporal	0.24	0.52 (0.34 - 0.79)	0.003
Left inferior temporal	0.24	0.53 (0.35 - 0.81)	0.003
Left temporal pole	0.42	1.37 (1.02 - 1.83)	0.04
Right banks STS	0.23	0.70 (0.53 - 0.94)	0.02
Right entorhinal	0.53	0.46 (0.35 - 0.62)	<.0001
Left parahippocampal	0.39	0.64 (0.51 - 0.82)	0.0004
Left superior parietal	0.20	1.52 (1.01 - 2.30)	0.05
Right fusiform	0.22	1.42 (1.02 - 1.99)	0.04
Right precuneus	0.18	0.55 (0.38 - 0.80)	0.002
Left lateral occipital	0.16	1.27 (0.91 - 1.78)	0.16
Left insula	0.22	1.30 (0.96 - 1.76)	0.09
c= 0.829			

Table 3.5b GWIR-corrected cortical thickness models for predicting all three groups. The c-statistics indicate the ability of the model to discriminate between the subject groups. Point estimates with 95% confidence intervals are presented. STS = superior temporal sulcus.

	unit	Point Estimate (C.I)	p-value
Age	6.70	0.71 (0.56 - 0.89)	0.003
Gender	1.00	1.29 (0.82 - 2.06)	0.27
Education	3.06	0.65 (0.52 - 0.81)	0.0001
Left rostral middle frontal	0.18	0.60 (0.40 - 0.88)	0.01
Right caudal middle frontal	0.22	0.72 (0.50 - 1.04)	0.08
Left medial orbitofrontal	0.21	0.75 (0.57 - 0.98)	0.03
Left pars opercularis	0.20	1.53 (1.10 - 2.12)	0.01
Right pars orbitalis	0.27	1.30 (0.98 - 1.73)	0.07
Left superior frontal	0.20	1.57 (1.00 - 2.45)	0.05
Right isthmus of the cingulate	0.26	1.30 (0.99 - 1.70)	0.06
Left middle temporal	0.24	0.56 (0.37 - 0.86)	0.008
Left inferior temporal	0.24	0.56 (0.37 - 0.84)	0.006
Left temporal pole	0.42	1.31 (0.98 - 1.76)	0.07
Right banks STS	0.23	0.74 (0.54 - 1.00)	0.05
Right entorhinal	0.53	0.47 (0.35 - 0.63)	<.0001
Left parahippocampal	0.39	0.68 (0.53 - 0.86)	0.002
Right superior parietal	0.20	2.20 (1.40 - 3.46)	0.0006
Right inferior parietal	0.21	0.68 (0.42 - 1.11)	0.12
Right fusiform	0.22	1.30 (0.93 - 1.82)	0.13
Right precuneus	0.18	0.51 (0.34 - 0.76)	0.001
Left lateral occipital	0.16	1.32 (0.95 - 1.83)	0.10
Left insula	0.22	1.29 (0.96 - 1.75)	0.09
c= 0.830			

Table 3.6a Results from ANOVA and Tukey's post-hoc analysis for differences in cortical thickness in the left hemisphere before and after GWIR correction in normal aging, MCI, and AD subject groups. The change in effect size after correctio is reflected in the F-ratio, whereby a value greater than 1 indicates an increased effect size. Degrees of freedom for each ANOVA is 2. For Tukey's columns, the letters represent the groupings for normal aging, MCI, and AD, respectively.

	Cortical Thickness				GWIR Corrected Cortical Thickness				
Cortical region	**r-square**	**F**	**P**	**Tukey**	**r-square**	**F**	**P**	**Tukey**	**F-ratio**
Left hemisphere									
Frontal pole	0.03	5.25	0.006	a,ab,b	0.03	5.34	0.005	a,ab,b	1.03
Rostral middle frontal	0.11	25.2	<.0001	a,b,c	0.11	25.14	<.0001	a,b,c	0.99
Caudal middle frontal	0.08	16.8	<.0001	a,b,c	0.08	16.75	<.0001	a,b,c	0.99
Lateral orbitofrontal	0.06	12.4	<.0001	a,a,b	0.06	12.48	<.0001	a,a,b	1.02
Medial orbitofrontal	0.08	16.9	<.0001	a,b,c	0.08	16.86	<.0001	a,b,c	0.99
Pars opercularis	0.03	6.28	0.002	a,ab,b	0.03	6.30	0.002	a,ab,b	1.01
Pars orbitalis	0.03	5.96	0.003	a,ab,b	0.03	6.10	0.003	a,ab,b	1.05
Pars triangularis	0.06	12.3	<.0001	a,b,b	0.06	12.20	<.0001	a,b,b	0.98
Superior frontal	0.06	13.8	<.0001	a,b,c	0.06	13.75	<.0001	a,b,c	0.96
Precentral	0.03	6.75	0.001	a,ab,b	0.03	6.49	0.0017	a,ab,b	0.92
Postcentral	0.05	9.7	<.0001	a,a,b	0.04	9.17	0.0001	a,a,b	0.08
Paracentral	0.01	1.77	0.17	a,a,a	0.01	1.74	0.18	a,a,a	0.97
Rostral anterior cingulate	0.03	6.24	0.002	a,ab,b	0.03	6.02	0.003	a,ab,b	0.93
Caudal anterior cingulate	0.004	0.8	0.45	a,a,a	0.004	0.79	0.45	a,a,a	0.98
Isthmus of the cingulate	0.09	18.7	<.0001	a,ab,b	0.09	19.06	<.0001	a,a,b	1.04
Posterior cingulate	0.04	7.28	0.0008	a,ab,b	0.04	7.27	0.0008	a,ab,b	1.59
Superior temporal	0.11	24.6	<.0001	a,b,c	0.11	24.66	<.0001	a,b,c	1.00
Middle temporal	0.18	42.4	<.0001	a,b,c	0.18	42.43	<.0001	a,b,c	1.00
Inferior temporal	0.18	44.7	<.0001	a,b,c	0.18	44.61	<.0001	a,b,c	1.00
Temporal pole	0.06	11.8	<.0001	a,b,c	0.06	12.70	<.0001	a,b,c	1.16
Transverse temporal	0.02	4.75	0.009	a,ab,b	0.02	4.80	0.009	a,ab,b	1.02
Banks sts	0.11	24.1	<.0001	a,b,c	0.11	23.84	<.0001	a,b,c	0.98
Entorhinal	0.14	33	<.0001	a,b,c	0.14	33.46	<.0001	a,b,c	1.03
Parahippocampus	0.08	17.2	<.0001	a,b,c	0.08	17.03	<.0001	a,b,c	0.98
Superior parietal	0.03	6.57	0.002	a,ab,b	0.03	6.43	0.002	a,ab,b	1.00
Inferior parietal	0.10	21.3	<.0001	a,b,c	0.10	21.37	<.0001	a,b,c	1.01
Supramarginal	0.09	19.5	<.0001	a,b,c	0.09	19.51	<.0001	a,b,c	1.00
Fusiform	0.13	29.8	<.0001	a,b,c	0.13	29.79	<.0001	a,b,c	1.00
Precuneus	0.07	15.4	<.0001	a,b,c	0.07	15.29	<.0001	a,b,c	0.99
Cuneus	0.004	0.71	0.49	a,a,a	0.003	0.54	0.58	a,a,a	0.58
Pericalcarine	0.01	2.91	0.06	a,ab,b	0.01	2.72	0.07	a,ab,b	6.24
Lateral occipital	0.04	7.74	0.0005	a,a,b	0.04	7.43	0.0007	a,a,b	0.92
Lingual	0.05	10.5	<.0001	a,a,b	0.05	10.12	<.0001	a,a,b	0.94
Insula	0.05	9.77	<.0001	a,a,b	0.05	9.58	<.0001	a,a,b	0.96

Table 3.6b Results from ANOVA and Tukey's post-hoc analysis for differences in cortical thickness in the right hemisphere before and after GWIR correction in normal aging, MCI, and AD subject groups. The change in effect size after correctio is reflected in the F-ratio, whereby a value greater than 1 indicates an increased effect size. Degrees of freedom for each ANOVA is 2. For Tukey's columns, the letters represent the groupings for normal aging, MCI, and AD, respectively.

Right hemisphere									
Frontal pole	0.04	7.26	0.0008	a,b,b	0.03	7.15	0.0009	a,b,b	0.97
Rostral middle frontal	0.10	21.3	<.0001	a,b,c	0.10	21.50	<.0001	a,b,c	1.02
Caudal middle frontal	0.07	15.8	<.0001	a,b,c	0.08	16.20	<.0001	a,b,c	1.06
Lateral orbitofrontal	0.06	11.6	<.0001	a,a,b	0.06	12.06	<.0001	a,a,b	1.07
Medial orbitofrontal	0.06	13	<.0001	a,b,c	0.06	13.04	<.0001	a,b,c	1.00
Pars opercularis	0.05	10.7	<.0001	a,a,b	0.05	10.84	<.0001	a,a,b	1.02
Pars orbitalis	0.04	7.51	0.0006	a,ab,b	0.04	7.50	0.0006	a,ab,b	1.00
Pars triangularis	0.04	9.38	0.0001	a,b,b	0.05	9.57	<.0001	a,b,b	1.04
Superior frontal	0.08	18.3	<.0001	a,b,c	0.09	18.87	<.0001	a,b,c	1.06
Precentral	0.02	4.21	0.02	a,ab,b	0.02	4.26	0.01	a,ab,b	1.02
Postcentral	0.02	5.01	0.007	a,ab,b	0.02	4.97	0.007	a,ab,b	0.08
Paracentral	0.02	4.42	0.01	a,ab,b	0.02	4.39	0.01	a,ab,b	0.99
Rostral anterior cingulate	0.01	2.39	0.09	a,ab,b	0.01	2.37	0.10	a,ab,b	0.98
Caudal anterior cingulate	0.01	1.21	0.30	a,a,a	0.01	1.22	0.30	a,a,a	1.02
Isthmus of the cingulate	0.06	12.5	<.0001	a,a,b	0.06	12.68	<.0001	a,a,b	1.04
Posterior cingulate	0.04	9.04	0.0001	a,b,c	0.04	9.22	0.0001	a,a,b	0.30
Superior temporal	0.09	20.2	<.0001	a,b,c	0.09	20.55	<.0001	a,b,c	1.03
Middle temporal	0.15	36	<.0001	a,b,c	0.16	36.54	<.0001	a,b,c	1.03
Inferior temporal	0.13	28.9	<.0001	a,b,c	0.13	29.40	<.0001	a,b,c	1.03
Temporal pole	0.08	18.3	<.0001	a,a,b	0.08	17.81	<.0001	a,a,b	0.95
Transverse temporal	0.003	0.51	0.60	a,a,a	0.003	0.52	0.59	a,a,a	1.04
Banks sts	0.13	29	<.0001	a,b,c	0.13	28.97	<.0001	a,b,c	1.00
Entorhinal	0.19	46.8	<.0001	a,b,c	0.19	46.38	<.0001	a,b,c	0.98
Parahippocampus	0.09	19.5	<.0001	a,b,c	0.09	19.19	<.0001	a,b,c	0.97
Superior parietal	0.02	4.48	0.01	a,ab,b	0.02	4.61	0.01	a,ab,b	1.06
Inferior parietal	0.11	24	<.0001	a,b,c	0.11	23.85	<.0001	a,b,c	0.99
Supramarginal	0.08	16.9	<.0001	a,b,c	0.08	17.09	<.0001	a,b,c	1.03
Fusiform	0.10	21.6	<.0001	a,b,c	0.10	22.37	<.0001	a,b,c	1.07
Precuneus	0.09	18.8	<.0001	a,b,c	0.09	19.02	<.0001	a,b,c	1.02
Cuneus	0.01	2.26	0.11	a,a,a	0.01	2.40	0.09	a,a,a	1.13
Pericalcarine	0.01	1.41	0.24	a,a,a	0.01	1.39	0.25	a,a,a	42.76
Lateral occipital	0.05	9.62	<.0001	a,a,b	0.05	9.39	0.0001	a,a,b	0.95
Lingual	0.04	7.94	0.0004	a,a,b	0.04	7.85	0.0005	a,a,b	0.98
Insula	0.05	10.9	<.0001	a,a,b	0.05	11.49	<.0001	a,a,b	1.12

References

Dale A.M., Fischl B. & Sereno M.I., 1999. Cortical Surface-Based Analysis I. Segmentation and Surface Reconstruction. *NeuroImage*, 9(2), pp.179–194.

DeLong, E.R., DeLong, D.M. & Clarke-Pearson, D.L., 1988. Comparing the Areas under Two or More Correlated Receiver Operating Characteristic Curves: A Nonparametric Approach. *Biometrics*, 44(3), pp.837–845.

Desikan, R.S. et al., 2006. An automated labeling system for subdividing the human cerebral cortex on MRI scans into gyral based regions of interest. *NeuroImage*, 31(3), pp.968–980.

Fischl, B., Sereno, M.I. & Dale, A. M., 1999. Cortical surface-based analysis - II: Inflation, flattening, and a surface-based coordinate system. Available at: http://discovery.ucl.ac.uk/145122/ [Accessed September 21, 2011].

Fischl, Bruce, Van der Kouwe, André, et al., 2004. Automatically Parcellating the Human Cerebral Cortex. *Cerebral Cortex*, 14(1), pp.11 –22.

Fischl, Bruce, Salat, David H, et al., 2004. Sequence-independent segmentation of magnetic resonance images. *NeuroImage*, 23 Suppl 1, pp.S69–84.

Fischl, Bruce et al., 2002. Whole Brain Segmentation. *Neuron*, 33(3), pp.341–355.

Fischl, Bruce & Dale, Anders M., 2000. Measuring the thickness of the human cerebral cortex from magnetic resonance images. *Proceedings of the National Academy of Sciences*, 97(20), pp.11050 –11055.

Gómez-Isla, T. et al., 1997. Neuronal loss correlates with but exceeds neurofibrillary tangles in Alzheimer's disease. *Annals of Neurology*, 41(1), pp.17–24.

Grignon, Y. et al., 1998. Cytoarchitectonic alterations in the supramarginal gyrus of late onset Alzheimer's disease. *Acta Neuropathologica*, 95(4), pp.395–406.

Grydeland, H. et al., 2012. Improved prediction of Alzheimer's disease with longitudinal white matter/gray matter contrast changes. *Human brain mapping*. Available at: http://www.ncbi.nlm.nih.gov/pubmed/22674625 [Accessed August 2, 2012].

Jack Jr., C.R. et al., 2008. The Alzheimer's disease neuroimaging initiative (ADNI): MRI methods. *Journal of Magnetic Resonance Imaging*, 27(4), pp.685–691.

Salat, D H et al., 2009. Age-associated alterations in cortical gray and white matter signal intensity and gray to white matter contrast. *NeuroImage*, 48(1), pp.21–28.

Salat, D.H. et al., 2011. Hippocampal degeneration is associated with temporal and limbic gray matter/white matter tissue contrast in Alzheimer's disease. *NeuroImage*, 54(3), pp.1795–1802.

Westlye, L.T. et al., 2009. Increased sensitivity to effects of normal aging and Alzheimer's disease on cortical thickness by adjustment for local variability in gray/white contrast: a multi-sample MRI study. *NeuroImage*, 47(4), pp.1545–1557.

Chapter 4 - Multimodal discrimination between normal aging, mild cognitive impairment, and Alzheimer's disease

INTRODUCTION

Alzheimer's disease (AD) is the most common form of dementia in our society today. It is a disorder that is found across the world and is currently affecting approximately 5.4 million Americans. Since age is the best known risk factor for AD, the incidence rate of AD is expected to nearly double within the next few decades as the American population ages (Anon 2012). The rate of development of AD is heightened in individuals with the amnestic form of mild cognitive impairment (MCI). Amnestic MCI is characterized by cognitive deficits primarily affecting memory, preserved overall cognitive and functional abilities, and the absence of a dementia (R. C. Petersen 2001). Individuals with MCI convert to AD at a rate of about 10 to 15% per year in comparison to approximately 1% per year in normal aging (R. C. Petersen 2001), making it imperative to generate effective methods for identifying individuals with MCI. This can be a challenge because the clinical presentation of MCI is heterogeneous, making it difficult to determine at what stage in the normal aging, MCI, AD spectrum an individual may be in. There are a number of factors that have been discussed as contributing to the differential diagnosis, including performance on neuropsychological tests, brain morphometric measurements, brain glucose uptake, and concentrations of biomarkers in cerebrospinal fluid (CSF).

Pathologically, AD and, to a lesser extent, MCI are characterized by the presence of intracellular neurofibrillary tangles (NFTs) and extracellular amyloid plaques. The NFTs are composed of insoluble hyperphosphorylated tau protein.

Normal tau protein, the non-hyperphosphorylated type, is involved in microtubule stabilization of the axonal cytoskeleton (Trojanowski et al. 1993). In the presence of NFTs, however, the integrity of the cytoskeleton is impaired, such that neurons are dysfunctional and there is synaptic and neuronal loss (Gómez-Isla et al. 1997; Mosconi 2005). In AD and MCI, NFTs accumulate in the locus coeruleus (Heiko Braak & Del Tredici 2011a; Heiko Braak & Del Tredici 2011b) hippocampus, entorhinal cortex, amygdala, and other limbic areas that are important for memory. As the disease progresses, the NFTs affect more neocortical areas, resulting in a deficit in other cognitive domains (H Braak & E. Braak 1991; H Braak & E. Braak 1995; Heiko Braak & Del Tredici 2011a; St George-Hyslop 2000). While NFTs have a predilection for medial temporal lobe and limbic structures, amyloid plaques tend to accumulate more in the association cortices and, as the disease progresses, affect more hippocampal structures (H Braak & E. Braak 1991; D. R. Thal et al. 2002). The extent of amyloid distribution is related to the severity of impairment on cognition (Hulette et al. 1998). Amyloid plaques are extracellular, are composed of insoluble fibrils of amyloid-beta (Aβ), and may be related to the hypometabolism that is observed using FDG PET (Mosconi 2005). The underlying pathology is nearly impossible to monitor *in vivo*, however, using imaging techniques, CSF sampling, and neuropsychological testing as biomarkers of the disease, it is possible to monitor disease progression. What remains unclear is which individual or combination of biomarkers provides the best differentiation between normal aging, MCI, and

AD? CSF levels of ABeta 1-42 (Aβ-42), total tau, and phosphorylated tau, structural brain changes as measured with MRI morphometry, and functional brain changes as measured with FDG PET have all been shown to be of some value.

There is evidence that there is free exchange of molecules between the brain and the CSF (Reiber & Peter 2001), which is the basis for the use for molecular analysis of CSF samples for biomarker of MCI and AD. In particular there are three major compounds that have been identified as being present in the CSF of AD patients, namely total tau (tTau), hyperphosphorylated tau (pTau), and Aβ-42 (Zetterberg et al. 2003). It has been reported that these markers are able to identify AD in its early stages with fairly high accuracy (Hansson et al. 2006) as increased levels of pTau and tTau have been observed in AD compared to normal aging (K Blennow et al. 1995; M. Ewers et al. 2007). CSF samples from both MCI and AD subjects shows decreased concentrations of Aβ-42 (M. Ewers et al. 2007), which may reflect an increased deposition of Aβ in aggregated plaques in the brain (Cedazo-Minguez & Winblad 2010).

One of the consequences of AD pathology is a disruption of synaptic function that may be indirectly measured via changes in glucose metabolism. FDG PET, a glucose analogue, is typically used as a marker of synaptic function, as metabolic changes are closely tied to glucose consumption. There is a relatively consistent pattern of decreased metabolism that occurs in AD. The regions that tend to show hypometabolism are the posterior

cingulate/retrosplenial cortex and the cortical structures in the parieto-temporal junction, such as the angular gyrus and precuneus. Some studies also indicate a decrease in hippocampal and entorhinal metabolism, although this is not consistently observed. There is not a consistent pattern for MCI (Mosconi et al. 2008).

As previously mentioned, one of the consequences of AD pathology is neuronal loss. This loss is visible *in vivo* through indirect methods, such as MRI. MRI enables researchers to examine the various ways in which atrophy can present itself, namely through changes in cortical surface area, thickness, or volume, of the cortical structures. Cortical thickness has been shown to be a particularly useful metric for tracking disease progression. Volumetric and cortical thickness changes have been observed consistently in MCI and AD, with the earliest detecTable 4.changes occurring in the entorhinal cortex hippocampus, spreading outward to other cortical and subcortical structures (Michael Ewers et al. 2011; R J Killiany et al. 2002; P. M. Thompson et al. 2003).

Ultimately the accumulation of NFTS and Aβ, and the resultant changes in synaptic function and neuronal loss, manifests as cognitive deficits that are quantified through the use of neuropsychological tests. Each test in a typical battery is meant to measure performance on different types of cognitive skills (e.g. executive function, visuospatial abilities, etc.) or forms of memory (e.g. long-term memory, recall, recognition). Neuropsychological measures, especially

those of memory function tend to readily identify individuals with AD but have more variability to them than the other measures discussed.

Each of the four modalities we discussed above has been implicated to be useful for discriminating normal aging, MCI, and AD. Since each of the modalities is to an extent independent of the other, it is conceivable that a combination of them would provide better discrimination than any individual method on its own. In the current study we explored this concept using a data-driven approach. Because each of these factors can provide independent information that can influence diagnosis as a whole, we also examined if we can increase the ability to differentiate groups by combining modalities.

Thus, the main aims were: 1) to determine the independent value of MRI, FDG PET, CSF sampling, and neuropsychological test scores in differentiating between normal aging, MCI, and AD groups, and 2) to determine the best combination of modalities to differentiate between normal aging, MCI and AD groups.

MATERIALS AND METHODS

Subjects

The data for use in this study were chosen from the larger pool of data that has been made publically available by the Alzheimer's Disease Neuroimaging Initiative. Data was screened to include all subjects who had both PET and MRI scans available for use on the ADNI/LONI website

(www.loni.ucla.edu/ADNI) at the time this study began. From this screened dataset, PET data from 21 subjects was of poor contrast and quality and had to be omitted from the analyses undertaken in this study. Three subjects were omitted due to missing information. This left us with data from 403 subjects. We present demographic information on this sample in Table 4.1.

As part of the ADNI, all subjects completed a battery of neuropsychological tests, On the basis of their cognitive status the subjects were classified by the ADNI clinical core as: (a) normal controls with normal cognition and memory, Clinical Dementia Rating (CDR) 0, and Mini Mental Status Exam (MMSE) between 24-30; (b) amnestic MCI with memory complaint verified by a study partner, memory loss measured by education-adjusted performance on the Logical Memory II subscale of the Wechsler Memory Scale-Revised (Wechsler 1987), preserved activities of daily living, CDR 0.5, MMSE between 24 and 30, and absence of dementia at time of baseline MRI scan; or (c) probable AD with memory complaint validated by an informant, abnormal memory function for age and education level, absence of depression, impaired activities of daily living, diminished cognition, CDR > 0.5, and MMSE between 20 - 26.

Alzheimer's Disease Neuroimaging Initiative

The ADNI was a 5-year non-randomized natural history non-treatment study utilizing data from multiple study centers across the United States and Canada. One of the main goals of the ADNI was to develop optimized methods and uniform standards for the acquisition of multicenter MRI and PET data on

normal control subjects and patients with MCI and AD in drug/treatment trials. For more information about the ADNI please refer to http://www.adni-info.org.

CSF Sampling

Detailed CSF collection and processing methods can be found in elsewhere (Shaw et al. 2011). Briefly, CSF samples obtained by lumbar puncture were examined for tTau. pTau, and Aβ-42 using an immunoassay method. These measures were performed by the ADNI Biomarker Core at the University of Pennsylvania School of Medicine.

Neuropsychological testing

For this study we analyzed the cognitive scores from the cognitive and neuropsychological tests taken at the first visit. CDR memory, CDR problem solving and judgment, Trails A, Trails B, Clock draw, Clock copy, digit span forward and backward, and the Rey's Auditory verbal 30 minute delay recognition, 30 minute recognition errors, and 30 minute recall were examined for their ability to differentiate between subject groups in this study.

MRI scans

For this study, we analyzed the T1-weighted MPRAGE baseline MRI scans from those acquired by the ADNI on 1.5T scanners from General Electric (GE), Philips Medical Systems (Philips), and Siemens Medical Solutions (Siemens). Specific pulse sequence guidelines can be found at http://www.loni.ucla.edu/ADNI/Research/Cores/index.shtml.

FDG-PET scans

For this study, we analyzed baseline FDG-PET scans from those acquired by the ADNI on GE, Philips, or Siemens scanners. Specific protocols for each scanner are available from the ADNI website (http://adni.loni.ucla.edu/research/protocols/pet-protocols/). These data were corrected for radiation attenuation and scatter using scanner-specific algorithms and each image was visually assessed for potential artifacts by the ADNI PET core at the University of Michigan. For this study we used the original PET data that was not pre-processed by the ADNI PET core so that we could have local control of all the processing steps as with the MRI scans.

Freesurfer Analysis

All MRI and FDG PET scans were processed with the Freesurfer 5.1.0 (Dale A.M. et al. 1999; B. Fischl et al. 1999), which is documented and freely available. The processing pipeline has been described in detail elsewhere (Dale A.M. et al. 1999; B. Fischl et al. 1999; Bruce Fischl et al. 2002; Bruce Fischl, André van der Kouwe, et al. 2004; Bruce Fischl, David H Salat, et al. 2004; Bruce Fischl & Anders M. Dale 2000). Briefly, for each subject, the 2 DICOM T1-weighted MRI datasets were motion corrected, averaged, segmented into gray matter, white matter, and cerebral spinal fluid (CSF), and intensity normalized. Cortical thickness measures were corrected for gray/white matter intensity ratio using residuals, as it was previously determined to increase the predictive ability of cortical thickness in our sample (Chapter 3). The gray/white matter intensity

ratio was calculated as previously described, but will be briefly outlined here (D H Salat et al. 2009; D.H. Salat et al. 2011). Gray matter tissue intensities were measured 35% through the thickness of the cortical ribbon. White matter tissue intensities were measured 1mm below the gray/white matter boundary, into the white matter. The GWIR was calculated by dividing the white matter by the gray matter intensity values. The ratios were then projected onto the cortical surface and smoothed with a Gaussian kernel with a full width at half maximum of 30mm. The cortex was parcellated into regions of interest (ROIs) based on gyral and sulcal structure using the Desikan/Killiany atlas(Desikan et al. 2006). In this study, the isthmus of the cingulate is the portion of the cingulate posterior to the marginal ramus. Many studies refer to this region as the posterior cingulate. For consistency we will refer to this region as the isthmus throughout and specify posterior cingulate when the hypometabolism extended anterior to the marginal ramus.

PET Processing

Once the T1-weighted MRI images were processed, the PET images were affine spatial transformed into "anatomical space" 1x1x1, 256x256x256, which was the same resolution as the transformed MRI images. The PET and MRI images were then co-registered using an automated Freesurfer boundary based application using 6 degrees of freedom (Douglas N Greve & Bruce Fischl 2009), such that no skewing or twisting of the data occurred (Figure 4.1). The resulting coregistration was visually assessed for accuracy and adjusted if necessary

(approximately 25% of the datasets). After the two datasets were co-registered, FDG uptake was measured in specific ROIs according to the cerebral cortex parcellations generated on the representative MRI images (Desikan et al. 2006). A total of 82 cortical and subcortical areas were examined for changes in MRI morphometry and FDG uptake related to MCI and AD relative to normal aging (Figures 2 and 3).

To control for individual global variations and to increase sensitivity of the method for differentiating between subject groups (Yakushev et al. 2008), the FDG uptake was normalized to regional activity in the cerebellum using residuals. The choice of reference region was based on the results from a previous study in which we tested which region was best suited for as a reference region for normalization in our subjects. Partial volume effects were also corrected for using an adapted gray matter mask (Daisuke Yanase et al. 2005).

Statistical Analysis

In order to assess the equality of the male-female distribution in the three diagnostic groups, χ^2 tests were performed. ANOVA was used in order to assess the age, education, and MMSE distributions in the three diagnostic groups. Hemisphere differences for both MRI and PET data were examined with paired t-tests and correlation analysis. If the t-tests showed no significant differences the two hemispheres they were averaged together. Age was correlated with each of

the morphometric and uptake variables, including cortical surface area, volume, cortical thickness, gray/white matter intensity ratio, and FDG uptake.

Logistic regression Analyses

In order to determine which ROIs and neuropsychological tests should be entered into the models for diagnostic group, we first performed step-wise logistic regression on each variable individually with entry and exit criteria of 0.20. If the odds ratio was below 0.75 or above 1.25 it was determined to be an adequate predictor on its own and was entered as a variable in the model for that modality. For each modality (e.g. cortical thickness, volume, cortical surface area, FDG uptake, CSF profile, and neuropsychological tests), all the variables that met criterion were placed into a second step-wise logistic regression with entry and exit criteria of 0.20 and diagnostic group as the dependent variable. Age, gender, and education were forced into the model, thus any variance that they contributed to diagnostic group was controlled for. To generate multi-modal models, the variables from modality specific model with the highest c-score were entered into another step-wise logistic regression using the same parameters as before. To examine the added effects of CSF biomarker concentrations on the multimodal model, we forced all the variables from the multimodal model into the CSF-multimodal model. In this way we could ensure that the variables contributing variance in the first multimodal model were repeated in the CSF-multimodal model in order to limit the changes in c-statistic to just the CSF

biomarker concentrations. In instances where a ROI was represented by more than one modality in the model (e.g. cortical thickness and FDG uptake), the modality accounting for the most variance in the model was included and the other was excluded. The same process was used to control for models in which both hemispheres were represented from the same modality. Pearson's correlation was used to assess collinearity amongst the predictor variables of the multimodal models.

RESULTS

Chi-square tests revealed no significant differences for distribution of males and females between groups ($df = 2$, $p = 0.3517$). Age was not significantly different between control, MCI, and AD groups, as indicated by ANOVA ($p = 0.6684$). The AD group had on average a year less education than normal and MCI groups, which, although small, was significant ($p < 0.05$). As expected, the MMSE scored also showed significant decreases in both the MCI and AD subject groups ($p < 0.05$).

Left/Right Hemisphere differences:

Volume, cortical thickness, and cortical surface area were significantly different between left and right hemispheres in the vast majority of regions (data not shown). There were also significant correlations between the hemispheres in all regions for volume, cortical thickness, and cortical surface area ($p < 0.05$). Although we observed significant correlations, we also observed widespread

significant hemisphere differences and decided to keep the hemispheres separate for all MRI measures. FDG PET showed no significant differences between hemispheres, so the data from the two hemispheres were averaged.

Models for predicting diagnostic group

MRI

Separate volume, cortical thickness, and cortical surface area models were generated and the variables contributing unique variance from each of these models were entered into a separate stepwise logistic regression model to generate a total MRI model.

AD vs. MCI

The MRI variables which contributed significant amounts of variance ($p < 0.05$) to the model discriminating AD from MCI included volume of the left hippocampus; cortical surface area of the left postcentral gyrus and right middle temporal; and cortical thickness of the left isthmus of the cingulate, left insula, left inferior temporal, right entorhinal, and of the right banks of the superior temporal sulcus. In addition, education was a significant predictor ($p = 0.0005$). Overall, the MRI model for AD vs. MCI generated a c-statistic of 0.861 (Hosmer-Lemeshow goodness of fit Chi-square = 4.86, $p = 0.77$, Cox and Snell generalized $R^2 = 0.33$, Nagelkerke $R^2 = 0.46$) (Table 4.2).

MCI vs. normal aging

The MRI variables which contributed significant amounts of variance ($p < 0.05$) to the model discriminating MCI from normal aging included volume of the left entorhinal, right hippocampus, right caudal anterior cingulate, and left caudal middle frontal; cortical surface area of the right inferior temporal and right paracentral gyri; and cortical thickness of the left middle temporal, left rostral middle frontal, right banks of the superior temporal sulcus, right inferior parietal, and left superior frontal regions. In addition, age ($p < 0.0001$) and gender ($p = 0.029$) were significant predictors. The MCI vs. normal aging model gave a c-statistic of 0.870 (Hosmer-Lemeshow goodness of fit Chi-square = 7.54, $p = 0.48$, Cox and Snell generalized $R^2 = 0.36$, Nagelkerke $R^2 = 0.50$) (Table 4.3).

AD vs. normal aging

The MRI variables that contributed significant amounts of variance ($p < 0.05$) to the model discriminating AD from normal aging included volume of the left entorhinal, left hippocampus, right caudal anterior cingulate, left rostral anterior cingulate, and right banks of the superior temporal sulcus; cortical surface area of the left caudal middle frontal and left inferior temporal; and cortical thickness of the right cuneus, left middle temporal, and left lateral occipital regions. In addition, age ($p - 0.0027$) and education ($p = 0.0023$) were significant predictors. Overall, the MRI model for normal control vs. AD gave a c-statistic of 0.986 (Hosmer-Lemeshow goodness of fit Chi-square = 0.68, $p = 1.0$, Cox and Snell generalized $R^2 = 0.70$, Nagelkerke $R^2 = 0.94$) (Table 4.4).

All three groups

The MRI variables which contributed significant amounts of variance ($p < 0.05$) to the model discriminating all three groups included volume of the left hippocampus and left caudal middle frontal; cortical surface area of the right fusiform; and cortical thickness of the right entorhinal, right superior parietal, left inferior temporal, left middle temporal, left temporal pole, right banks of the superior temporal sulcus, right rostral middle frontal, left medial orbitofrontal, left pars opercularis, left lateral occipital, and right precuneus regions. In addition, age ($p < 0.0001$), gender ($p = 0.011$), and education ($p = 0.0006$) all contributed significantly to the model. Overall, the MRI model for differentiating all three groups gave a c-statistic of 0.879 (Cox and Snell generalized $R^2 = 0.53$, Nagelkerke $R^2 = 0.60$) (Table 4.5).

FDG PET

AD vs. MCI

FDG metabolism in a number of regions significantly contributed to the model differentiating AD from MCI. These regions, along with education ($p = 0.0006$), were the inferior temporal, postcentral, and putamen. Overall, the FDG PET model provided a c-statistic of 0.726 (Hosmer-Lemeshow goodness of fit Chi-square = 9.47, $p = 0.30$, Cox and Snell generalized $R^2 = 0.15$, Nagelkerke $R^2 = 0.22$) (Table 4.6).

MCI vs. normal aging

FDG metabolism in a number of regions significantly contributed to the model differentiating MCI from normal aging. These regions were the entorhinal, fusiform, inferior temporal, and isthmus of the cingulate. Overall, the model provided a c-statistic of 0.688 (Hosmer-Lemeshow goodness of fit Chi-square = 4.29, p = 0.83, Cox and Snell generalized R^2 = 0.11, Nagelkerke R^2 = 0.15) (Table 4.7).

AD vs. normal aging

FDG metabolism in a number of regions significantly contributed to the model differentiating AD from normal aging. These regions, along with education (p = 0.0087), were the entorhinal, middle temporal, paracentral, postcentral, parahippocampus, and the temporal pole. Overall, the model provided a c-statistic of 0.879 (Hosmer-Lemeshow goodness of fit Chi-square = 3.89, p = 0.87, Cox and Snell generalized R^2 = 0.41, Nagelkerke R^2 = 0.55) (Table 4.8).

All three groups

FDG metabolism in a number of regions significantly contributed to the model differentiating all three groups. These regions, along with education (p = 0.0004), were the entorhinal, inferior parietal, isthmus of the cingulate, and the postcentral gyrus. The model provided a c-statistic of 0.735 (Cox and Snell generalized R^2 = 0.22, Nagelkerke R^2 = 0.25), respectively (Table 4.9).

Neuropsychological tests

AD vs. MCI

The neuropsychological tests which contributed significant variance to the model differentiating AD from MCI were the digit span backwards, trails A, and the RAVLT 30 minute delay and delay errors. Education was also significant. Overall, the neuropsychological test model for AD vs. MCI gave a c-statistic of 0.876 (Hosmer-Lemeshow goodness of fit Chi-square = 10.55, p = 0.23, Cox and Snell generalized R^2 = 0.44, Nagelkerke R^2 = 0.62) (Table 4.10).

MCI vs. normal aging

The neuropsychological tests which contributed significant variance to the model differentiating MCI from normal aging were the clock score, digit span backwards, trails B, and the RAVLT 30 minute delay and delay errors. Age was also significant. The model provided a c-statistic of 0.841 (Hosmer-Lemeshow goodness of fit Chi-square = 8.79, p = 0.36, Cox and Snell generalized R^2 = 0.29, Nagelkerke R^2 = 0.41) (Table 4.11).

AD vs. normal aging

The neuropsychological tests which contributed significant variance to the model differentiating AD from normal aging were the clock score, digit span forward, and the RAVLT 30 minute delay and delay errors. The model provided a

c-statistic of 0.9692 (Hosmer-Lemeshow goodness of fit Chi-square = 10.50, p = 0.23, Cox and Snell generalized R^2 = 0.69, Nagelkerke R^2 = 0.92) (Table 4.12).

All three groups

The neuropsychological tests which contributed significant variance to the model differentiating all three groups were the clock score, digit span backward, trails A and B, and the RAVLY 30 minute delay and delay errors. This model provided a c-statistic of 0.878 (Cox and Snell generalized R^2 = 0.63, Nagelkerke R^2 = 0.73) (Table 4.13).

CSF measures

AD vs. MCI

In the CSF model for differentiating AD from MCI, education was the only significant predictor (p = 0.01). There were trends for both Aβ-1-42 and pTau (p = 0.069 and 0.063, respectively). The c-statistic for this model was 0.685 and accounted for 11% of the variance, according to Nagelkerke R^2 (Hosmer-Lemeshow goodness of fit Chi-square = 6.55, p = 0.59, Cox and Snell generalized R^2 = 0.08, Nagelkerke R^2 = 0.11) (Table 4.14).

AD vs. normal

The CSF model for differentiating AD from normal aging included Aβ-1-42 and tTau along with age, gender, and education. Both of the CSF measures of pathology were significant (p < 0.0001 and p = 0.0004, respectively), along with education (p < 0.05). The overall model was able to discriminate well between

the groups with a c-statistic of 0.904. This accounted for approximately 60% of the variance, with a Nagelkerke R-square of 0.604 (Hosmer-Lemeshow goodness of fit Chi-square = 8.55, p = 0.38, Cox and Snell generalized R^2 = 0.45) (Table 4.15).

MCI vs. normal

The CSF model for differentiating MCI from normal aging included Aβ-1-42 and tTau, both of which were significant predictors (p = 0.0005 and 0.0025, respectively). The model had a c-statistic of 0.775 (Hosmer-Lemeshow goodness of fit Chi-square = 0.775, p = 0.51, Cox and Snell generalized R^2 = 0.20, Nagelkerke $R^{2 = 0.28}$). Neither age, gender, nor education were significant predictors (Table 4.16).

All three groups

For differentiating all three groups with CSF measures of pathology, Aβ-1-42 and tTau were both significant predictors, along with education (p = <0.0001, 0.0011, and 0.03, respectively). Neither age nor gender were significant. Overall the model had a c-statistic of 0.753 and accounted for approximately 28% of the variance (Cox and Snell generalized R^2 = 0.24, Nagelkerke R^2 = 0.28) (Table 4.17).

Multi-modal

Once a final model for each modality was completed, they were combined into a multi-modal model with the main goal of obtaining a model that better

discriminated between groups. Because fewer subjects had a CSF sample, and because lumbar puncture is a fairly invasive procedure, we first examined the imaging and cognitive test modalities together without CSF measures and then we made new multimodal models with added CSF to see if this improved the discriminability.

AD vs. MCI

When differentiating between AD and MCI the c-statistic was 0.918 (Hosmer-Lemeshow goodness of fit Chi-square = 10.55, p = 0.23, Cox and Snell generalized R^2 = 0.44, Nagelkerke R^2 = 0.62) in the final multi-modal model, which included neuropsychological tests and MRI. FDG PET variables did not contribute any additional variance to the model (Table 4.18). The model after the addition of both Aβ-1-42 and pTau had a c-statistic of 0.943 (Hosmer-Lemeshow goodness of fit Chi-square = 8.85, p = 0.36, Cox and Snell generalized R^2 = 0.51, Nagelkerke R^2 = 0.70) (Table 4.19).

MCI vs. normal aging

For differentiating between MCI and normal aging subjects the c-statistic was 0.925 (Hosmer-Lemeshow goodness of fit Chi-square = 6.77, p = 0.56, Cox and Snell generalized R^2 = 0.46, Nagelkerke R^2 = 0.64) using MRI, FDG PET, and neuropsychological test variables (Table 4.20). The second model including CSF variables to the model was better able to discriminate with a c-statistic of 0.972 (Hosmer-Lemeshow goodness of fit Chi-square = 3.20, p = 0.92, Cox and

Snell generalized R^2 = 0.59, Nagelkerke R^2 = 0.81). Of the CSF variables, both total tau and Aβ-1-42 were added (Table 4.21).

AD vs. normal aging

When differentiating between AD and normal aging the c-statistic was 0.939 (Hosmer-Lemeshow goodness of fit Chi-square = 0.66, p = 0.72, Cox and Snell generalized R^2 = 0.74, Nagelkerke R^2 = 0.99) in the final multi-modal model, which included only neuropsychological tests and MRI. FDG PET again did not contribute any additional variance to the model. The difficulty here is that when gender is forced into the model, it becomes unreliable, with a number of extreme odds ratios for the predictor variables, although the c-statistic here was 1.00. In order to address this issue, each variable was examined with respect to the other variables and, it was determined that not forcing gender into the model resolved the reliability issue. Thus, the final model for differentiating normal aging vs. AD does not include gender. Age and education along with left hippocampal volume and AVLT 30 minute delay scores composed the model, which had an overall c-statistic of 0.996 (Hosmer-Lemeshow goodness of fit Chi-square = 0.49, p = 1.0, Cox and Snell generalized R^2 = 0.70, Nagelkerke R^2 = 0.94). All the variables were significant except for education (Table 4.22). With the addition of CSF, the c-statistic increased to 0.998 (Hosmer-Lemeshow goodness of fit Chi-square = 0.33, p = 1.0, Cox and Snell generalized R^2 = 0.33, Nagelkerke R^2 = 0.95). CSF concentrations of aβ-1-42 were in the model, although did not make a significant contribution (p = 0.07) (Table 4.23).

All three groups

When differentiating between all three groups the c-statistic was 0.928 (Cox and Snell generalized R^2 = 0.6334, Nagelkerke R^2 = 0.7248) in the final multi-modal model (Table 4.24). The model for differentiating all three groups included neuropsychological tests, MRI, and FDG PET variables. After the addition of CSF samples to the candidate variables of the model, the c-statistic increased to 0.946 (Cox and Snell generalized R^2 = 0.68, Nagelkerke R^2 = 0.78). The CSF variable included was Aβ-1-42, which was a significant predictor (Table 4.25).

DISCUSSION

In this study we created a set of models that characterize the MRI morphometric, FDG PET, CSF, and neuropsychological test variables that are best able to discriminate between normal aging, MCI, and AD. We addressed two main hypotheses: 1) MRI, FDG PET, CSF, and neuropsychological test scores on their own can distinguish between normal aging, MCI, or AD subject groups, and 2) combining modalities increases the predictability of the model.

MRI, FDG PET, CSF, and neuropsychological testing models for predicting normal aging, MCI, and AD

Each modality on its own was able to distinguish between the groups to some degree; however, MRI provided a better discrimination than FDG PET, CSF biomarker concentraion, or neuropsychological tests. FDG PET and CSF

biomarker concentration providing the least discrimination depending on which groups were being compared. To our knowledge only a limited number of studies have compared these four modalities, there are a number of studies that have examined discrimination between normal aging and MCI or AD in MRI and FDG PET. We will discuss how our results for both individual and multimodal models relate to the literature below.

MRI

Our combined MRI model was the result of a stepwise logistic regression whereby the pool of variables available for the model were those that were independent predictors from three separate models, each examining a different aspect of three-dimensional MRI-derived structures, namely volume, cortical thickness, and cortical surface area. This was necessary as a data-limiting step but has the added benefit of not limiting the model to only one morphometric measurement. In each of our MRI models, there were variables from each type of measurement that contributed independent variance to the model. This indicates that it may be counter productive to limit MCI and AD studies to only cortical thickness, but that volume and cortical surface area may also be important indicators of disease. It has previously been suggested that cortical thickness changes more in AD than cortical surface area when the effects of age are removed (Dickerson, Feczko, et al. 2009). Dickerson et al. (Dickerson, Feczko, et al. 2009) failed to observe an effect of AD on cortical surface area in the perirhinal cortex or the parahippocampal gyrus. Our study, on the other hand

showed that there were a number of regions in which cortical surface area was affected by both MCI and AD even after the effects of age were accounted for, suggesting that this measure may have been unduly overlooked in the past even though it is not able to discriminate between groups as well as cortical thickness. Cortical surface area may be linked to brain volume in that it may represent cortical columns, whereas cortical thickness may represent the number of cells within a column (Courchesne et al. 2000; Rakic 1988), however, the underlying cellular mechanism of cortical surface area is not well understood. It has also been suggested that cortical surface area may be influenced by a variety of factors such as synaptogenesis, dendritic arborization, intracortical myelination, and connectivity (Eyler et al. 2011). Changes in MRI volume are highly correlated with post-mortem measures of tissue volume, which suggests that the volume loss observed in this study likely reflects neuronal loss. Cortical thickness changes are thought to reflect loss of neurons and neuropil. Studies that examine ante-mortem cortical thickness with post-mortem neuron counts show high levels of agreement.

In our MRI models for differentiating normal aging from MCI, volumes of both the right hippocampus and the left entorhinal cortex were significant predictors, while the left hippocampal volume and right entorhinal cortical thickness were significant predictors for AD vs. MCI, suggesting that there is not only hemisphere effects, whereby one hemisphere is affected before the other,

but also that different types of geometry are more effective than others at differentiating different stages of the disease.

Previous studies suggest the entorhinal volume, hippocampus volume (De Santi S. et al. 2001; Kawachi et al. 2006; K B Walhovd, A M Fjell, Brewer, et al. 2010), amygdala (Kawachi et al. 2006), and inferior temporal lobe volume to be predictive of AD (Schmand et al. 2011). Other studies also suggest that retrosplenial thickness is able to predict AD (K B Walhovd, A M Fjell, Brewer, et al. 2010), while other still rely on what is known as the "cortical signature of AD", which is a set of 10 cortical thicknesses that have been shown to change consistently in AD (Dickerson, Bakkour, et al. 2009). One benefit of the current study to previous studies is that we did not examine only a few preselected regions, but rather included the entire cortical and subcortical gray matter. To directly test the benefit of not limiting our data to regions that change most with AD, we created a model that included only the "cortical signature regions", along with age, and education, to see which model differentiated normal aging from AD best. We found that our data-driven approach was better able to differentiate groups, with a significantly larger c-statistic ($c = 0.90$ for signature and $R = 0.98$ for our model, $p = 0.0002$). In addition, regions typically associated with the signature of Alzheimer's disease were not all in the models differentiating disease group, suggesting that although the "Alzheimer's signature" regions may change most in the disease that they are not optimal for differentiating disease states. Thus, this paper indicates additional brain regions that might be targeted

for future studies and perhaps for assisted in clinical diagnosis. Although significant changes were observed throughout the cortex, not all these regions were able to contribute unique and independent variance to the models.

FDG PET

Not surprisingly, FDG PET did not perform as well as MRI or neuropsychological test scores for distinguishing between diagnostic groups. This finding is in agreement with a number of previous studies (Schmand et al. 2011; K B Walhovd et al. 2009; K B Walhovd, A M Fjell, Brewer, et al. 2010) and at odds with others that have found evidence for better prediction with FDG PET than with MRI (De Santi S. et al. 2001; Kawachi et al. 2006; Matsunari et al. 2007). While some of these discrepancies may be accounted for by sample, scanner, and scanning protocol, a portion of the difference may be accounted for by differences in post-processing methods. While here we present data from a data-driven ROI-based approach that re-sampled the PET data into MRI space, many of the other studies use a-priori ROIs or else use a voxel-based approach using relatively large voxels, which may be less sensitive to group changes, particularly in small structures or those that may show more anatomical variability. Another post-processing difference lies in the treatment of partial volume effects and normalization region. We controlled for partial volume effects, which diminished some of the group differences (Chapter 2) and may have contributed to its relatively poor performance compared to MRI morphometric variables. Most of the studies citing an increased ability of FDG PET to detect AD

compared to normal aging do not adjust for partial volume errors that occur in PET imaging in atrophic structures, which likely artificially inflates the ability of FDG PET to predict group (Kawachi et al. 2006; Matsunari et al. 2007; D. Zhang et al. 2011). We also normalized to the cerebellum, rather than the pons or whole brain based on results of one of our previous studies (Chapter 2).

In the individual FDG PET model, a number of regions contributed independent variance to the models. Surprisingly some cortical regions typically preserved in the disease contributed variance to the models differentiating AD from both MCI and normal aging, such as the para- and post-central gyri. Closer examination of the odds ratios and ANOVA results from these regions indicate for both regions, AD showed increased metabolism and the odds ratios were greater than one, indicating that increased metabolism in these two regions is suggestive of AD. It is not clear at this point whether this is protective for these AD subjects, as the subjects enrolled in the ADNI had relatively mild AD.

Regions common to all four models were the amygdala and inferior temporal cortex. The entorhinal cortex was in models predicting either MCI or AD from normal aging, but not when comparing MCI to AD. This supports the notion of early involvement of the entorhinal cortex. Previous studies have indicated that although it changes early in the disease, FDG uptake in the entorhinal cortex contributes to models classifying normal aging and AD (K B Walhovd, A M Fjell, Brewer, et al. 2010) and that it may in fact be an important area for classifying MCI and normal aging (De Santi S. et al. 2001) . The isthmus of the cingulate

was also affected when comparing MCI to normal aging, which suggests that the region changes early in the disease and that, while the decrease in activity may also be present in AD, that by then it no longer contributed unique variance to the model, likely because other regions contribute more or overlapping variance to the model. Previous studies have suggested that glucose metabolism in the temporal neocortex is a predictor for differentiating MCI from AD. Our results also indicate that the inferior temporal cortex, as well as the postcentral gyrus and putamen are significant predictors to the model differentiating MCI from AD.

Neuropsychological tests

There are a number of benefits to using neuropsychological tests for determining diagnostic group, including its low cost relative to MRI, PET, and CSF sampling. There is also no risk to the patient. On the other hand, these tests may not be as specific to differential diagnoses, they can take a long time to administered, and have the most variability of any of the variables being discussed in this study. That being said, what do these tests contribute on their own and which tests are most effective at distinguishing normal aging, MCI, and AD from one another? Our results indicate that for this sample of normal aging, MCI, and mild AD, there were a number of tests common to all models.

Among the common tests were clock drawing test score, RAVLT 30 minute delay, and RAVLT delay errors. For differentiating normal aging from MCI, the earliest stage in the progression, Trails B and digit span backwards were also predictors. As the disease progresses to AD, Trails B has a higher

odds ratio, indicating that poorer performance is more highly related to AD than it was to MCI. In addition, Trails A and digit span forward, were predictors in the normal aging vs. AD model. In the model differentiating MCI from AD, a mix of visuospatial ability, executive function, and memory were in the model, as indicated by the presence of Trail A and digit span backward tests. Taken together, these results show that different combinations of tests were better at differentiating normal aging from MCI than differentiating MCI from AD, and normal aging from AD. This is not surprising given the progression of the disease and the basement effects that may be observed in tasks that require more memory and executive function, such as Trails B.

CSF models

We examined which of three biomarkers found in CSF contributed to models differentiating between normal aging, MCI, and AD. Aβ-1-42 contributed variance to each of the models, which reached statistical significance in all models except for the MCI vs. AD model. The type of tau, total or 181-p, was not consistent between models. Total tau contributed to each of the models with the exception of differentiating AD from MCI. In this model it was pTau that contributed variance, rather than tTau. The ratio of tTau to Aβ-1-42 has been indicated as a unique predictor of diagnostic group previously (K B Walhovd, A M Fjell, Brewer, et al. 2010), however, in a ratio measurement it is unknown whether it is the Aβ-1-42 or the tTau driving the predictive value. tTau and pTau are typically associated with neuronal and axonal damage, *while* Aβ-1-42 is a

reflection of the amyloid burden in the brain. Although CSF measures may be useful in identifying individuals at risk for disease progression, they are not as useful as MRI or neuropsychological tests at differentiating between the groups (Schmand et al. 2011). This may be in part because the CSF measures are not exclusively brain derived, nor do they provide insight as to the localization of the AD-related pathology.

Multimodal models

While each modality on its own had some predictive value, we wanted to determine whether they were independent measure and to do this we combined them to see if this resulted in better models. Indeed, combining modalities increased the overall discriminability of the models, with the exception of AD vs. normal aging, in which MRI on its own showed higher discriminability index than the multimodal model. The addition of CSF variables further increased the c-statistic in all scenarios, such that multimodal including CSF provided the highest degree of discrimination.

When differentiating normal aging from MCI, both volume and FDG uptake in the entorhinal cortex contributed significantly to the model. Correlation analysis indicates that the variables were independent factors, likely because the FDG PET data had been corrected for atrophy effects, so that any changes in metabolism observed are true representations of brain function and are not mixed with atrophy results. Although FDG PET showed significant decreases in AD compared to both normal aging and FDG PET, no regions provided any

additional variance to the model after including MRI and cognitive measures suggesting that MRI and neuropsychological test scores on their own could adequately distinguish between the groups.

Limitations

There are a few limitations of the present study. The first is that there is a larger proportion of males to females throughout the entire ADNI sample. This is consistent throughout each of the diagnostic groups, however, and was included in each of our models to control for this. The other limitation with sample is that the ADNI subjects may not be representative of the entire population due to the restrictions on subject enrollment. The MCI and normal aging groups in particular, might be more diverse in the general population.

Although ADNI collected genetic information on its participants, we did not examine genetic variables, such as ApoE status, which has been shown to influence rate of disease progression in a dose-dependent manner. Also, not all the subjects in our sample had CSF data, which resulted in a smaller sample for the multimodal model including CSF.

CONCLUSION

This study shows that combining modalities better differentiates between normal aging and MCI subject groups. It is important to be able to distinguish individuals with MCI as early as possible. By looking outside the typical *a priori* regions, we may increase the number of individuals identified. These individuals

should be followed over a longer period of time to determine who declines in memory and executive function and the brain regions associated with these changes.

A set of MRI, FDG PET, CSF, and neuropsychological variables that best differentiates between normal aging, MCI, and AD subject groups has been determined in a large sample from the ADNI database.

Table 4.1 Demographic information

	Subjects (male/female)	**Age mean years (std dev)**	**Education Mean (std dev)**	**MMSE**
Normal Aging	105 (64/41)	75.81 (4.75)	15.90 (3.12)	28.98 (1.12)
MCI	204 (137/67)	75.44 (7.22)	15.80 (2.88)	27.15 (1.71)[a]
AD	94 (56/38)	74.91 (7.37)	14.61 (3.21)[a,b]	23.48 (2.14)[a,b]

[a] significant difference from normal aging ($p < 0.05$), [b] significant difference from MCI ($p < 0.05$).

Table 4.2. MRI model for differentiating AD and MCI groups. The model provided a c-statitisc of 0.861.

	Unit	Odds Ratio	Lower CI	Upper CI	p-value
Age	7.27	0.80	0.57	1.13	0.20
Gender		1.33	0.68	2.60	0.41
Education	3.04	0.56	0.40	0.77	0.0005
Left hippocampus volume	563.50	0.66	0.43	0.99	0.05
Left fusiform volume	1278.50	1.44	0.98	2.12	0.06
Left postcentral surface area	412.10	0.60	0.42	0.86	0.006
Right middle temporal surface area	332.70	0.63	0.43	0.91	0.01
Right lateral occipital surface area	609.60	0.73	0.51	1.03	0.07
Left isthmus of the cingulate cortical thickness	0.26	0.49	0.30	0.78	0.003
Right entorhinal cortical thickness	0.53	0.61	0.41	0.92	0.02
Left inferior temporal cortical thickness	0.24	0.39	0.23	0.65	0.0004
Left posterior cingulate cortical thickness	0.19	1.51	0.98	2.31	0.06
Right banks STS cortical thickness	0.23	0.58	0.39	0.84	0.004
Left insula cortical thickness	0.22	1.91	1.23	2.96	0.004

Table 4.3. MRI model for differentiating MCI and normal aging groups. The model provided a c-statitisc of 0.870.

	Unit	Odds Ratio	Lower CI	Upper CI	p-value
Age	6.50	0.43	0.62	0.29	<.0001
Gender		0.46	0.93	0.23	0.03
Education	2.96	0.80	1.10	0.58	0.17
Right hippocampus volume	549.30	0.38	0.60	0.24	<.0001
Right caudal anterior cingulate volume	397.40	2.04	2.91	1.43	<.0001
Left caudal middle frontal volume	1067.30	0.46	0.66	0.31	<.0001
Left entorhinal volume	445.10	0.64	0.92	0.44	0.02
Right parahippocampus volume	327.30	0.75	1.06	0.54	0.10
Left pericalcarine surface area	212.50	1.39	1.97	0.99	0.06
Right postcentral surface area	414.30	1.32	1.94	0.89	0.17
Right inferior temporal surface area	390.70	0.66	0.93	0.46	0.02
Right paracentral surface area	190.00	1.42	2.00	1.00	0.05
Left middle temporal cortical thickness	0.22	0.46	0.78	0.27	0.004
Left rostral middle frontal cortical thickness	0.17	0.51	0.94	0.27	0.03
Left medial orbitofrontal cortical thickness	0.21	0.78	1.13	0.54	0.19
Right banks STS cortical thickness	0.22	0.61	0.97	0.39	0.04
Right supramarginal cortical thickness	0.19	0.66	1.21	0.36	0.17
Right inferior parietal cortical thickness	0.19	3.37	6.60	1.72	0.0004
Left superior frontal cortical thickness	0.20	2.76	5.29	1.44	0.002

Table 4.4. MRI model for differentiating AD and normal aging groups. The model provided a c-statitisc of 0.986.

	Unit	Odds Ratio	Lower CI	Upper CI	p-value
Age	6.11	0.05	0.36	0.008	0.003
Gender		0.32	4.03	0.03	0.38
Education	3.22	0.04	0.30	0.004	0.002
Left hippocampus volume	614.50	0.003	0.09	<0.001	0.0008
Right caudal anterior cingulate volume	404.20	27.75	251.33	3.06	0.003
Left rostral anterior cingulate volume	404.50	13.23	83.44	2.10	0.006
Left entorhinal volume	450.80	0.04	0.30	0.005	0.002
Right banks STS volume	475.20	0.05	0.37	0.007	0.003
Left insula volume	680.30	15.77	130.46	1.91	0.01
Left caudal middle frontal surface area	355.10	0.02	0.18	0.003	0.0003
Left inferior temporal surface area	459.30	0.07	0.67	0.008	0.02
Right cuneus cortical thickness	0.14	0.08	0.62	0.01	0.02
Left middle temporal cortical thickness	0.26	<0.001	0.02	<0.001	0.0006
Left lateral occipital cortical thickness	0.16	40.80	436.26	3.82	0.002

Table 4.5. MRI model for differentiating between all three groups. The model provided a c-statitisc of 0.879.

	Unit	Odds Ratio	Lower CI	Upper CI	p-value
Age	6.70	0.52	0.40	0.67	<.0001
Gender	0.48	0.74	0.58	0.93	0.01
Education	3.06	0.67	0.54	0.84	0.0006
Left hippocampus surface area	580.50	0.42	0.31	0.58	<.0001
Left caudal middle frontal surface area	1042.70	0.57	0.44	0.75	<.0001
Right parahippocampus surface area	331.00	0.80	0.62	1.03	0.09
Right supramarginal surface area	1324.90	1.32	0.99	1.74	0.05
Left inferior parietal surface area	1682.90	0.77	0.58	1.02	0.07
Right fusiform volume	348.00	0.68	0.54	0.87	0.002
Right superior parietal cortical thickness	0.20	2.07	1.34	3.20	0.001
Right isthmus of the cingulate cortical thickness	0.26	1.29	0.98	1.71	0.07
Left temporal pole cortical thickness	0.42	1.37	1.02	1.85	0.04
Left postcentral cortical thickness	0.16	0.74	0.53	1.03	0.07
Left middle temporal cortical thickness	0.24	0.61	0.39	0.95	0.03
Right entorhinal cortical thickness	0.53	0.60	0.44	0.82	0.001
Right rostral middle frontal cortical thickness	0.18	0.61	0.41	0.91	0.02
Left inferior temporal cortical thickness	0.24	0.52	0.34	0.81	0.003
Left medial orbitofrontal cortical thickness	0.21	0.73	0.56	0.97	0.03
Left lateral occipital cortical thickness	0.16	1.75	1.25	2.47	0.001
Right banks STS cortical thickness	0.23	0.68	0.50	0.92	0.01
Right insula cortical thickness	0.23	1.35	0.97	1.88	0.08
Left pars opercularis cortical thickness	0.20	1.55	1.10	2.19	0.01
Left superior frontal cortical thickness	0.20	1.51	0.99	2.31	0.06
Right lateral orbitofrontal cortical thickness	0.21	1.29	0.91	1.82	0.15
Right precuneus cortical thickness	0.18	0.44	0.29	0.66	0.0001

Table 4.6. FDG PET model for differentiating AD and MCI groups. The model provided a c-statitisc of 0.726.

	Unit	Odds Ratio	Lower CI	Upper CI	p-value
Gender	1	0.716	0.406	1.265	0.25
Education	3.0423	0.61	0.461	0.808	0.0006
Age	7.0892	1.085	0.811	1.452	0.5811
Inferior temporal FDG	1337.9	0.552	0.408	0.749	0.0001
Postcentral FDG	1564	1.779	1.285	2.463	0.0005
Putamen FDG	2407.4	1.425	1.043	1.946	0.0262

Table 4.7. FDG PET model for differentiating MCI and normal aging groups. The model provided a c-statitisc of 0.688.

	Unit	Odds Ratio	Lower CI	Upper CI	p-value
Gender	1.00	1.51	0.87	2.61	0.14
Education	2.96	0.86	0.66	1.12	0.25
Age	6.48	0.80	0.61	1.04	0.10
Entorhinal FDG	1349.30	0.55	0.36	0.84	0.005
Fusiform FDG	1235.90	2.44	1.34	4.43	0.004
Inferior temporal FDG	1301.00	0.58	0.34	0.98	0.04
Isthmus of the cingulate FDG	2007.90	0.59	0.39	0.90	0.01

Table 4.8. FDG PET model for differentiating AD and normal aging groups. The model provided a c-statitisc of 0.879.

	Unit	Odds Ratio	Lower CI	Upper CI	p-value
Gender	1.00	1.07	0.45	2.55	0.88
Education	3.25	0.57	0.38	0.87	0.01
Age	5.93	1.05	0.71	1.57	0.81
Entorhinal FDG	1508.90	0.10	0.03	0.33	0.0001
Isthmus of the cingulate FDG	2183.60	0.42	0.12	1.50	0.18
Middle temporal FDG	1686.00	0.23	0.11	0.50	0.0002
Paracentral FDG	2075.20	2.47	1.02	5.99	0.05
Parahippocampus FDG	1576.20	4.22	1.22	14.58	0.02
Postcentral FDG	1575.60	3.69	1.46	9.28	0.01
Precuneus FDG	2083.10	0.33	0.10	1.09	0.07
Temporal pole FDG	1264.50	3.13	1.13	8.66	0.03

Table 4.9. FDG PET model for differentiating between all three groups. The model provided a c-statitisc of 0.876.

	Unit	Odds Ratio	Lower CI	Upper CI	p-value
Gender	1.00	1.05	0.69	1.59	0.83
Education	3.07	0.69	0.56	0.85	0.0004
Age	6.59	1.00	0.81	1.23	0.98
Entorhinal FDG	1405.30	0.72	0.57	0.91	0.007
Inferior parietal FDG	1761.90	0.60	0.44	0.82	0.002
Isthmus of the cingulate FDG	1974.20	0.59	0.43	0.80	0.0008
Postcentral FDG	1517.70	2.68	1.99	3.60	<.0001
Pallidum FDG	710.90	1.23	0.99	1.53	0.06

Table 4.10. Neuropsyhological test model for differentiating between AD and MCI. The model provided a c-statitisc of 0.876.

	Unit	Odds Ratio	Lower CI	Upper CI	p-value
Age	7.26	1.18	0.85	1.65	0.33
Gender		1.42	0.73	2.75	0.31
Education	3.03	0.69	0.50	0.95	0.02
Clock drawing	1.15	0.71	0.50	1.01	0.06
Digit span backward	2.16	0.62	0.43	0.89	0.01
Trails A	30.70	2.29	1.56	3.37	<.0001
RAVLT 30 minute delayed recall	3.15	0.18	0.09	0.38	<.0001
RAVLT 30 minute delayed recognition errors	2.56	1.42	1.05	1.92	0.02

Table 4.11. Neuropsyhological test model for differentiating between MCI and normal aging. The model provided a c-statitisc of 0.841.

	Unit	Odds Ratio	Lower CI	Upper CI	p-value
Age	6.49	0.70	0.51	0.94	0.02
Gender		0.95	0.51	1.75	0.86
Education	2.96	1.32	0.97	1.78	0.08
Clock drawing	0.89	0.70	0.50	0.97	0.03
Digit span backward	2.14	0.69	0.51	0.93	0.02
Trails B	63.44	1.50	1.03	2.18	0.03
RAVLT 30 minute delayed recall	4.10	0.36	0.25	0.51	<.0001
RAVLT 30 minute delayed recognition errors	2.16	1.57	0.98	2.51	0.06

Table 4.12. Neuropsyhological test model for differentiating between AD and normal aging. The model provided a c-statitisc of 0.992.

	Unit	Odds Ratio	Lower CI	Upper CI	p-value
Age	6.11	0.63	0.24	1.61	0.33
Gender		0.35	0.05	2.55	0.30
Education	3.22	0.85	0.31	2.36	0.75
Clock drawing	1.23	0.21	0.05	0.88	0.03
Digit span forward	2.07	0.26	0.10	0.67	0.005
Trails A	32.71	5.03	0.63	40.24	0.13
Trails B	87.58	2.92	0.81	10.50	0.10
RAVLT 30 minute delayed recall	4.45	0.01	<0.001	0.07	<.0001
RAVLT 30 minute delayed recognition errors	2.32	3.53	1.27	9.84	0.02

Table 4.13. Neuropsyhological test model for differentiating between all three groups. The model provided a c-statitisc of 0.878.

	Unit	Odds Ratio	Lower CI	Upper CI	p-value
Age	6.70	0.88	0.71	1.10	0.25
Gender		1.09	0.69	1.72	0.72
Education	3.06	1.01	0.80	1.27	0.94
Clock drawing	1.09	0.71	0.55	0.92	0.009
Digit span forward	1.99	0.79	0.60	1.02	0.07
Digit span backward	2.24	0.72	0.54	0.95	0.02
Trails A	27.98	1.57	1.17	2.11	0.003
Trails B	78.81	1.44	1.08	1.92	0.01
RAVLT 30 minute delayed recall	4.00	0.33	0.23	0.47	<.0001
RAVLT 30 minute delayed recognition errors	2.37	1.51	1.18	1.94	0.001
RAVLT 30 minute delayed recognition	3.97	0.77	0.57	1.03	0.08

Table 4.14. CSF biomarker model for differentiating between MCI and AD. The model provided a c-statitisc of 0.685.

	Unit	Odds Ratio	Lower CI	Upper CI	p-value
Age	7.25	1.13	0.77	1.66	0.52
Gender	1.00	0.97	0.45	2.11	0.95
Education	3.23	0.62	0.43	0.90	0.01
aBeta 1-42	51.31	0.68	0.44	1.03	0.07
Phosphorylated tau	19.47	1.44	0.98	2.12	0.06

Table 4.15. CSF biomarker model for differentiating between MCI and normal aging. The model provided a c-statitisc of 0.775.

	Unit	Odds Ratio	Lower CI	Upper CI	p-value
Age	6.45	1.04	0.70	1.54	0.84
Gender	1.00	1.42	0.64	3.19	0.39
Education	3.01	0.98	0.67	1.41	0.89
aBeta 1-42	59.43	0.50	0.34	0.74	0.0005
Total tau	54.52	2.80	1.44	5.46	0.003

Table 4.16. CSF biomarker model for differentiating between AD and normal aging. The model provided a c-statitisc of 0.904.

	Unit	Odds Ratio	Lower CI	Upper CI	p-value
Age	6.36	1.51	0.86	2.64	0.15
Gender	1.00	1.02	0.31	3.37	0.98
Education	3.46	0.55	0.31	1.00	0.05
aBeta 1-42	58.94	0.23	0.12	0.46	<0.0001
Total tau	56.29	4.70	2.00	11.06	0.0004

Table 4.17. CSF biomarker model for differentiating between all three groups. The model provided a c-statitisc of 0.753.

	Unit	Odds Ratio	Lower CI	Upper CI	p-value
Age	6.73	1.09	0.83	1.44	0.53
Gender	1.00	1.31	0.73	2.36	0.36
Education	3.21	0.73	0.56	0.96	0.03
aBeta 1-42	57.40	0.45	0.33	0.61	<0.0001
Total tau	59.00	1.70	1.24	2.35	0.001

Table 4.18. Multimodal model without CSF for differentiating between AD and MCI. The model provided a c-statitisc of 0.918.

	Unit	Odds Ratio	Lower CI	Upper CI	p-value
Gender	1.00	1.06	0.48	2.34	0.88
Age	7.23	0.91	0.61	1.36	0.65
Education	3.04	0.59	0.40	0.87	0.008
Left hippocampus volume	563.40	0.54	0.31	0.94	0.03
Left postcentral surface area	415.70	0.67	0.46	0.98	0.04
Right lateral occipital surface area	611.10	0.57	0.38	0.85	0.006
Right entorhinal cortical thickness	0.53	0.55	0.34	0.89	0.01
Left inferior temporal cortical thickness	0.24	0.45	0.26	0.79	0.005
Left insula cortical thickness	0.22	2.29	1.34	3.93	0.003
Clock drawing	1.14	0.70	0.46	1.05	0.08
Digit span backward	2.19	0.50	0.32	0.78	0.002
Trails A	29.73	2.26	1.41	3.62	0.0007
RAVLT 30 minute delayed recall	3.12	0.29	0.13	0.63	0.002
RAVLT 30 minute delayed recognition errors	2.58	1.36	0.96	1.93	0.09

Table 4.19. Multimodal model with CSF for differentiating between AD and MCI. The model provided a c-statitisc of 0.943.

	Unit	Odds Ratio	Lower CI	Upper CI	p-value
Gender	1.00	0.91	0.24	3.42	0.88
Age	7.27	0.99	0.53	1.85	0.98
Education	3.24	0.48	0.25	0.92	0.03
Left hippocampus volume	545.50	0.81	0.35	1.88	0.62
Left postcentral surface area	446.40	0.74	0.40	1.36	0.33
Right lateral occipital surface area	616.60	0.43	0.21	0.86	0.02
Right entorhinal cortical thickness	0.52	0.37	0.17	0.82	0.01
Left inferior temporal cortical thickness	0.23	0.32	0.13	0.77	0.01
Left insula cortical thickness	0.20	2.48	1.03	5.95	0.04
Clock drawing	1.11	0.65	0.34	1.24	0.19
Digit span backward	2.17	0.30	0.14	0.63	0.001
Trails A	32.68	2.63	1.30	5.32	0.007
RAVLT 30 minute delayed recall	2.74	0.31	0.13	0.78	0.01
RAVLT 30 minute delayed recognition errors	2.76	2.37	1.28	4.40	0.006
aBeta 1-42	51.47	0.41	0.20	0.86	0.02
Phosphorylated tau	19.52	0.63	0.32	1.24	0.18

Table 4.20. Multimodal model without CSF for differentiating between MCI and normal aging. The model provided a c-statitisc of 0.925.

	Unit	Odds Ratio	Lower CI	Upper CI	p-value
Gender	1.00	1.33	0.59	2.97	0.49
Age	6.49	0.33	0.20	0.53	<.0001
Education	2.96	1.20	0.81	1.79	0.37
Right hippocampus volume	550.30	0.37	0.21	0.66	0.0007
Right caudal anterior cingulate volume	399.10	2.01	1.33	3.03	0.0009
Left caudal middle frontal volume	1071.40	0.41	0.26	0.65	0.0001
Left entorhinal volume	443.90	0.57	0.37	0.88	0.01
Right postcentral surface area	415.20	1.49	0.96	2.32	0.08
Right inferior temporal surface area	394.40	0.63	0.41	0.95	0.03
Left rostral middle frontal cortical thickness	0.17	0.53	0.26	1.09	0.08
Left medial orbitofrontal cortical thickness	0.20	0.60	0.39	0.94	0.03
Left superior frontal cortical thickness	0.19	2.44	1.18	5.05	0.02
Clock drawing	0.89	0.52	0.34	0.80	0.003
Digit span backward	2.15	0.56	0.37	0.83	0.004
RAVLT 30 minute delayed recall	4.12	0.45	0.29	0.70	0.0004
RAVLT 30 minute delayed recognition errors	2.20	2.01	1.05	3.87	0.04
Entorhinal FDG	1353.90	0.56	0.37	0.84	0.005

Table 4.21. Multimodal model with CSF for differentiating between MCI and normal aging. The model provided a c-statitisc of 0.972.

	Unit	Odds Ratio	Lower CI	Upper CI	p-value
Gender	1.00	2.44	0.40	14.79	0.33
Age	6.44	0.52	0.22	1.22	0.13
Education	3.00	1.36	0.61	3.00	0.45
Right hippocampus volume	557.30	0.54	0.19	1.57	0.26
Right caudal anterior cingulate volume	387.00	3.41	1.41	8.23	0.006
Left caudal middle frontal volume	1109.80	0.15	0.05	0.49	0.002
Left entorhinal volume	447.90	0.76	0.34	1.70	0.50
Right postcentral surface area	363.70	0.81	0.36	1.83	0.61
Right inferior temporal surface area	424.50	0.43	0.18	1.03	0.06
Left rostral middle frontal cortical thickness	0.17	0.79	0.16	4.04	0.78
Left medial orbitofrontal cortical thickness	0.20	0.30	0.13	0.72	0.007
Left superior frontal cortical thickness	0.20	4.58	0.99	21.13	0.05
Clock drawing	0.96	0.29	0.12	0.73	0.008
Digit span backward	2.17	0.58	0.26	1.28	0.18
RAVLT 30 minute delayed recall	4.02	0.13	0.04	0.43	0.0009
RAVLT 30 minute delayed recognition errors	2.32	1.35	0.33	5.59	0.68
Entorhinal FDG	1448.70	0.42	0.19	0.97	0.04
aBeta 1-42	59.92	0.42	0.17	1.03	0.06
Total tau	55.48	2.98	0.94	9.46	0.06

Table 4.22. Multimodal model without CSF for differentiating between AD and normal aging. The model provided a c-statitisc of 0.996.

	Unit	Odds Ratio	Lower CI	Upper CI	p-value
Age	0.60	0.006	0.06	6.27	0.02
Education	3.20	0.06	0.44	3.49	0.42
Left hippocampus volume	0.20	<0.001	0.004	608.50	0.006
RAVLT 30 minute delayed recall	0.08	<0.001	<0.001	4.43	0.004

Table 4.23. Multimodal model with CSF for differentiating between AD and normal aging. The model provided a c-statitisc of 0.998.

Variable	Unit	Odds Ratio	Lower CI	Upper CI	p-value
Age	6.36	0.04	0.002	0.68	0.03
Education	3.46	0.25	0.02	3.82	0.32
Left hippocampus volume	608.80	0.002	<0.001	0.35	0.02
RAVLT 30 minute delayed recall	4.42	<0.001	<0.001	0.11	0.01
aBeta 1-42	58.94	0.06	0.003	1.29	0.07

Table 4.24. Multimodal model without CSF for differentiating between all three groups. The model provided a c-statitisc of 0.928.

	Unit	Odds Ratio	Lower CI	Upper CI	p-value
Gender	1.00	1.44	0.82	2.54	0.21
Age	6.59	0.59	0.43	0.80	0.0007
Education	3.07	0.82	0.63	1.08	0.16
Left hippocampus volume	579.70	0.40	0.27	0.60	<.0001
Left caudal middle frontal volume	1047.10	0.53	0.38	0.73	0.0001
Right superior parietal cortical thickness	0.20	2.21	1.34	3.62	0.002
Right isthmus of the cingulate cortical thickness	0.26	1.28	0.92	1.78	0.15
Left temporal pole cortical thickness	0.42	1.33	0.94	1.88	0.10
Left postcentral cortical thickness	0.16	0.64	0.44	0.93	0.02
Right entorhinal cortical thickness	0.53	0.58	0.40	0.85	0.005
Left inferior temporal cortical thickness	0.24	0.50	0.32	0.77	0.002
Left medial orbitofrontal cortical thickness	0.21	0.69	0.51	0.95	0.02
Left lateral occipital cortical thickness	0.16	1.76	1.19	2.60	0.005
Right banks STS cortical thickness	0.23	0.72	0.50	1.04	0.08
Right insula cortical thickness	0.23	1.47	1.03	2.11	0.04
Left pars opercularis cortical thickness	0.19	1.60	1.09	2.33	0.02
Right precuneus cortical thickness	0.18	0.63	0.39	1.02	0.06
Clock drawing	1.09	0.72	0.52	0.98	0.04
Digit span forward	1.97	0.71	0.52	0.97	0.03
Digit span backward	2.25	0.65	0.47	0.90	0.009
Trails A	27.24	1.77	1.26	2.49	0.001
RAVLT 30 minute delayed recall	4.01	0.44	0.29	0.67	0.0001
RAVLT 30 minute delayed recognition errors	2.40	1.65	1.22	2.23	0.001
RAVLT 30 minute delayed recognition	4.03	0.77	0.55	1.09	0.14
Isthmus of the cingulate FDG	1971.50	0.69	0.49	0.96	0.03
Postcentral FDG	1521.50	1.39	0.99	1.95	0.06
Pallidum FDG	712.30	1.27	0.98	1.64	0.07

Table 4.25. Multimodal model with CSF for differentiating between all three groups. The model provided a c-statitisc of 0.946.

Variable	Unit	Odds Ratio	Lower CI	Upper CI	p-value
Gender	1.00	0.97	0.40	2.33	0.94
Age	6.68	0.69	0.42	1.12	0.14
Education	3.24	0.78	0.51	1.19	0.25
Left hippocampus volume	570.20	0.52	0.28	0.95	0.03
Left caudal middle frontal volume	1079.60	0.65	0.40	1.08	0.09
Right superior parietal cortical thickness	0.19	2.25	0.98	5.16	0.06
Right isthmus of the cingulate cortical thickness	0.26	1.20	0.73	1.97	0.47
Left temporal pole cortical thickness	0.42	1.87	1.10	3.18	0.02
Left postcentral cortical thickness	0.15	0.48	0.25	0.93	0.03
Right entorhinal cortical thickness	0.53	0.53	0.30	0.96	0.03
Left inferior temporal cortical thickness	0.24	0.45	0.24	0.87	0.02
Left medial orbitofrontal cortical thickness	0.20	0.64	0.40	1.03	0.07
Left lateral occipital cortical thickness	0.15	1.62	0.89	2.94	0.11
Right banks STS cortical thickness	0.23	1.12	0.63	1.99	0.70
Right insula cortical thickness	0.22	1.20	0.68	2.14	0.53
Left pars opercularis cortical thickness	0.18	1.29	0.70	2.37	0.41
Right precuneus cortical thickness	0.19	0.63	0.29	1.35	0.24
Clock drawing	1.07	0.65	0.41	1.03	0.06
Digit span forward	1.93	1.03	0.64	1.65	0.91
Digit span backward	2.25	0.51	0.32	0.82	0.005
Trails A	28.21	1.52	0.91	2.54	0.11
RAVLT 30 minute delayed recall	3.89	0.31	0.16	0.62	0.0009
RAVLT 30 minute delayed recognition errors	2.61	2.10	1.34	3.30	0.001
RAVLT 30 minute delayed recognition	3.78	0.77	0.46	1.29	0.32
Isthmus of the cingulate FDG	1921.70	0.55	0.31	0.95	0.03
Postcentral FDG	1549.70	1.22	0.69	2.15	0.49
Pallidum FDG	597.50	1.25	0.78	1.99	0.35
aBeta 1-42	58.13	0.58	0.36	0.91	0.02

REFERENCES

Anon, 2012. 2012 Alzheimer's disease facts and figures. *Alzheimer's and Dementia*, 8(2), pp.131–168.

Blennow, K et al., 1995. Tau protein in cerebrospinal fluid: a biochemical marker for axonal degeneration in Alzheimer disease? *Molecular and chemical neuropathology / sponsored by the International Society for Neurochemistry and the World Federation of Neurology and research groups on neurochemistry and cerebrospinal fluid*, 26(3), pp.231–245.

Braak, H & Braak, E., 1991. Neuropathological stageing of Alzheimer-related changes. *Acta neuropathologica*, 82(4), pp.239–259.

Braak, H & Braak, E., 1995. Staging of Alzheimer's disease-related neurofibrillary changes. *Neurobiology of aging*, 16(3), pp.271–278; discussion 278–284.

Braak, Heiko & Del Tredici, K., 2011a. Alzheimer's pathogenesis: is there neuron-to-neuron propagation? *Acta Neuropathologica*, 121(5), pp.589–595.

Braak, Heiko & Del Tredici, K., 2011b. The pathological process underlying Alzheimer's disease in individuals under thirty. *Acta neuropathologica*, 121(2), pp.171–181.

Cedazo-Minguez, A. & Winblad, B., 2010. Biomarkers for Alzheimer's disease and other forms of dementia: Clinical needs, limitations and future aspects. *Experimental Gerontology*, 45(1), pp.5–14.

Courchesne, E. et al., 2000. Normal brain development and aging: quantitative analysis at in vivo MR imaging in healthy volunteers. *Radiology*, 216(3), pp.672–682.

Dale A.M., Fischl B. & Sereno M.I., 1999. Cortical Surface-Based Analysis I. Segmentation and Surface Reconstruction. *NeuroImage*, 9(2), pp.179–194.

Desikan, R.S. et al., 2006. An automated labeling system for subdividing the human cerebral cortex on MRI scans into gyral based regions of interest. *NeuroImage*, 31(3), pp.968–980.

Dickerson, B.C., Feczko, E., et al., 2009. Differential effects of aging and Alzheimer's disease on medial temporal lobe cortical thickness and surface area. *Neurobiology of Aging*, 30(3), pp.432–440.

Dickerson, B.C., Bakkour, A., et al., 2009. The Cortical Signature of Alzheimer's Disease: Regionally Specific Cortical Thinning Relates to Symptom Severity in

Very Mild to Mild AD Dementia and Is Detectable in Asymptomatic Amyloid-Positive Individuals. *Cerebral Cortex*, 19(3), pp.497–510.

Ewers, M. et al., 2007. Multicenter assessment of CSF-phosphorylated tau for the prediction of conversion of MCI. *Neurology*, 69(24), pp.2205–2212.

Ewers, Michael et al., 2011. Staging Alzheimer's disease progression with multimodality neuroimaging. *Progress in Neurobiology*, 95(4), pp.535–546.

Eyler, L.T. et al., 2011. Genetic and Environmental Contributions to Regional Cortical Surface Area in Humans: A Magnetic Resonance Imaging Twin Study. *Cerebral Cortex*, 21(10), pp.2313–2321.

Fischl, B., Sereno, M.I. & Dale, A. M., 1999. Cortical surface-based analysis - II: Inflation, flattening, and a surface-based coordinate system. Available at: http://discovery.ucl.ac.uk/145122/ [Accessed September 21, 2011].

Fischl, Bruce, Van der Kouwe, André, et al., 2004. Automatically Parcellating the Human Cerebral Cortex. *Cerebral Cortex*, 14(1), pp.11 –22.

Fischl, Bruce, Salat, David H, et al., 2004. Sequence-independent segmentation of magnetic resonance images. *NeuroImage*, 23 Suppl 1, pp.S69–84.

Fischl, Bruce et al., 2002. Whole Brain Segmentation. *Neuron*, 33(3), pp.341–355.

Fischl, Bruce & Dale, Anders M., 2000. Measuring the thickness of the human cerebral cortex from magnetic resonance images. *Proceedings of the National Academy of Sciences*, 97(20), pp.11050 –11055.

Gómez-Isla, T. et al., 1997. Neuronal loss correlates with but exceeds neurofibrillary tangles in Alzheimer's disease. *Annals of Neurology*, 41(1), pp.17–24.

Greve, Douglas N & Fischl, Bruce, 2009. Accurate and robust brain image alignment using boundary-based registration. *NeuroImage*, 48(1), pp.63–72.

Hansson, O. et al., 2006. Association between CSF biomarkers and incipient Alzheimer's disease in patients with mild cognitive impairment: a follow-up study. *Lancet neurology*, 5(3), pp.228–234.

Hulette, C.M. et al., 1998. Neuropathological and neuropsychological changes in "normal" aging: evidence for preclinical Alzheimer disease in cognitively normal individuals. *Journal of neuropathology and experimental neurology*, 57(12), pp.1168–1174.

Kawachi, T. et al., 2006. Comparison of the diagnostic performance of FDG-PET and VBM-MRI in very mild Alzheimer's disease. *European Journal of Nuclear Medicine and Molecular Imaging*, 33(7), pp.801–809.

Killiany, R J et al., 2002. MRI measures of entorhinal cortex vs hippocampus in preclinical AD. *Neurology*, 58(8), pp.1188–1196.

Matsunari, I. et al., 2007. Comparison of 18F-FDG PET and optimized voxel-based morphometry for detection of Alzheimer's disease: aging effect on diagnostic performance. *Journal of Nuclear Medicine: Official Publication, Society of Nuclear Medicine*, 48(12), pp.1961–1970.

Mosconi, L., 2005. Brain glucose metabolism in the early and specific diagnosis of Alzheimer's disease. *European Journal of Nuclear Medicine and Molecular Imaging*, 32(4), pp.486–510.

Mosconi, L., Pupi, A. & De Leon, M.J., 2008. Brain glucose hypometabolism and oxidative stress in preclinical Alzheimer's disease. *Annals of the New York Academy of Sciences*, 1147, pp.180–195.

Petersen, R. C., 2001. Current Concepts in Mild Cognitive Impairment. *Archives of Neurology*, 58(12), pp.1985–1992.

Rakic, P., 1988. Specification of cerebral cortical areas. *Science (New York, N.Y.)*, 241(4862), pp.170–176.

Reiber, H. & Peter, J.B., 2001. Cerebrospinal fluid analysis: disease-related data patterns and evaluation programs. *Journal of the neurological sciences*, 184(2), pp.101–122.

Salat, D H et al., 2009. Age-associated alterations in cortical gray and white matter signal intensity and gray to white matter contrast. *NeuroImage*, 48(1), pp.21–28.

Salat, D.H. et al., 2011. Hippocampal degeneration is associated with temporal and limbic gray matter/white matter tissue contrast in Alzheimer's disease. *NeuroImage*, 54(3), pp.1795–1802.

De Santi S. et al., 2001. Hippocampal formation glucose metabolism and volume losses in MCI and AD. *Neurobiology of Aging*, 22(4), pp.529–539.

Schmand, B. et al., 2011. Value of Neuropsychological Tests, Neuroimaging, and Biomarkers for Diagnosing Alzheimer's Disease in Younger and Older Age Cohorts. *Journal of the American Geriatrics Society*, 59(9), pp.1705–1710.

Shaw, L.M. et al., 2011. Qualification of the analytical and clinical performance of CSF biomarker analyses in ADNI. *Acta Neuropathologica*, 121(5), pp.597–609.

St George-Hyslop, P.H., 2000. Molecular genetics of Alzheimer's disease. *Biological psychiatry*, 47(3), pp.183–199.

Thal, D.R. et al., 2002. Phases of Aβ-deposition in the human brain and its relevance for the development of AD. *Neurology*, 58(12), pp.1791–1800.

Thompson, P.M. et al., 2003. Dynamics of Gray Matter Loss in Alzheimer's Disease. *The Journal of Neuroscience*, 23(3), pp.994–1005.

Trojanowski, J.Q. et al., 1993. Altered Tau and Neurofilament Proteins in Neuro-Degenerative Diseases: Diagnostic Implications for Alzheimer's Disease and Lewy Body Dementias. *Brain Pathology*, 3(1), pp.45–54.

Walhovd, K.B. et al., 2010. Combining MR imaging, positron-emission tomography, and CSF biomarkers in the diagnosis and prognosis of Alzheimer disease. *AJNR. American Journal of Neuroradiology*, 31(2), pp.347–354.

Walhovd, K.B. et al., 2009. Multimodal imaging in mild cognitive impairment: Metabolism, morphometry and diffusion of the temporal-parietal memory network. *NeuroImage*, 45(1), pp.215–223.

Wechsler, D., 1987. *WMS-R: Wechsler Memory Scale--Revised manual*, Psychological Corp., Harcourt Brace Jovanovich.

Yakushev, I. et al., 2008. Choice of reference area in studies of Alzheimer's disease using positron emission tomography with fluorodeoxyglucose-F18. *Psychiatry Research*, 164(2), pp.143–153.

Yanase, Daisuke et al., 2005. Brain FDG PET study of normal aging in Japanese: effect of atrophy correction. *European Journal of Nuclear Medicine and Molecular Imaging*, 32(7), pp.794–805.

Zetterberg, H., Wahlund, L.-O. & Blennow, Kaj, 2003. Cerebrospinal fluid markers for prediction of Alzheimer's disease. *Neuroscience letters*, 352(1), pp.67–69.

Zhang, D. et al., 2011. Multimodal classification of Alzheimer's disease and mild cognitive impairment. *NeuroImage*, 55(3), pp.856–867.

Chapter 5 - Multimodal imaging and CSF biomarkers associated with baseline cognitive function and predictive of future cognitive decline in normal aging, mild cognitive impairment, and Alzheimer's disease

INTRODUCTION

Alzheimer's disease (AD) is characterized by a progressive decline in cognitive abilities. Initial symptoms typically present as difficulties with memory tasks, where a rapid rate of forgetting is often found, followed by deficits in executive function, ultimately affecting visuospatial abilities and attention in the later stages of the disease. The cognitive deficits seen throughout mild cognitive impairment (MCI) and AD have been shown to correlate with the degree of pathology in post-mortem tissue analysis as well as *in vivo* imaging measures (Gómez-Isla et al. 1997; Mufson et al. 2012; K B Walhovd, A M Fjell, A M Dale, et al. 2010; PA et al. 2010). However, many of these studies only report one or two tests in the same subjects, thus we do not have a complete picture as to the neural correlates of the wide range of neuropsychological functions in normal aging, MCI, and AD. Tests that involve memory, such as delayed recall, have been examined to greater depths than simpler tasks, such as Trails A and few studies to our knowledge have examine the full extent of cognitive abilities in the same subjects.

Insight into structure-function relationships in the brain can be gained by studying multiple tests and their imaging correlates both at baseline and over time using measures expressed as average annual change in the same subjects. Although tests, such as delayed recall have been extensively studied in AD, the brain regions that are predictive of decline and baseline performance are not consistent in these reports. Often there are variations reported, which may be the

results of the subjects in the sample or the version of the test being used. Thus, by studying the same sample of subjects over time using the same measures, we will be able to obtain a more cohesive and broad picture of the interaction between cognitive functions and imaging variables. In this study we sought to identify the MRI morphometric and FDG PET metabolic variables that are associated with baseline cognitive performance and those that are able to predict future cognitive decline. For this study, cognitive decline was defined as the annualized percent change (APC), which was calculated as the total amount of change in score divided by the time between the first and last incidences of the testing. Linear regression models were used to identify the variables that best predicted neuropsychological decline and baseline scores. Thus, we created a series of stepwise linear regression models to predict baseline performance and APC in a battery of neuropsychological tests in normal aging, MCI, and AD groups. We hypothesized that MRI and FDG PET would both be able to predict future cognitive performance. We also hypothesized that combining metabolism and morphometry would increase the total amount of variance that the models accounted for.

METHODS

Subjects

The data for use in this study were chosen from the larger pool of data that has been made publically available by the Alzheimer's Disease

Neuroimaging Initiative. Data was screened to include all subjects who had both PET and MRI scans available for use on the ADNI/LONI website (www.loni.ucla.edu/ADNI) at the time this study began. From this screened dataset, PET data from 21 subjects was of poor contrast and quality and had to be omitted from the analyses undertaken in this study. Three subjects were omitted due to missing information. This left us with data from 403 subjects. Approximately half of the total subjects from ADNI also underwent lumbar puncture to obtain CSF samples. In our subjects, 55 normal aging, 103 MCI, and 51 AD subjects had CSF sample data. We present demographic information on this sample in Table 5.1.

As part of the ADNI, all subjects completed a battery of neuropsychological tests, On the basis of their cognitive status the subjects were classified by the ADNI clinical core as: (a) normal controls with normal cognition and memory, Clinical Dementia Rating (CDR) 0, and Mini Mental Status Exam (MMSE) between 24-30; (b) amnestic MCI with memory complaint verified by a study partner, memory loss measured by education-adjusted performance on the Logical Memory II subscale of the Wechsler Memory Scale-Revised[(Wechsler 1987)], preserved activities of daily living, CDR 0.5, MMSE between 24 and 30, and absence of dementia at time of baseline MRI scan; or (c) probable AD with memory complaint validated by an informant, abnormal memory function for age and education level, absence of depression, impaired activities of daily living, diminished cognition, CDR > 0.5, and MMSE between 20 - 26.

Alzheimer's Disease Neuroimaging Initiative

The ADNI was a 5-year non-randomized natural history non-treatment study utilizing data from multiple study centers across the United States and Canada. One of the main goals of the ADNI was to develop optimized methods and uniform standards for the acquisition of multicenter MRI and PET data on normal control subjects and patients with MCI and AD in drug/treatment trials. For more information about the ADNI please refer to http://www.adni-info.org.

CSF Sampling

Detailed CSF collection and processing methods can be found in elsewhere (Shaw et al. 2011). Briefly, CSF samples obtained by lumbar puncture were examined for tTau. pTau, and Aβ-42 using an immunoassay method. These measures were performed by the ADNI Biomarker Core at the University of Pennsylvania School of Medicine.

Neuropsychological testing

The baseline and subsequent follow-up cognitive scores were utilized as our variables of interest. The time each subject was followed varies, thus the longitudinal cognitive data was converted to annualized percent change (APC), which was calculated as the average change in cognitive score from year to year. These values were then z-transformed. The cognitive tests of interest were Trails A, Trails B, Clock draw, digit span forward, digit span backward, and RAVLT 30

minute delayed recall and recognition. Baseline and APC measurements were assessed within each diagnostic group.

MRI scans

For this study, we analyzed the T1-weighted MPRAGE baseline MRI scans from those acquired by the ADNI on 1.5T scanners from General Electric (GE), Philips Medical Systems (Philips), and Siemens Medical Solutions (Siemens). Specific pulse sequence guidelines can be found at http://www.loni.ucla.edu/ADNI/Research/Cores/index.shtml.

FDG-PET scans

For this study, we analyzed baseline FDG-PET scans from those acquired by the ADNI on GE, Philips, or Siemens scanners. Specific protocols for each scanner are available from the ADNI website (http://adni.loni.ucla.edu/research/protocols/pet-protocols/). These data were corrected for radiation attenuation and scatter using scanner-specific algorithms and each image was visually assessed for potential artifacts by the ADNI PET core at the University of Michigan. For this study we used the original PET data that was not pre-processed by the ADNI PET core so that we could have local control of all the processing steps as with the MRI scans.

Freesurfer Analysis

All MRI and FDG PET scans were processed with the Freesurfer 5.1.0 (Dale A.M. et al. 1999; B. Fischl et al. 1999), which is documented and freely

available. The processing pipeline has been described in detail elsewhere (Dale A.M. et al. 1999; B. Fischl et al. 1999; Bruce Fischl et al. 2002; Bruce Fischl, André van der Kouwe, et al. 2004; Bruce Fischl, David H Salat, et al. 2004; Bruce Fischl & Anders M. Dale 2000). Briefly, for each subject, the 2 DICOM T1-weighted MRI datasets were motion corrected, averaged, segmented into gray matter, white matter, and cerebral spinal fluid (CSF), and intensity normalized. Cortical thickness measures were corrected for gray/white matter intensity ratio using residuals, as it was previously determined to increase the predictive ability of cortical thickness in our sample (in preparation). The gray/white matter intensity ratio was calculated as previously described, but will be briefly outlined here (D H Salat et al. 2009; D.H. Salat et al. 2011). Gray matter tissue intensities were measured 35% through the thickness of the cortical ribbon. White matter tissue intensities were measured 1mm below the gray/white matter boundary, into the white matter. The GWIR was calculated by dividing the white matter by the gray matter intensity values. The ratios were then projected onto the cortical surface and smoothed with a Gaussian kernel with a full width at half maximum of 30mm. The cortex was parcellated into regions of interest (ROIs) based on gyral and sulcal structure using the Desikan/Killiany atlas (Desikan et al. 2006). In this study, the isthmus of the cingulate is the portion of the cingulate posterior to the marginal ramus. Many studies refer to this region as the posterior cingulate. For consistency we will refer to this region as the isthmus throughout

and specify posterior cingulate when the hypometabolism extended anterior to the marginal ramus.

PET Processing

Once the T1-weighted MRI images were processed, the PET images were affine spatial transformed into "anatomical space" 1x1x1, 256x256x256, which was the same resolution as the transformed MRI images. The PET and MRI images were then co-registered using an automated Freesurfer boundary based application using 6 degrees of freedom (Douglas N Greve & Bruce Fischl 2009), such that no skewing or twisting of the data occurred. The resulting coregistration was visually assessed for accuracy and adjusted if necessary (approximately 25% of the datasets). After the two datasets were co-registered, FDG uptake was measured in specific ROIs according to the cerebral cortex parcellations generated on the representative MRI images (Desikan et al. 2006). A total of 82 cortical and subcortical areas were examined for changes in MRI morphometry and FDG uptake related to MCI and AD relative to normal aging.

To control for individual global variations and to increase sensitivity of the method for differentiating between subject groups (Yakushev et al. 2008), the FDG uptake was normalized to regional activity in the cerebellum using residuals. The choice of reference region was based on the results from a previous study in which we tested which region was best suited for as a reference region for normalization in our subjects. Partial volume effects were

also corrected for using an adapted gray matter mask (Daisuke Yanase et al. 2005).

Statistical Analysis

In order to assess the equality of the male-female distribution in the three diagnostic groups, χ^2 tests were performed. ANOVA was used in order to assess the age, education, and MMSE distributions in the three diagnostic groups. Hemisphere differences for both MRI and PET data were examined with paired t-tests and correlation analysis. If the t-tests showed no significant differences the two hemispheres they were averaged together. Age was correlated with each of the morphometric and uptake variables, including cortical surface area, volume, cortical thickness, gray/white matter intensity ratio, and FDG uptake. The difference in baseline cognitive tests and APC between groups was determined using ANOVA with Tukey's post-hoc comparison.

Linear regression Analyses

A stepwise linear regression was used to identify the baseline MRI morphometry, FDG PET, and CSF sample variables that were associated with baseline cognitive performance and predictive of future APC within each diagnostic group. To determine which CSF and imaging variables should be entered into the linear regression models, we first performed a linear regression on each variable individually to ensure that on its own the variable could account for a minimum amount of variance in the cognitive test. If the standardized

estimate was greater or equal to an absolute value of 0.15, then it was enabled as a variable for the stepwise linear regression models. The stepwise linear regression models had entry and exit criteria of 0.20. Age, gender, and education were included in each of the models to control for the variance that they may have contributed to the cognitive variables. To generate multi-modal models, the variables that contributed to the individual modality models were entered into another stepwise linear regression with the same entry and exit criteria as before. Standardized estimates were used to put the predictor variables in the same scale, such that holding all other variables constant, a one standard deviation change in one predictor variable, results in a one standard deviation change (in the direction of the sign) of the dependent cognitive variable. Pearson's correlation and variance inflation factor were used to assess collinearity amongst the predictor variables of the multimodal models.

RESULTS

Age and gender were not significantly different between groups, as measured with ANOVA and chi-square, respectively. Education was significantly lower in the AD group compared to normal and MCI. As expected, MMSE scores were significantly lower in MCI and further decreased in AD.

Cognitive scores at baseline and decline by diagnostic group

Baseline scores differed between groups in two main patterns: 1) a stepwise significant decrease between normal aging and MCI, and again

between MCI and AD, and 2) significant decreases in AD, but no change between normal aging and MCI. Trails B, clock score, digit span backward, and the AV 30 minute delay, delay total, and delay errors shared the first pattern, whereas Trails A and digit span forward showed the second pattern. The details are shown in Table 5.2.

Differences in APC between groups showed three main patterns: 1) significantly increased decline in AD compared to both normal and MCI, as seen in clock score, digit span backward, and AV 30 minute delay, 2) significantly increased decline in AD compared to normal, but not MCI, as observed in Trails B and digit span forwards, and 3) no significant differences in amount of decline between groups, as seen with AV delayed recognition and Trails A.

Linear Regression Models

After an initial linear regression on each of the individual morphometric, metabolic, and CSF biomarkers, the variables that accounted for enough variance of the cognitive tasks on their own were eligible to be entered into the stepwise linear regression model for baseline and decline in cognitive performance. Age, gender, and education were accounted for in each of the models. We will present only the significant contributors in the text.

Normal aging

Baseline clock drawing scores

MRI accounted for 43% of the variance (R^2 = 0.48, Adj. R^2 = 0.43, F = 9.89, p < ,0.0001), FDG PET accounted for 32% of the variance (R^2 = 0.37, Adj. R^2 = 0.32, F = 7.66, p < 0.0001), and CSF did not account for any variance. Combining imaging modalities increased the prediction accounting for 49% of the variance (R^2 = 0.54, Adj. R^2 = 0.49, F = 10.35, p < 0.0001). Age and education showed significant associations with clock drawing. Cuneus hypermetabolism and larger cortical thickness of the right pericalcarine and surface area of the left caudal middle frontal and left pars triangularis were associated with worse clock draw scores. Thinner cortex in the right posterior cingulate and smaller surface area of the right lingual gyrus were also associated with worse clock drawing scores. The full models can be found in Table 5.3.

Longitudinal clock drawing scores

Clock drawing scores increased over time in the normal group by an average of 0.11 (sd = 0.83). Because this study focuses on predicting future decline, we will not discuss the longitudinal clock drawing models for normal aging further.

Baseline digit span forward

MRI variables attributed for 36% of the variance (R^2 = 0.43, Adj. R^2 = 0.36, F = 6.34, p < 0.0001, FDG PET accounted for 10% of the variance (R^2 = 0.14,

Adj. R^2 = 0.10, F = 3.80, p = 0.0066), and CSF did not contribute any variance. The combination of modalities did not improve upon the adjusted R^2 values beyond MRI alone (R^2 = 0.42, Adj. R^2 = 0.36, F = 6.42, p < 0.0001). Larger surface area in the right pars orbitalis were significantly associated with shorter digit spans, while smaller cortical thickness in the right pericalcarine and smaller volume in the right isthmus of the cingulate were significantly associated with worse digit spans. The full models can be found in Table 5.4.

Longitudinal digit span forward change

For subjects in the normal aging group, the average APC for digit span forward was an increase of 0.13 (sd = 0.35). Because this study focuses on predicting future decline, we will not discuss the longitudinal digit span forward models for normal aging further.

Baseline digit span backward

MRI accounted for 31% of the variance (R^2 = 0.38, Adj. R^2 = 0.31, F = 5.64, p < 0.0001) and FDG PET accounted for 5% of the variance (R^2 = 0.09, Adj. R^2 = 0.05, F = 2.35, p = 0.06). No CSF variables made it through the cutoff steps. Combining MRI morphometry and FDG PET metabolism accounted for 36% of the variance (R^2 = 0.42, Adj. R^2 – 0.36, F = 6.98, p < 0.0001). In the multimodal model, larger cortical thickness in the left entorhinal, larger volumes in the right anterior cingulate and right pars triangularis, and larger surface area in the right transverse temporal were associated with worse scores on the digit

span backward in normal aging. Smaller cortical thickness in the right pericalcarine and smaller surface area in the left isthmus of the cingulate were also associated with wore scores on the digit span backward. The full models can be found in Table 5.5.

Longitudinal digit span backward

In the group diagnosed as normal aging at baseline, digit span backward score improved an average of 0.13 per year (sd = 0.35). Because this study focuses on predicting future decline, we will not discuss the longitudinal digit span backward models for normal aging further.

Baseline Trails A

MRI accounted for 34% of the variance (R^2 = 0.42, Adj. R^2 = 0.34, F = 5.46, $p < 0.0001$), FDG PET accounted for 14% of the variance (R^2 = 0.18, Adj. R^2 = 0.14, F = 4.10, p = 0.0021), and CSF variables did not pass the initial cutoff values. Combining MRI morphometry and FDG PET metabolism accounted for 36% of the variance (R^2 = 0.45, Adj. R^2 = 0.36, F = 5.25, $p < 0.0001$). Older ages were associated with longer time to complete for Trails A. Larger volume in the right temporal pole, larger surface areas in the left insula and right lateral orbitofrontal regions, and hypermetabolism in the insula were associated with longer times to complete Trails A in normal aging. Smaller cortical thickness in the right transverse temporal, smaller surface area in the left rostral middle

frontal, as well as hypometabolism in the frontal pole were associated with longer times to complete Trails A. The full models can be found in Table 5.6.

Longitudinal Trails A change

The average APC for Trails A in normal aging was 0.14 (sd = 0.49), indicating that it took more time to complete the test on future visits. This change was predicted best from combining MRI and FDG PET (R^2 = 0.36, Adj. R^2 = 0.29, F = 4.91, p < 0.0001). Larger baseline volume in the right temporal pole and surface area in the left banks of the superior temporal sulcus were predictive of greater decline during follow-up. Smaller baseline cortical thickness in the right posterior cingulate, volume in the right thalamus, surface area in the right inferior temporal, and hypometabolism of the precentral gyrus were associated with greater decline in Trails A at follow-up, as reflected in the positive APC. The full models can be found in Table 5.7.

Baseline Trails B

MRI accounted for 35% of the variance (R^2 = 0.42, Adj. R^2 = 0.35, F = 6.19, p < 0.0001). Neither FDG PET nor CSF variables made it through the initial cutoff steps. Older age was associated with worse performance. Higher volume in the right temporal pole and higher surface area in the right superior temporal and right middle temporal areas were associated with longer times (e.g. worse performance) to complete Trails B. Smaller volume in the right precentral, and

smaller surface area in the right inferior parietal were associated with worse performance on Trails B. The full models can be found in Table 5.8.

Longitudinal Trails B

Time to complete trails B decreased on average by 0.06 (sd 0.01). Because this study focuses on predicting future decline, we will not discuss the longitudinal Trails B models for normal aging further.

Baseline AV 30 minute delayed recall (Recall)

MRI accounted for 40% of the variance (R^2 = 0.48, Adj. R^2 = 0.40, F = 5.93, $p < 0.0001$), FDG PET accounted for 7% of the variance (R^2 = 0.11, Adj. R^2 = 0.07, F = 2.85, p = 0.03), and CSF accounted for 9% of the variance (R^2 = 0.16, Adj. R^2 = 0.09, F = 2.32, p = 0.07). Combining MRI morphometry and FDG PET metabolism accounted for 38% of the variance (R^2 = 0.46, Adj. R^2 = 0.38, F = 5.53, $p < 0.0001$), while combining CSF biomarker concentrations with the imaging measures, 40% of the variance in baseline AV 30 minute delayed recall was accounted for (R^2 = 0.58, Adj. R^2 = 0.40, F = 3.13, p = 0.002). Age, gender, and education were significantly associated with delayed recall. Larger volume in the left thalamus, and right isthmus of the cingulate, larger surface area of the right posterior cingulate, and hypermetabolism in the paracentral gyrus were associated with worse AV 30 minute delayed recall scores. Smaller surface area in the right inferior temporal was associated with worse AV 30 minute delayed recall scores. The full models can be found in Table 5.9.

Longitudinal AV 30 minute delayed recall (Recall)

The average APC for AV 30 minute delayed recall was 0.14 (sd = 0.86). Because this study focuses on predicting future decline, we will not discuss the longitudinal 30 minute RAVLT delayed recall models for normal aging further.

Baseline AV delayed recognition (Recognition)

MRI accounted for 42% of the variance (R^2 = 0.49, Adj. R^2 = 0.42, F = 6.72, p < 0.0001), FDG PET accounted for 7% of the variance (R^2 = 0.12, Adj. R^2 = 0.07, F = 2.52, p = 0.04), and CSF accounted for 10% of the variance (R^2 = 0.17, Adj. R^2 = 0.10, F = 2.53, p = 0.05). Combing MRI morphometry and FDG PET metabolism accounted for 45% of the variance (R^2 = 0.53, Adj. R^2 = 0.45, F = 7.15, p < 0.0001), while combining CSF biomarker concentrations with the imaging measures accounted for only 37% of the variance (R^2 = 0.55, Adj. R^2 = 0.37, F = 3.02, p = 0.003). Age and gender with significantly associated with recognition scores. Larger volumes in the left temporal pole and left thalamus, larger surface area in the right supramarginal gyrus, and hypermetabolism in the hippocampus were associated with poorer recognition scores. Smaller volume in the right accumbens, and smaller surface area in the left insula were significantly associated with poorer recognition scores in the multimodal model. The full models can be found in Table 5.10.

Longitudinal AV delayed recognition scores (Recognition)

Subjects categorized as normal aging at baseline declined on average 0.005 (sd = 1.16). Because this study focuses on predicting future decline, we will not further discuss the longitudinal recognition scores for normal aging.

MCI

Baseline Clock drawing

In MCI subjects, MRI accounted for 18% of the variance (R^2 = 0.21, Adj. R^2 = 0.18, F = 6.48, p < 0.0001) and FDG PET accounted for 3% of the variance (R^2 = 0.05, Adj. R^2 = 0.03, F = 2.47, p = 0.05). No CSF variables made it through the initial cutoff values. Combining MRI morphometry and FDG PET metabolism accounted for 20% of the variance (R^2 = 0.24, Adj. R^2 = 0.20, F = 6.17, p < 0.0001). Education was significantly associated with clock draw scores. Larger surface area in the right transverse temporal was significantly associated with lower scores in the multimodal model. Smaller cortical thickness in the right isthmus of the cingulate and right caudal middle frontal and surface area in the right inferior parietal lobule were significantly associated with lower scores in the multimodal model. The full models can be found in Table 5.11.

Longitudinal Clock drawing

In subjects diagnosed with MCI at baseline, the average APC in clock draw scores was 0.03 (sd = 0.59), thus it increased slightly every year. Because

this study focuses on predicting future decline, we will not further discuss the longitudinal clock drawing models for MCI.

Baseline Digit span forward

In MCI, MRI accounted for 5% of the variance (R^2 = 0.08, Adj. R^2 = 0.05, F = 2.66, p = 0.02). Neither FDG PET nor CSF variables made it through the initial cutoffs for entry as variables in the stepwise linear regression models. Age was significantly associated with baseline digit span forward. Smaller cortical thickness in the right pericalcarine and smaller volumes in the left pallidum and left were significantly associated with lower digit spans. The full models can be found in Table 5.12.

Longitudinal Digit span forward

Digit span forward score APC increased on average of 0.004 (sd = 0.59) in subjects diagnosed with MCI at baseline. Because this study focuses on predicting future decline, we will not further discuss the longitudinal digit span forward models for MCI.

Baseline Digit span backward

In MCI, MRI accounted for 10% of the variance (R^2 = 0.13, Adj. R^2 = 0.10, F = 4.95, p < 0.0001), FDG-PET variables did not make it through the initial cutoffs, and CSF biomarker concentrations accounted for 4% of the variance (R^2 = 0.08, Adj. R^2 = 0.04, F = 2.05, p = 0.09). Combining MRI morphometry with CSF biomarker concentrations, the model accounts for 12% of the variance (R^2 =

0.18, Adj. R^2 = 0.12, F = 2.93, p = 0.008). Gender was significantly associated with worse scores. Lower concentration of $a\beta_{1\text{-}42}$ in the CSF was significantly associated with lower scores as was smaller volume in the left frontal pole. The full models can be found in Table 5.13.

Longitudinal digit span backward

The average APC for digit span backward in MCI was 0.04 (sd = 0.73). Because this study focuses on predicting future decline, we will not further discuss the longitudinal digit span backward models for MCI.

Baseline Trails A

In MCI, MRI accounted for 11% of the variance (R^2 = 0.14, Adj. R^2 = 0.11, F = 4.68, p < 0.0001), FDG PET accounted for 12% of the variance (R^2 = 0.15, Adj. R^2 = 0.12, F = 5.53, p < 0.0001), but no CSF variables made it into the model. Combining FDG PET and MRI accounted for 17% of the variance (R^2 = 0.20, Adj. R^2 = 0.17, F = 6.76, p < 0.0001). Education was significantly associated with baseline Trails A. Thinner cortex in the left isthmus of the cingulate, smaller surface area in the right supramarginal gyrus, and hypometabolism in the precuneus were all significantly associated with longer times to complete Trails A in the multimodal model. The full models can be found in Table 5.14.

Longitudinal Trails A

In the MCI group, the average APC for Trails A was -0.06 (sd = 0.70), indicating that it required less time to complete at follow-up. Because this study focuses on predicting future decline, we will not further discuss the longitudinal Trails A models for MCI.

Baseline Trails B

MRI accounted for 27% of the variance (R^2 = 0.30, Adj. R^2 = 0.27, F = 10.49, $p < 0.0001$), FDG PET accounted for 17% of the variance (R^2 = 0.22, Adj. R^2 = 0.17, F = 5.02, $p < 0.0001$), and no CSF variables made it through the initial cutoff stages. Combining MRI morphometry and FDG PET metabolism accounted for 30% of the variance (R^2 = 0.34, Adj. R^2 = 0.30, F = 10.27, $p < 0.0001$). Education was significantly associated with Trails B in the MCI group. Smaller cortical thickness of the left cingulate, smaller volume of the left inferior parietal, smaller surface areas in the right superior frontal, and hypometabolism in the supramarginal gyrus were significantly associated with increased times to complete Trails B in MCI at baseline. The full models can be found in Table 5.15.

Longitudinal Trails B

In the MCI group, the Trails B APC was -0.03 (sd = 0.50), indicating less time to complete the test at follow-up. Because this study focuses on predicting future decline, we will not further discuss the longitudinal Trails B models for MCI.

Baseline AV 30 minute delayed recall

MRI accounted for 31% of the variance (R^2 = 0.35, Adj. R^2 = 0.31, F = 9.26, p < 0.0001), FDG PET accounted for 1% of the variance (R^2 = 0.03, Adj. R^2 = 0.01, F = 1.61.p = 0.17), and CSF accounted for 4% of the variance (R^2 = 0.08, Adj. R^2 = 0.04, F = 1.99, p = 0.10). Combining MRI morphometry accounted for 30% of the variance (R^2 = 0.34, Adj. R^2 = 0.30, F = 8.47, p < 0.0001), while combining CSF and imaging modalities accounted for 23% of the variance (R^2 = 0.32, Adj. R^2 = 0.23, F = 3.48, p = 0.0003). Age and gender were significantly associated with baseline recall scores in MCI subjects. Larger cortical thickness in the right supramarginal gyrus and larger surface area in the left postcentral gyrus were associated with lower scores. Smaller cortical thickness in the right superior parietal and left insula and smaller volume in the hippocampus were significantly associated with lower scores. The full models can be found in Table 5.16.

Longitudinal AV 30 minute delayed recall

MCI subjects showed an average APC for AV 30 minute delayed recall of -0.03 (sd = 0.61). MRI accounted for 26% of the variance (R^2 = 0.31, Adj. R^2 = 0.26, F = 96.36, p < 0.0001), FDG PET accounted for 1% of the variance (R^2 = 0.04, Adj. R^2 = 0.01, F = 1.41.p = 0.23). Combining MRI morphometry and FDG PET metabolism accounted for 26% of the variance (R^2 = 0.31, Adj. R^2 = 0.26, F = 6.21, p < 0.0001), while combing CSF biomarker concentrations with imaging markers accounted for 12% of the variance (R^2 = 0.26, Adj. R^2 = 0.12, F = 1.85, p

= 0.07). Older age was significantly predictive of greater change. Larger baseline cortical thickness in the left superior parietal, larger baseline volumes in the left entorhinal, left posterior cingulate, and left caudate, and larger baseline surface areas in the right postcentral and left pars opercularis were predictive of greater decline in the multimodal model. The full models can be found in Table 5.17.

Baseline AV delayed recognition

MRI accounted for 15% of the variance (R^2 = 0.18, Adj. R^2 = 0.15, F = 5.35, $p < 0.0001$), while no FDG PET or CSF biomarker concentration variables made it through the initial cutoff steps. Age was a significant predictor of recognition scores. Larger surface area in the left postcentral gyrus was significantly associated with lower AV delayed recognition scores. Smaller cortical thickness in the right middle temporal and volume in the left hippocampus were significantly associated with poorer performance on the AV delayed recognition. The full models can be found in Table 5.18.

Longitudinal AV delayed recognition

MCI subjects showed an average APC for AV delayed recognition score of 0.05 (sd = 0.50), indicating better performance during follow-up. Because this study focuses on predicting future decline, we will not further discuss the longitudinal delayed recognition models for MCI.

AD

Baseline Clock drawing

In AD, MRI accounted for 35% of the variance (R^2 = 0.43, Adj. R^2 = 0.35, F = 5.62, p < 0.0001), FDG PET accounted for 6% of the variance (R^2 = 0.10, Adj. R^2 = 0.06, F = 2.41, p = 0.06), and CSF accounted for 1% of the variance (R^2 = 0.09, Adj. R^2 = 0.01, F = 1.17, p = 0.34). Combining MRI morphometry and FDG PET metabolism accounted for 38% of the variance (R^2 = 0.47, Adj. R^2 = 0.38, F = 5.58, p < 0.0001). Adding CSF biomarker concentrations to imaging variables accounted for 30% of the variance (R^2 = 0.49, Adj. R^2 = 0.30, F = 2.53, p = 0.02). Larger cortical thickness in the left parahippocampal gyrus and the left precuneus and hypermetabolism in the cuneus were significantly associated with lower clock draw scores. Smaller cortical thickness in the right temporal pole, and left inferior parietal and smaller surface area in the left superior frontal were associated with lower clock draw scores. The full models can be found in Table 5.19.

Longitudinal Clock drawing

In the AD group, the average APC was -0.28 (sd = 0.83) for clock draw. MRI accounted for 32% of the variance (R^2 = 0.41, Adj. R^2 = 0.32, F = 4.53, p < 0.0001). No FDG PET variables made it through the initial cutoff stage. Although CSF concentration of pTau made it through the initial cutoff, it did not contribute any additional variance beyond that offered by age, gender, and education in the

linear regression model. Larger baseline cortical thickness in the right fusiform, larger volume in the left paracentral gyrus, and larger baseline surface area of the left lateral occipital regions were predictive of higher APC in clock draw in the AD group. Smaller baseline cortical thickness in the right pericalcarine and smaller baseline surface areas in the left pars triangularis, left entorhinal, and right parahippocampus were significantly predictive of greater APC in clock draw. The full models can be found in Table 5.20.

Baseline Digit span forward

MRI accounted for 36% of the variance (R^2 = 0.44, Adj. R^2 = 0.36, F = 5.81, $p < 0.0001$), FDG PET accounted for less than one percent of the variance (R^2 = 0.04, Adj. R^2 = -0.008, F = 0.82, p = 0.52). No CSF variables made it through the initial cutoff values. Combining MRI morphometry and FDG PET metabolism accounted for 38% R^2 = 0.45, Adj. R^2 = 0.38, F = 5.83, $p < 0.0001$). Education was significantly associated with digit span forward. Larger surface areas in the right pars triangularis, left postcentral gyrus, and left entorhinal, and hypermetabolism in the precuneus were significantly associated with worse performance on the digit span forward task. In addition, smaller volumes in the left pars orbitalis and smaller surface area in the right middle temporal were significantly associated with worse performance on the baseline digit span forward task in the AD subject group. The full models can be found in Table 5.21.

Longitudinal digit span forward

The average APC for the AD group was -0.21 (sd = 0.96). MRI accounted for 30% of the variance (R^2 = 0.37, Adj. R^2 = 0.30, F = 5.45, p < 0.0001), no FDG PET variables made it through the initial cutoff stages, and CSF accounted for 14% of the variance (R^2 = 0.20, Adj. R^2 = 0.14, F = 2.95, p = 0.03). Combining MRI morphometry with CSF biomarker concentration accounted for 35% of the variance (r^2 = 0.48, Adj. R^2 = 0.35, F = 3.69, p = 0.002). Age was significantly predictive of future decline. Larger baseline concentrations of $a\beta_{1\text{-}42}$ in the CSF were predictive of greater decline at follow-up, as was larger baseline surface area in the left superior frontal in the multimodal model for the AD group. The full models can be found in Table 5.22.

Baseline digit span backward

MRI accounted for 31% of the variance (R^2 = 0.38, Adj. R^2 = 0.31, F == 5.17, p < 0.0001), FDG PET accounted for 6% of the variance (R^2 = 0.10, Adj. R^2 = 0.06, F = 2.39, p = 0.06), and CSF accounted for 5% of the variance (R^2 = 0.13, Adj. R^2 = 0.05, F = 1.67, p = 0.17). Combining MRI morphometry and FDG PET metabolism accounted for 31% of the variance (R^2 = 0.38, Adj. R^2 = 0.31, F = 4.91, p < 0.0001). Combining CSF biomarker concentration with imaging variables accounted for 37% of the variance (R^2 = 0.50, Adj. R^2 = 0.37, F = 3.70, p = 0.002). Larger volume in the left pallidum and larger surface areas in the right cuneus, left fusiform were significantly associated with lower scores on the digit span backward. Smaller volume in the left inferior parietal and smaller surface

areas in the right rostral middle frontal and left precuneus were significantly associated with lower scores on the digit span backward. The full models can be found in Table 5.23.

Longitudinal Digit span backward

The average APC for the AD group was -0.21 (sd = 0.98). MRI accounted for 23% of the variance (R^2 = 0.31, Adj. R^2 = 0.23, F = 4.11, p = 0.0002), FDG PET accounted for 8% of the variance (R^2 = 0.12, Adj. R^2 = 0.08, F = 3.01, p = 0.02), and No CSF biomarker concentration variables made it through the initial cutoffs for entry into the model. Combining MRI morphometric and FDG PET metabolic variables increased the variability to 25% (R^2 = 0.32, Adj. R^2 = 0.25, F = 4.27, p = 0.0001). Gender was a significant predictor of decline. Larger baseline surface areas in the left isthmus of the cingulate and left caudal middle frontal were significantly predictive of greater APC at follow-up for digit span backward in AD subjects. Smaller baseline cortical thicknesses in the right cuneus and left frontal pole at baseline were significantly predictive of greater APC at follow-up. The full models can be found in Table 5.24.

Baseline Trails A

MRI accounted for 35% of the variance (R^2 = 0.44, Adj. R^2 = 0.35, F = 5.23, p < 0.0001), FDG PET accounted for 3% of the variance (R^2 = 0.07, Adj. R^2 = 0.03, F = 1.70, p = 0 .16), and CSF accounted for 17% of the variance (R^2 = 0.24, Adj. R^2 = 0.17, F = 3.63, p = 0.01). Combining MRI morphometry and FDG

PET metabolism accounted for 30% of the variance (R^2 = 0.37, Adj. R^2 = 0.30, F = 5.86, p < 0.0001). Combining CSF with imaging markers accounted for 49% of the variance (R^2 = 0.64, Adj. R^2 = 0.49, F = 4.18, p = 0.0004). Smaller cortical thickness in the right transverse temporal, smaller volume in the left inferior parietal, smaller surface area in the right pars triangularis were significantly associated with longer times to complete Trails A. The full models can be found in Table 5.25.

Longitudinal Trails A

The average APC for the AD group was -0.02 (sd = 0.72), in other words, with time, the time to complete Trails A in the AD group decreased. We did not include these models in this paper, as we focus on cognitive decline, and the AD subject showed improvements in performance over time.

Baseline trails B

MRI accounted for 32% of the variance (R^2 = 0.40, Adj. R^2 = 0.32, F = 5.02, p < 0.0001), FDG PET accounted for 12% of the variance (R^2 = 0.16., Adj. R^2 = 0.12, F = 3.53, p = 0.006), and CSF accounted for 10% of the variance (R^2 = 0.17,d. r^2 = 0.10, F = 2.37, p = 0.07). Combining MRI morphometry and FDG PET metabolism accounted for 35% of the variance (R^2 = 0.43, Adj. R^2 = 0.35, F = 5.34, p < 0.0001). Combining CSF with imaging variables accounted for 42% of the variance (R^2 = 0.52, Adj. R^2 = 0.41, F = 4.66, p = 0.0003). Education significantly predicted baseline Trails B in AD subjects. Larger surface area in the

right isthmus of the cingulate was significantly associated with longer times to complete Trails B. Larger concentrations of tTau in the CSF were significantly associated with longer times to complete Trails B. Smaller cortical thickness in the left precuneus, smaller volumes in the left temporal pole, and smaller surface area in the right insula were significantly associated with longer times to complete Trails B. The full models can be found in Table 5.26.

Longitudinal Trails B

For the AD group, the average APC on Trails B was 0.15 (sd = 1.21). MRI accounted for 24% of the variance (R^2 = 0.32, Adj. R^2 = 0.24, F = 3.92, p = 0.0002) and FDG PET accounted for 4% of the variance (R^2 = 0.08, Adj. R^2 = 0.04, F = 1.82, p = 0.13). No CSF variables made it through the initial cutoffs. Combining MRI morphometry with FDG PET metabolism accounted for 25% of the variance (R^2 = 0.34, Adj. R^2 = 0.25, F = 4.0, p = 0.0002). Smaller baseline volume in the right lateral orbitofrontal, and smaller baseline surface area in the right postcentral gyrus were predictive of greater decline during the follow-up period. Larger baseline volumes in the left rostral middle frontal and left hippocampus and larger baseline surface areas in the right entorhinal and left frontal pole were predictive of greater decline in Trails B during follow-up. The full models can be found in Table 5.27.

Baseline AV 30 minute delayed recall

In the AD group, MRI accounted for 29% of the variance (R^2 = 0.37, Adj. R^2 = 0.29, F = 4.74, p < 0.0001) and FDG PET accounted for 7% of the variance (R^2 = 0.12, Adj. R^2 = 0.07, F = 2.32, p = 0.05). No CSF variables made it through the initial cutoff. Combining MRI morphometry and FDG PET metabolism increased the variance accounted for to 34% (R^2 = 0.43, Adj. R^2 = 0.34, F = 4.75, p < 0.0001). Larger cortical thickness in the right lingual, larger surface areas in the right rostral middle frontal and right lateral occipital, and hypermetabolism in the supramarginal gyrus were significantly associated with lower scores on AV 30 minute delayed recall at baseline in the AD group. Smaller cortical thickness in the right superior temporal and smaller surface areas in the right paracentral gyrus were significantly associated with worse performance on AV 30 minute delayed recall at baseline. The full models can be found in Table 5.28.

Longitudinal AV 30 minute delayed recall

The average APC for the AD group on AV 30 minute delays scores was -0.41 (sd = 0.38). MRI accounted for 68% of the variance (R^2 = 0.78, Adj. R^2 = 0.68, F = 7.65, p = 0.0001) and FDG PET accounted for less that one percent of the variance (R^2 = 0.11, Adj. R^2 = -0.04, F = 0.72, p = 0.59). No CSF biomarker variables made it through the initial cutoff. Combining MRI morphometry and FDG PET metabolism accounted for 78% of the variance (R^2 = 0.86, Adj. R^2 = 0.78, F = 10.40, p < 0.0001). Larger baseline cortical thickness in the parahippocampal gyrus and larger baseline surface area in the left pericalcarine

were significantly predictive of greater decline during follow-up. Smaller baseline volumes in the superior parietal, right frontal pole and smaller baseline surface areas in the right inferior parietal were significantly predictive of higher APC during the follow-up interval. The full models can be found in Table 5.29.

Baseline AV delayed recognition

MRI accounted for 36% of the variance (R^2 = 0.42, Adj. R^2 = 0.36, F = 6.89, $p < 0.0001$) and FDG PET accounted for 11% of the variance (R^2 = 0.16, Adj. R^2 = 0.11, F = 3.21, p = 0.01). No CSF biomarker concentration variables made it through the initial cutoffs. Combining MRI morphometry and FDG PET metabolism accounted for 35% of the variance (R^2 = 0.42, Adj. R^2 = 0.35, F = 6.34, $p < 0.0001$). Age was significantly associated with delayed recognition scores. Larger cortical thickness in the right transverse temporal, larger volumes in the left frontal pole and brainstem, and hypermetabolism in the superior temporal were significantly associated with lower AD delayed recognition scores. In addition, smaller cortical thickness in the left entorhinal and smaller surface area in the right superior temporal were significantly associated with lower AV delayed recognition scores in the AD subject group at baseline. The full models can be found in Table 5.30.

Longitudinal AV delayed recognition

The average APC was -0.10 (sd = 0.63), thus the group decreased in their AV delayed recognition score over time. MRI accounted for 20% of the variance

(R^2 = 0.28, Adj. R^2 = 0.20, F = 3.41, p = 0.0014) and FDG PET accounted for 4% of the variance (R^2 = 0.09, Adj. R^2 = 0.04, F = 1.93, p = 0.11). No CSF biomarker baseline concentrations made it through the initial cutoffs. Combining MRI morphometry and FDG PET metabolism accounted for 23% of the variance (R^2 = 0.30, Adj. R^2 = 0.23, F = 4.08, p = 0.0004). Larger baseline cortical thickness in the left isthmus of the cingulate and larger baseline volume in the left lingual were significantly predictive of increased APC for AV delayed recognitions. In addition, smaller baseline volume in the left entorhinal, smaller baseline surface areas in the right fusiform, and baseline hypometabolism in the posterior cingulate were significantly predictive of increased APC during follow-up. The full models can be found in Table 5.31.

DISCUSSION

In this study, we identified the baseline morphometric, metabolic, and CSF biomarker variables associated with baseline performance and decline in clock drawing, trails A and B, digit span forward and backward, and RAVLT delayed recall and recognition. We addressed two main hypotheses: MRI and FDG PET would independently account for variance in baseline neuropsychological test scores; and combining both modalities would improve prediction. In addition, we assessed the contribution of CSF biomarker concentrations to account for variance in neuropsychological performance at baseline and amount of average annualized decline in cognition. The results of this study indicate that MRI performs better than FDG PET or CSF measures at accounting for variance in

the neuropsychological measures at every stage of disease. Combining modalities did not consistently improve the adjusted R^2 values, nor did FDG PET and CSF alone account for any variance. In many instances, no FDG PET or CSF biomarker concentration variables made it through the initial cutoff stages of building the models. Each of the tests was associated with measures related to widespread regions in the brain, which suggests that each of these tests involves a network of neuronal processing for efficient function. In addition, different regions were typically predictive of baseline performance and decline within each group, and the regions and types of measures varied between groups illustrating the complex nature of structure-function relationships and the impact of disease upon them.

A number of imaging variables showed opposite relationships than originally anticipated (e.g. larger volumes predicting worse test scores or greater decline). While we are still investigating the exact origins of this negative relationship, in some cases it is likely the result of interactions between variables in the model, such as precentral FDG metabolism in MCI for Trails A. This interpretation is supported by the assessment run during the screening process, where regression was run using each variable separately and the directionality of the relationship was opposite to that found in the final multivariate model. Other instances where this may be the case is FDG metabolism of the pericalcarine and inferior parietal in baseline normal aging clock score, FDG metabolism in the superior temporal, superior frontal, and fusiform for MCI baseline Trails B,

cortical thickness in the right supramarginal gyrus for baseline MCI delayed recall, left precuneus cortical thickness for baseline AD clock drawing, and FDG metabolism for the postcentral gyrus in Trails A normal aging decline.

For the inverse relationships that are not the result of potential interaction effects, one potential explanation is that is represents a compensatory mechanism. This phenomenon is not well understood, but has been observed previously (Browndyke et al. 2012; Caroli et al. 2010; Clément & Belleville 2010; Clément et al. 2012; Guedj et al. 2009; Leyhe et al. 2009; Mufson et al. 2012; Qi et al. 2010). The underlying premise being that these brain regions are more associated with a specific task than would normally be the case to help cope with the loss of function in related structures (e.g. the pericalcarine may be compensating for decreased visuospatial processing abilities in other brain regions). Undoubtedly, this accounts for some of the inverse relationships that we observed. Finally, it is feasible that when looking at APC, the relationships with directions opposite to that expected are a byproduct of more rapid and variable rates of disease progression. More studies are needed for us to better understand these complex relationships.

Clock Drawing

The clock drawing test utilizes a number of cognitive functions, including visuospatial ability, executive function, comprehension, motor ability, and semantic memory (Leyhe et al. 2009; Rouleau et al. 1992; Royall et al. 1998; Shulman 2000). It has been argued that difficulties in clock drawing mostly reflect

impairments of visuospatial ability (Mendez et al. 1992; Sunderland et al. 1989), while others have argued that it is more heavily influenced by semantic memory and executive function (Libon et al. 1996; Rouleau et al. 1992; Tuokko et al. 1992). Our results would suggest that multiple cognitive systems are associated with performance of the clock drawing test. In all groups frontal, parietal, and temporal regions were associated with clock draw scores, although the specific regions differed. In normal aging, left surface areas in the caudal middle frontal and pars triangularis were predictive of baseline performance, while in MCI the cortical thickness in the right caudal middle frontal was associated with baseline performance. In AD the frontal regions changed to the left superior frontal and left pars orbitalis. These results indicate that poorer performance on the clock drawing test may be related to increased levels of frontal lobe damage, agreeing with the argument in favour of frontal executive functioning involvement. In addition, nearly the entire right occipital lobe was involved with baseline performance in normal aging, but these areas were not associated with baseline performance in either MCI or AD. The posterior and isthmus of the cingulate were predictive of baseline performance in normal aging and MCI, respectively, which supports the notion that this test involves some memory component, as these regions are heavily connected to the hippocampus and MTL structures. Providing further support for a memory component is that the left parahippocampal gyrus was predictive of baseline scores in the AD group, suggesting that decrease cortical thickness in this region is associated with lower

scores on the clock drawing test. Clock drawing scores has previously been shown to be inversely related to tangle counts in the parietal lobe and the parahippocampal gyrus, as well as to neuronal count in the parahippocampal gyrus (Förstl et al. 1993). In addition, evidence suggests that the right parahippocampus, which in our case was predictive of APC in the AD group, is required for spatial memory and for accurate schematic spatial representations of familiar environments (Bohbot et al. 1998; Bohbot et al. 2000; Johnsrude et al. 1999; Moscovitch et al. 2005; Owen et al. 1996). Perhaps in normal aging and MCI, the spatial memory and representations are not impaired enough to see associations with the parahippocampal gyrus. Also, the switch from left to right hemisphere in association with baseline and decline in the AD group suggests that perhaps the left hemisphere is affected first, followed by the right hemisphere. Visual information is processed in two streams, the dorsal, or where, and the ventral, or what, pathways. Because MCI and AD affect structures in both of these streams (e.g. parietal and temporal), one might expect to see associations between both parietal and temporal structures with clock drawing performance. In fact, we observed increasing involvement of both the parietal and temporal regions with increasing disease severity. In addition, more temporal structures were predictive of future APC than parietal structures. It has previously been shown that the right posterior temporal lobe is associated with semantic knowledge about the clock's minute hand (Leyhe et al. 2009), while the parietal lobe plays more of a role in detecting spatial relationships among

objects, which might be important for proper numbering of the clock (Ungerleider & Haxby 1994). The parietal lobe has also been associated with spatial construction ability and figure design ability, as damage to this area causes impairment on spatial reconstruction ability (Takahashi et al. 2008). In our subjects, the parietal lobe was increasingly involved with clock drawing abilities as the disease progressed. In addition, the types of variables involved reflects the idea that glucose metabolism is affected prior to structural changes in AD, with changes in FDG associated with baseline performance in normal aging and structural MRI measures associated with baseline performance in both MCI and AD groups. Interestingly, it was the inferior parietal lobule that showed this pattern.

Trails A

The neural correlates of Trails A are not well identified and it has not been well characterized on its own in normal aging, MCI, and AD, as it tends to be used in conjunction with Trails B. We examined both tests individually, rather than taking the ratio of the two, because with ratios, it is unknown whether it is the numerator or denominator that is the driving force behind the relationship. Trails A is thought to reflect abilities in visual scanning, graphomotor and psychomotor speed, and attention, as such, we would expect to see associations with the occipital areas, precentral gyrus, and regions critical to attention. Indeed, our results support each of these roles of Trails A. At baseline, visual regions were left lateralized and were observed in the lateral occipital and lingual areas in

normal aging and AD, respectively. In the MCI group, the left lateral occipital volume was predictive of decline, while the baseline left cortical thickness of the pericalcarine was predictive of decline in AD. The occipital cortex has previously been implicated in object-based attention (Hou & Liu 2012), in agreement with our results. Reflecting the motor component of Trails A, baseline scores were associated with the precentral gyrus in normal aging and MCI groups. Baseline FDG uptake in the precentral and postcentral gyri was predictive of APC in the normal aging group, while surface area of the left paracentral gyrus was predictive of APC in the MCI group, confirming the role of brain regions controlling motor function in Trails A. Attention has also been implicated in Trails A. There are various forms of attention that may be more closely linked with distinct brain regions. Selective attention, whereby attention is focused on a single stimulus, while ignoring irrelevant information, is modulated by posterior parietal systems. These areas are important for orienting and shifting attention and may be modulated by basal ganglia structures (R. J. Perry & Hodges 1999). According to the Posner model, the intraparietal sulcus/superior parietal lobe and the temporoparietal junction are involved orienting attention to the appropriate location along with the frontal eye fields and inferior frontal gyrus (Steven E Petersen & Michael I Posner 2012; M I Posner & S E Petersen 1990). We observed supramarginal and inferior parietal associations in baseline performance of Trails A in MRI and AD subject groups. In addition, the pars triangularis portion of the inferior frontal was associated with baseline Trails A in

the AD group. This region along with the pars orbitalis was also predictive of APC in AD. In our subjects, Trails A was not predicted by the frontal eye fields, which are located in the caudal middle frontal gyrus (Blanke et al. 2000), but rather by the rostral middle frontal gyrus at baseline and APC. Thus, our results support the attention component of Trails A. We observed a significant increase in time to complete Trails A in the AD group as baseline. This may be the result of poor working memory, as reflected by increased involvement of memory structures in the model, or decreased attentional capacity, as indicated by greater involvement of attentional structures. In MCI and AD, as disease severity increased, more temporal and parietal regions were associated with Trails A, indicating that completion of the task relied more heavily on the memory network. This is also supported by the influence of baseline cortical thickness of the right isthmus of the cingulate on APC in MCI and AD groups. Similarly, the temporal lobe at baseline was predictive of APC in all three groups, particularly in the inferior temporal and banks of the superior temporal sulcus. Based on this we can conclude that our data-driven approach successfully identified neural correlates of Trails A components in our three subject groups and that MRI was able to predict baseline and APC performance better than FDG PET.

Trails B

Similar to Trails A, Trails B also involves visual scanning, graphomotor and psychomotor speed and attention. However, because the test requires the switching between numbers and letters, there are components of cognitive

flexibility and set shifting, both of which are typically thought of as part of the executive function domain, which is mainly thought to be the realm of the frontal lobes. Thus, we might expect to observe involvement from the frontal lobe, reflecting set shifting abilities, the medial temporal and cingulate regions, reflecting working memory abilities required to keep track of where one is in the sequence of numbers/letters, and perhaps occipital regions reflecting the visual processing component of the test. Previous studies using fMRI have shown increased activation compared to Trails A in the left middle frontal gyrus, precentral gyrus, cingulate, superior frontal, medial frontal, insula, paracentral, and middle and superior temporal areas (Zakzanis et al. 2005). In addition, previous studies have suggested that the strongest predictor of Trails B performance is atrophy of the medial temporal lobe (Oosterman et al. 2010). The same study also cited correlations between performance on Trails B and working memory, executive function, speed, attention, and episodic memory, thus the regions critical to each of these skills may very likely be associated with Trails B baseline performance or APC. In fact, Pa and colleagues (PA et al. 2010) reported widespread correlations with trails B switch performance, involving gray matter of the frontal, parietal, temporal, and occipital lobes. Our results show that there is increasing involvement of frontal regions and decreased involvement of temporal regions in MCI and AD compared to normal aging. In addition, temporal and frontal regions tended to be the most predictive of APC, reflecting the roles of memory and executive processing in Trails B.

Digit Span Forward

Digit span forward is thought to be a measure of attention (Cohen & Jr 1993). It may be associated more with the left hemisphere than the right hemisphere, as brain injury to the left hemisphere can lead to an impaired digit span (F. W. Black 1986). Although our results showed about equal representation of the left and right hemispheres at baseline, we did observe an increased representation of the left hemisphere when predicting APC. In this case, 6 of the regions were in the right hemisphere, while 12 were in the left hemisphere. In the AD group, the variables most highly associated with digit span forward were the right middle temporal, left postcentral gyrus, left pars orbitalis, and the left entorhinal cortex. In MCI, the left hippocampus and right pericalcarine were most highly associated with digit span forward, while in normal aging, it was the right pars orbitalis, right pericalcarine, and right rostral middle frontal. There is a noticeable shift as the disease progresses to involve more memory structures, such as the hippocampus and entorhinal cortex, which indicates that the task becomes less of an attention task and more of a memory task as memory function worsens. It is not surprising that the pars orbitalis is involved, as it plays a role in speech production, what is interesting is the shift from the right hemisphere to the left hemisphere in normal aging and AD, respectively. The left pars orbitalis is the location of Broca's area and is typically thought to be involved in speech production, while the right pars orbitalis has been implicated in error inhibition on verbal tasks (Geva et al. 2012), inhibitory

control (Poirel et al. 2012). The middle temporal gyrus is involved in a number of cognitive processes, one of which is language processing (Cabeza & Nyberg 2000). Thus, our results indicate that as the AD progresses from normal aging through MCI, the brain regions involved are those subserving memory and language processing regions.

Digit Span Backward

Digit span backward is thought to be a measure of the capacity of verbal working memory (R. Li et al. 2012). It involves storage and maintenance of the numbers in working memory as well as transformation of the data to reorder the numbers into reverse sequence. The highest predictors of baseline performance in normal aging were the right pericalcarine, right rostral middle frontal, left isthmus of the cingulate, and metabolism in the paracentral gyrus. In MCI subjects, MRI morphometry in the left frontal pole and left paracentral gyrus and, in AD subjects, the right rostral middle frontal, left inferior parietal, left pallidum, and right cuneus were most highly associated with digit span backward. The dorsolateral prefrontal cortex and inferior parietal lobule have previously been associated with digit span backward performance in neurodegenerative disorders (Amici et al. 2007). Involvement of the isthmus of the cingulate hints at the memory component of the task. This region was also predictive of APC in the normal and AD groups, while the caudal anterior cingulate was predictive of decline in MCI subjects.

RAVLT Delayed Recall

Baseline recall scores in normal aging were most highly associated with paracentral metabolism and MRI morphometry in the right isthmus of the cingulate, right inferior temporal, and right caudal middle frontal regions. Recall score in MCI were most highly associated with right superior parietal, right supramarginal, and left hippocampal morphometry. Scores in AD were most associated with MRI morphometry in the right superior temporal, right lingual, and right rostral middle frontal regions, along with metabolism in the entorhinal and supramarginal gyrus. Hippocampal associations with recall in the MCI group provide support for the thought that there may be a connection between episodic memory and NFT pathology in the medial temporal lobes. The associations between frontal and parietal regions with recall scores is not surprising, as these regions have been shown to subserve working memory ability (Champod & Michael Petrides 2007). The posterior/isthmus of the cingulate as well as the precuneus and prefrontal regions are highly interconnected with the medial temporal lobes and have previously been shown to play a role in memory function. The prefrontal cortex contributes to encoding and retrieval of accurate memory (M. P. Alexander et al. 2009; Blumenfeld & Ranganath 2007), with the left ventrolateral prefrontal cortex being critical to semantic access at memory encoding (Logan et al. 2002; Otten et al. 2001). In our study, surface area in the right posterior cingulate and metabolism in the isthmus of the cingulate were predictive of recall score in normal aging and MCI, respectively. In a study

examining the correlations between baseline FDG metabolism and subsequent decline in verbal memory in pre-MCI individuals, the posterior cingulate, bilateral parietal, and left prefrontal were all correlated with higher rates of decline. Interestingly, in the same study, those who did not decline, but remained in the normal aging category at follow-up, showed significant correlations in the posterior and mid-cingulate regions with verbal memory decline. This indicates that it may be increased involvement of the parietal and frontal lobes that is predictive of future decline, more than the cingulate, as the cingulate was involved with verbal memory in both those who did not decline and those who did (Caselli et al. 2008). Interestingly, in a study with AD subjects examining various stages of recall based on the immediate recall trials and delayed recall and recognition trials of the RAVLT, different brain regions were implicated at different stages of recall. In the early immediate recall trials (e.g. trials 1 through 3), the scores were correlated with cortical thickness of the inferior parietal, middle frontal, temporal pole, and supramarginal gyrus. Later immediate recall trials (e.g. 5 plus) were correlated with the medial temporal lobe and temporal pole. In delayed recall, the hippocampus correlated with performance (Wolk & Dickerson 2011). In our study, the hippocampus did not predict recall scores in the AD population. We did observe, however, associations with the entorhinal, rostral middle frontal, superior temporal, and the supramarginal gyrus, which were associated with earlier recall trials in the Wolk study (Wolk & Dickerson 2011). The hippocampus was implicated in the MCI group for recall, which would

suggest that in our method, the hippocampus is more sensitive to early rather than late deficits in recall.

One difficulty in assessing the impact of deficits in recall is that it may represent problems in either learning or in retention, since both would affect the ability to recall information after delays. Although the present study did not separate the results into retention and learning, a previous study in MCI subjects examined high vs. low retainers and learners (Chang et al. 2010). They observed that both learning and retention were significantly correlated with cortical thickness in the lateral and medial frontal cortex, lateral temporal, medial temporal, anterior temporal, parietal, and anterior and posterior cingulate cortices. Meanwhile, retention on its own, after removing the effects of learning, showed correlations with the anterior, medial, and ventral temporal lobe, entorhinal, parahippocampus, temporal pole, fusiform, and hippocampus. Thus, retention tended to involve more medial structures, while learning was more widespread. When this is applied to our results, we can conclude based on the regions predictive of recall scores, that in normal aging, recall is mainly affected by difficulties with retention, as predominantly temporal regions were involved. In our MCI and AD subjects, we observed more widespread changes, involving temporal as well as frontal and parietal regions, suggesting that as memory deficits progress, there becomes more difficulties in both learning and retention. It is also possible that as medial temporal regions become increasingly atrophic, that they are no longer able to mediate memory function and other brain regions

are recruited. This has been observed in functional imaging studies that show the compensatory involvement of a number of regions including the frontal (Clément & Belleville 2010; Clément & Belleville 2012; Clément et al. 2012) and cingulate cortices (Caroli et al. 2010; Clément et al. 2012). Of note, in the AD group we observed involvement of the medial orbitofrontal regions with recall scores. The medial orbitofrontal cortex is associated with the ability to inhibit irrelevant information (Happaney et al. 2004; D. T. Stuss & M. P. Alexander 2007), this suggests that in AD, the subjects are not able to inhibit the incorrect information to correctly identify which words to recall (e.g. the test words, rather than the interference words).

RAVLT Delayed Recognition

Recall requires the generation of the mental representation of the original stimuli, whereas in the recognition condition, the original stimuli are presented again intermixed with distracter stimuli. Previous studies have shown that in AD, recognition more is heavily dependent on perirhinal and entorhinal cortices, rather than the hippocampus, which is implicated in delayed recall(Kerchner et al. 2012; Wolk & Dickerson 2011). In our subjects, the hippocampus was predictive of baseline performance in MCI and normal aging, while the entorhinal cortex was predictive of baseline performance in AD. In addition, the entorhinal cortex was predictive of APC in the AD group. This supports the theory that recognition relies on the entorhinal cortex in AD, but it also suggests that the hippocampus is more predictive of recognition at earlier stages of dementia. Our

results conflict to some degree with a recent study by Walhovd (K B Walhovd, A M Fjell, A M Dale, et al. 2010), in which entorhinal metabolism accounted for 15% of the variance in recognition scores in normal aging, while the parahippocampal gyrus accounted for the most variance in the MCI group and genetic variables, rather than imaging variables, predicted AD recognition scores. In our study, the parahippocampal gyrus did not predict baseline of APC in any group, which may be the result of differences in post-processing or other methodological differences. In addition, our FDG PET data was more strictly corrected for partial volume effects, which likely contributed to some of the discrepancies as well. The medial temporal lobes are thought to be associated with memories that are automatically retrieved given the appropriate cues, whereas memory that involves strategies and context (Strategic, explicit memory), may involve more prefrontal areas. Along these line, we observed greater temporal and cingulate involvement than prefrontal involvement in baseline performance, but when predicting future change in MCI and AD, there were a number of inferior frontal regions that contributed to the model. Given that the task is auditory, it is not surprising that a number of auditory processing areas, such as the middle and superior temporal gyri are associated with recognition scores on the RAVLT.

CONCLUSION

At baseline, we observed progressively worse scores on neuropsychological tests of visuospatial abilities, attention, executive function,

delayed recall, recognition, and working memory in MCI and AD at baseline. However, over time, the MCI group declined mainly on delayed recall, whereas the AD group declined on everything but Trails A. We generated statistical models for predicting baseline performance and future decline within MCI and AD of scores from a number of neuropsychological tests, which address specific cognitive functions. Overall, the models indicate that MRI was better able to predict baseline scores and future decline than either FDG PET of CSF biomarker concentrations. The brain regions that were associated with each tasks highlighted the types of cognitive skills required for successful completion of the test and also highlighted that these regions, when damaged, can result in poor memory, executive function, and visuospatial abilities.

The results of this study provide insight into which types of cognitive functions might be best used in clinical trials as indices of disease severity and amount of decline. As increasing number of drug trials fail in later stages of testing, it is imperative to reanalyze the types of markers used to measure the success or failure of the treatments. The results of this study suggest that the imaging and CSF biomarkers most telling of disease severity and decline may be outside the medial temporal lobes and that perhaps it is these other regions, such as the frontal, parietal, and cingulate cortices that may be more telling clinical end points.

Table 5.1 Demographic information

	Baseline Subjects (m/f)	**Age mean years (std dev)**	**Education Mean (std dev)**	**MMSE**
Normal Aging	105 (64/41)	75.81 (4.75)	15.90 (3.12)	28.98 (1.12)
MCI	204 (137/67)	75.44 (7.22)	15.80 (2.88)	27.15 (1.71)[a]
AD	94 (56/38)	74.91 (7.37)	14.61 (3.21)[a,b]	23.48 (2.14)[a,b]

[a] significant difference from normal aging ($p < 0.05$), [b] significant difference from MCI ($p < 0.05$).

Table 5.2a. Baseline ANOVA results showing mean (sd) scores from each of the neuropsychological and cognitive tests for normal aging, MCI, and AD. Tukey's post-hoc results are presented in the last three columns, whereby a change in letter between groups indicates a significant change.

	df	Mean normal aging (sd)	Mean MCI (sd)	Mean AD (sd)	F-value	P-value	Normal Aging	MCI	AD
CDR Memory	2	0 (0)	0.57 (0.19)	1.03 (0.34)	586.87	<.0001	c	b	a
CDR judgement and problem solving	2	0.03 (0.13)	0.37 (0.25)	0.86 (0.36)	262.05	<.0001	c	b	a
CDR global	2	0 (0)	0.5 (0)	0.80 (0.25)	1169.73	<.0001	c	b	a
MMSE	2	28.98 (1.12)	27.15 (1.71)	23.48 (2.14)	272.07	<.0001	a	b	c
Clock draw	2	4.58 (0.76)	4.24 (0.93)	3.33 (1.31)	42.45	<.0001	a	b	c
Digitspan forward	2	8.68 (2.03_	8.10 (1.91)	7.19 (1.83)	15.05	<.0001	a	a	b
Digit Span backward	2	7.17 (2.12)	6.16 (2.07)	4.66 (2.00)	36.97	<.0001	a	b	c
Trails A	2	93.36 (44.79)	125.86 (68.69)	192.26 (94.19)	49.81	<.0001	b	b	a
Trails B	2	37.36 (13.40)	43.37 (21.50)	70.24 (38.73)	50.75	<.0001	c	b	a
RAVLT 30 minute delayed recall	2	7.31 (3.83)	3.07 (3.44)	0.61 (1.33)	114.9	<.0001	a	b	c
RAVLT 30 minute delayed recognition	2	12.51 (2.93)	10.00 (3.59)	7.31 (3.98)	53.96	<.0001	a	b	c
RAVLT 30 minute delayed recognition errors	2	0.82 (1.14)	2.00 (2.44)	3.19 (2.64)	28.14	<.0001	c	b	a

Table 5.2b. Annual percent change (APC) ANOVA results showing mean (sd) APC from each of the neuropsychological and cognitive tests for normal aging, MCI, and AD during follow-up. Tukey's post-hoc results are presented in the last three columns, whereby a change in letter between groups indicates a significant change.

	df	Mean APC normal aging (sd)	Mean APC MCI (sd)	Mean APC AD (sd)	F-value	P-value	Normal Aging	MCI	AD
Clock draw	2	0.11 (0.83)	0.03 (0.59)	-0.28 (0.83)	8.3	0.0003	a	a	b
Digit span forward	2	0.12 (0.55)	0.004 (0.59)	-0.15 (0.98)	3.98	0.02	a	ab	b
Digit span backward	2	0.13 (0.35)	0.04 (0.73)	-0.21 (0.96)	6.21	0.002	a	a	b
Trails A	2	0.14 (0.49)	-0.06 (0.70)	-0.02 (0.72)	3.27	0.04	a	a	a
Trails B	2	-0.06 (0.01)	-0.03 (0.50)	0.15 (1.21)	2.86	0.06	b	ab	a
RAVLT 30 minute delayed recall	2	0.14 (0.86)	-0.03 (0.61)	-0.41 (0.38)	7.12	0.001	a	a	b
RAVLT 30 minute delayed recognition	2	-0.005 (1.16)	0.05 (0.50)	-0.10 (0.63)	1.25	0.29	a	a	a

Table 5.3. Models predicting baseline clock drawing in normal aging subjects. The MRI model accounted for 43% of the variance, FDG PET accounted for 32% of the variance, and combining modalities accounted for 49% of the variance.

	MRI MODEL			FDG PET MODEL			MULTIMODAL MODEL		
	Parameter Estimate	p-value	Standardized Estimate	Parameter Estimate	p-value	Standardized Estimate	Parameter Estimate	p-value	Standardized Estimate
Age	-0.06	<.0001	-0.35	-0.05	0.001	-0.31	-0.06	<.0001	-0.36
Gender	-0.14	0.26	-0.09	-0.05	0.72	-0.03	-0.06	0.63	-0.04
Education	0.07	0.001	0.30	0.08	0.0002	0.34	0.07	0.0003	0.30
Right pericalcarine cortical thickness	-2.05	0.003	-0.23	--	--	--	-1.88	0.01	-0.21
Right posterior cingulate cortical thickness	1.49	0.0002	0.31	--	--	--	1.45	0.0003	0.30
Left caudal middle frontal surface area	-0.0003	0.09	-0.13	--	--	--	-0.0003	0.05	-0.15
Left pars triangularis surface area	-0.001	<.0001	-0.34	--	--	--	-0.001	0.0002	-0.31
Right temporal pole surface area	0.002	0.13	0.12	--	--	--	0.002	0.08	0.13
Right lingual surface area	0.0004	0.02	0.19	--	--	--	0.0004	0.05	0.16
Cuneus FDG PET	--	--	--	-0.0002	0.01	-0.58	-0.0001	0.01	-0.22
Inferior parietal FDG PET	--	--	--	0.0001	0.19	0.22	--	--	--
Lateral occipital FDG PET	--	--	--	-0.0001	0.06	-0.25	--	--	--
Pericalcarine FDG PET	--	--	--	0.0001	0.06	0.31	--	--	--

Table 5.4. Models predicting baseline digit span forward in normal aging subjects. The MRI model accounted for 36% of the variance, FDG PET accounted for 10% of the variance, and combining modalities accounted for 36% of the variance.

	MRI MODEL			FDG PET MODEL			MULTIMODAL MODEL		
	Parameter Estimate	p-value	Standardized Estimate	Parameter Estimate	p-value	Standardized Estimate	Parameter Estimate	p-value	Standardized Estimate
Age	-0.07	0.05	-0.17	-0.07	0.07	-0.18	-0.05	0.20	-0.12
Gender	-0.39	0.30	-0.09	-0.03	0.94	-0.01	-0.37	0.33	-0.09
Education	0.11	0.05	0.17	0.15	0.03	0.23	0.13	0.03	0.21
Rright pericalcarine cortical thickness	6.12	0.003	0.26	--	--	--	5.71	0.01	0.25
Left fusiform cortical thickness	-1.59	0.16	-0.14	--	--	--	-2.50	0.01	-0.22
Right rostral middle frontal cortical thickness	-2.39	0.06	-0.20	--	--	--	--	--	--
Right isthmus of the cingulate volume	0.001	0.04	0.18	--	--	--	0.001	0.02	0.21
Right superior parietal surface area	0.0004	0.18	0.12	--	--	--	--	--	--
Left superior temporal surface area	0.001	0.17	0.13	--	--	--	0.001	0.12	0.15
Right pars orbitalis surface area	-0.01	0.0003	-0.34	--	--	--	-0.01	0.003	-0.28
Left inferior parietal surface area	0.001	0.06	0.16	--	--	--	0.001	0.04	0.18
Pallidum FDG PET	--	--	--	-0.001	0.06	-0.19	-0.001	0.03	-0.19

Table 5.5. Models predicting baseline digit span backward in normal aging subjects. The MRI model accounted for 31% of the variance, FDG PET accounted for 5% of the variance, and combining modalities accounted for 36% of the variance.

	MRI MODEL			FDG PET MODEL			MULTIMODAL MODEL		
	Parameter Estimate	p-value	Standardized Estimate	Parameter Estimate	p-value	Standardized Estimate	Parameter Estimate	p-value	Standardized Estimate
Age	-0.07	0.06	-0.17	-0.04	0.36	-0.09	-0.07	0.07	-0.15
Gender	-0.37	0.34	-0.09	-0.26	0.57	-0.06	-0.28	0.46	-0.07
Education	0.08	0.20	0.12	0.09	0.18	0.14	0.09	0.14	0.14
Right pericalcarine cortical thickness	10.72	<.0001	0.44	--	--	--	10.62	<.0001	0.44
Left entorhinal cortical thickness	-0.71	0.15	-0.13	--	--	--	-0.79	0.12	-0.14
Right rostral middle frontal cortical thickness	-2.81	0.02	-0.22	--	--	--	--	--	--
Right rostral anterior cingulate volume	-0.001	0.06	-0.16	--	--	--	-0.001	0.01	-0.21
Right pars triangularis volume	-0.0004	0.14	-0.13	--	--	--	-0.001	0.05	-0.18
Left isthmus of the cingulate surface area	0.004	0.02	0.20	--	--	--	0.004	0.02	0.20
Right transverse temporal surface area	-0.01	0.03	-0.20	--	--	--	-0.01	0.01	-0.24
Paracentral FDG PET	--	--	--	0.0002	0.02	0.23	--	--	--

Table 5.6. Models predicting baseline Trails A in normal aging subjects. The MRI model accounted for 34% of the variance, FDG PET accounted for 14% of the variance, and combining modalities accounted for 36% of the variance.

	MRI MODEL			FDG PET MODEL			MULTIMODAL MODEL		
	Parameter Estimate	p-value	Standardized Estimate	Parameter Estimate	p-value	Standardized Estimate	Parameter Estimate	p-value	Standardized Estimate
Gender	2.06	0.43	0.08	-2.24	0.43	-0.08	0.12	0.96	0.004
Education	0.36	0.36	0.08	-0.09	0.84	-0.02	0.19	0.63	0.04
Left caudal anterior cingulate cortical thickness	-4.67	0.18	-0.12	--	--	--	--	--	--
Right transverse temporal cortical thickness	-9.49	0.03	-0.20	--	--	--	-10.83	0.02	-0.22
Right temporal pole volume	0.01	0.002	0.27	--	--	--	0.01	0.01	0.23
Left lateral occipital volume	-0.002	0.04	-0.18	--	--	--	-0.001	0.07	-0.16
Right caudate volume	-0.01	0.02	-0.21	--	--	--	-0.01	0.06	-0.17
Left rostral middle frontal surface area	-0.01	0.01	-0.28	--	--	--	-0.01	0.004	-0.30
Left insula surface area	0.02	0.01	0.26	--	--	--	0.02	0.09	0.17
Right precentral surface area	-0.01	0.03	-0.23	--	--	--	-0.01	0.06	-0.20
Right lateral orbitofrontal surface area	0.02	0.004	0.27	--	--	--	0.02	0.01	0.26
Frontal pole FDG PET	--	--	--	-0.002	0.001	-0.39	-0.001	0.04	-0.21
Insula FDG PET	--	--	--	0.003	0.002	0.34	0.002	0.01	0.24

Table 5.7. Models predicting APC of Trails A in normal aging subjects. The MRI model accounted for 22% of the variance, FDG PET accounted for 8% of the variance, and combining modalities accounted for 29% of the variance.

	MRI MODEL			FDG PET MODEL			MULTIMODAL MODEL		
	Parameter Estimate	p-value	Standardized Estimate	Parameter Estimate	p-value	Standardized Estimate	Parameter Estimate	p-value	Standardized Estimate
Age	-0.01	0.29	-0.10	-0.004	0.68	-0.04	-0.01	0.24	-0.11
Gender	0.09	0.37	0.09	0.10	0.36	0.10	0.15	0.13	0.15
Education	0.02	0.32	0.10	0.04	0.02	0.25	0.02	0.20	0.12
Right posterior cingulate cortical thickness	-0.79	0.01	-0.26	--	--	--	-0.66	0.02	-0.21
Right temporal pole volume	0.001	0.002	0.30	--	--	--	0.001	0.001	0.31
Right pars orbitalis volume	-0.0002	0.20	-0.12	--	--	--	-0.0003	0.07	-0.17
Right thalamus volume	-0.0002	0.04	-0.19	--	--	--	-0.0002	0.02	-0.21
Right rostral middle frontal surface area	-0.0001	0.14	-0.14	--	--	--	--	--	--
Right inferior temporal surface area	-0.0003	0.01	-0.25	--	--	--	-0.0003	0.01	-0.24
Left banks STS surface area	0.001	0.01	0.24	--	--	--	0.001	0.01	0.26
Postcentral FDG PET	--	--	--	0.0001	0.11	0.39	--	--	--
Precentral FDG PET	--	--	--	-0.0002	0.01	-0.62	-0.0001	0.001	-0.31

Table 5.8. Model predicting baseline Trails B in normal aging subjects. The MRI model accounted for 35% of the variance.

	MRI MODEL		
	Parameter Estimate	**p-value**	**Standardized Estimate**
Age	1.76	0.04	0.19
Gender	0.90	0.91	0.01
Education	-2.29	0.07	-0.16
Right temporal pole volume	0.04	0.003	0.26
Right precentral volume	-0.01	0.001	-0.32
Left pallidum volume	-0.04	0.08	-0.15
Right accumbens volume	-0.08	0.08	-0.15
Right superior temporal surface area	0.04	0.004	0.28
Right midtemporal surface area	0.03	0.005	0.26
Left parahippocampal surface area	0.08	0.10	0.14
Right inferior parietal surface area	-0.02	0.02	-0.21

Table 5.9. Models predicting baseline RAVLT 30 minute delayed recall in normal aging subjects. The MRI model accounted for 40% of the variance, FDG PET accounted for 7% of the variance, and CSF accounted for 9% of the variance. Combining imaging modalities accounted for 38% of the variance, while combining all modaliites accounted for 40% of the variance. Param. Est. = Parameter Estimate, Std. Est. = Standardized Estimate.

	MRI MODEL			FDG PET MODEL			CSF MODEL			MODEL			MULTIMODAL MODEL		
	Param. Est.	p-value	Std. Est.	Param. Est.	p-value	Std. Est.	Param. Est.	p-value	Std. Est.	Param. Est.	p-value	Std. Est.	Param. Est.	p-value	Std. Est.
Age	-0.23	0.001	-0.28	-0.14	0.07	-0.19	-0.12	0.24	-0.16	-0.24	0.001	-0.31	-0.28	0.01	-0.40
Gender	1.08	0.11	0.14	0.90	0.27	0.12	0.73	0.50	0.10	1.04	0.14	0.13	2.27	0.04	0.31
Education	0.13	0.22	0.11	0.25	0.05	0.21	0.39	0.02	0.34	0.21	0.06	0.17	0.48	0.002	0.43
Left superior parietal volume	-0.0005	0.03	-0.21	--	--	--	--	--	--	-0.001	0.01	-0.25	-0.0003	0.36	-0.13
Right isthmus of the cingulate volume	-0.003	0.02	-0.23	--	--	--	--	--	--	-0.004	0.004	-0.30	-0.01	0.003	-0.48
Right pericalcarine volume	0.002	0.03	0.20	--	--	--	--	--	--	0.002	0.08	0.16	0.0002	0.92	0.02
Right lateral occipital volume	-0.0004	0.07	-0.17	--	--	--	--	--	--	--	--	--	0.0002	0.64	0.07
Left thalamus volume	-0.001	0.04	-0.17	--	--	--	--	--	--	-0.002	0.02	-0.20	-0.002	0.03	-0.27
Left transverse temporal surface area	-0.01	0.07	-0.15	--	--	--	--	--	--	-0.01	0.05	-0.17	-0.01	0.07	-0.24
Right caudal middle frontal surface area	0.002	0.01	0.24	--	--	--	--	--	--	0.002	0.01	0.24	0.001	0.46	0.10
Left fusiform surface area	-0.002	0.02	-0.20	--	--	--	--	--	--	-0.001	0.16	-0.13	0.0004	0.78	0.04
Left entorhinal surface area	0.01	0.10	0.13	--	--	--	--	--	--	--	--	--	0.002	0.68	0.05
Right inferior temporal surface area	0.002	0.01	0.22	--	--	--	--	--	--	0.002	0.02	0.20	0.003	0.04	0.26
Right posterior cingulate surface area	-0.004	0.07	-0.15	--	--	--	--	--	--	-0.004	0.11	-0.14	-0.01	0.05	-0.24
Paracentral FDG PET	--	--	--	-0.0004	0.02	-0.23	--	--	--	-0.0002	0.14	-0.13	-0.0004	0.13	-0.21
Phosphorylated tau	--	--	--	--	--	--	-0.04	0.19	-0.18	--	--	--	-0.05	0.09	-0.22

Table 5.10. Models predicting baseline RAVLT 30 minute delayed recognition in normal aging subjects. The MRI model accounted for 42% of the variance, FDG PET accounted for 7% of the variance, and CSF accounted for 10% of the variance. Combining imaging modalities accounted for 45% of the variance, while combining all modaliites accounted for 37% of the variance. Param. Est. = Parameter Estimate, Std. Est. = Standardized Estimate

	MRI MODEL			FDG PET MODEL			CSF MODEL			MODEL			MULTIMODAL MODEL		
	Param. Est.	p-value	Std. Est.	Param. Est.	p-value	Std. Est.	Param. Est.	p-value	Std. Est.	Param. Est.	p-value	Std. Est.	Param. Est.	p-value	Std. Est.
Age	-0.10	0.07	-0.16	-0.06	0.34	-0.10	-0.14	0.05	-0.27	-0.11	0.05	-0.17	-0.28	0.01	-0.40
Gender	1.35	0.01	0.23	1.21	0.06	0.20	1.22	0.11	0.23	1.24	0.02	0.20	2.27	0.04	0.31
Education	-0.06	0.47	-0.06	-0.12	0.24	-0.12	0.04	0.72	0.05	-0.06	0.44	-0.06	0.48	0.002	0.43
Right banks STS cortical thickness	-1.80	0.12	-0.13	--	--	--	--	--	--	-2.18	0.07	-0.16	-0.0003	0.36	-0.13
Left isthmus of the cingulate volume	-0.002	0.03	-0.19	--	--	--	--	--	--	-0.001	0.12	-0.13	-0.01	0.003	-0.48
Left temporal pole volume	-0.003	0.0001	-0.31	--	--	--	--	--	--	-0.003	0.0002	-0.32	0.0002	0.92	0.02
Right lateral occipital volume	-0.0004	0.03	-0.19	--	--	--	--	--	--	-0.0003	0.06	-0.16	0.0002	0.64	0.07
Left thalamus volume	-0.001	0.07	-0.15	--	--	--	--	--	--	-0.001	0.04	-0.18	-0.002	0.03	-0.27
Right accumbens volume	0.01	0.02	0.19	--	--	--	--	--	--	0.01	0.002	0.27	-0.01	0.07	-0.24
Right cuneus surface area	0.002	0.19	0.11	--	--	--	--	--	--	--	--	--	0.001	0.46	0.10
Right fusiform surface area	0.001	0.07	0.16	--	--	--	--	--	--	--	--	--	0.0004	0.78	0.04
Left insula surface area	0.004	0.02	0.21	--	--	--	--	--	--	0.01	0.0004	0.30	0.002	0.68	0.05
Right supramarginal surface area	-0.002	0.01	-0.23	--	--	--	--	--	--	-0.002	0.02	-0.20	0.003	0.04	0.26
Hippocampus FDG PET	--	--	--	-0.0004	0.09	-0.18	--	--	--	-0.0004	0.06	-0.16	-0.01	0.05	-0.24
Thalamus FDG PET	--	--	--	-0.0004	0.08	-0.18	--	--	--	-0.0003	0.17	-0.12	-0.0004	0.13	-0.21
Phosphorylated tau	--	--	--	--	--	--	0.03	0.03	0.31	--	--	--	-0.05	0.09	-0.22

Table 5.11. Models predicting baseline clock drawing in MCI subjects. The MRI model accounted for 18% of the variance, FDG PET accounted for 3% of the variance, and combining modalities accounted for 20% of the variance.

	MRI MODEL			FDG PET MODEL			MULTIMODAL MODEL		
	Parameter Estimate	p-value	Standardized Estimate	Parameter Estimate	p-value	Standardized Estimate	Parameter Estimate	p-value	Standardized Estimate
Age	-0.0004	0.96	-0.003	-0.01	0.37	-0.07	-0.0003	0.98	-0.002
Gender	-0.05	0.69	-0.03	-0.03	0.84	-0.01	-0.03	0.82	-0.02
Education	0.04	0.08	0.12	0.05	0.05	0.14	0.04	0.05	0.13
Right isthmus of the cingulate cortical thickness	0.56	0.03	0.16	--	--	--	0.52	0.05	0.15
Right caudal middle frontal cortical thickness	0.86	0.02	0.17	--	--	--	0.85	0.02	0.18
Right banks STS volume	0.0003	0.10	0.11	--	--	--	0.0003	0.12	0.11
Right transverse temporal surface area	-0.004	0.001	-0.22	--	--	--	-0.004	0.002	-0.21
Right inferior parietal surface area	0.0003	0.01	0.17	--	--	--	0.0003	0.002	0.22
Inferior temporal FDG PET	--	--	--	0.0001	0.04	0.15	0.0001	0.17	0.09

Table 5.12. Model predicting baseline digit span forward in MCI subjects. The MRI model accounted for 5% of the variance.

	MRI MODEL		
	Parameter Estimate	p-value	Standardized Estimate
Age	-0.04	0.03	-0.17
Gender	-0.07	0.81	-0.02
Education	0.02	0.70	0.03
Right pericalcarine cortical thickness	-2.89	0.04	-0.15
Left pallidum volume	-0.001	0.07	-0.13
Left hippocampus volume	-0.001	0.04	-0.16

Table 5.13. Models predicting baseline digit span backward in MCI subjects. The MRI model accounted for 10% of the variance, CSF biomarkers accounted for 4% of the variance, and combining modalities accounted for 12% of the variance.

	MRI MODEL			CSF MODEL			MULTIMODAL MODEL		
	Parameter Estimate	p-value	Standardized Estimate	Parameter Estimate	p-value	Standardized Estimate	Parameter Estimate	p-value	Standardized Estimate
Age	0.001	0.96	0.003	-0.02	0.49	-0.07	-0.01	0.74	-0.03
Gender	0.50	0.09	0.11	0.88	0.05	0.20	0.95	0.03	0.21
Education	0.03	0.50	0.05	0.05	0.45	0.08	0.04	0.61	0.05
Left isthmus of the cingulate volume	0.001	0.09	0.12	--	--	--	0.0002	0.74	0.03
Left frontal pole volume	0.004	0.001	0.23	--	--	--	0.004	0.01	0.28
Left paracentral surface area	0.002	0.01	0.18	--	--	--	0.001	0.26	0.11
ABETA142	--	--	--	0.01	0.04	0.20	0.01	0.03	0.21

Table 5.14. Models predicting baseline Trails A in MCI subjects. The MRI model accounted for 11% of the variance, FDG PET accounted for 12% of the variance, and combining modalities accounted for 17% of the variance.

	MRI MODEL			FDG PET MODEL			MULTIMODAL MODEL		
	Parameter Estimate	p-value	Standardized Estimate	Parameter Estimate	p-value	Standardized Estimate	Parameter Estimate	p-value	Standardized Estimate
Age	-0.26	0.21	-0.09	-0.03	0.88	-0.01	-0.15	0.46	-0.05
Gender	2.04	0.51	0.04	-0.04	0.99	-0.001	2.11	0.48	0.05
Education	-0.79	0.12	-0.11	-1.15	0.02	-0.16	-0.99	0.04	-0.14
Left isthmus of the cingulate cortical thickness	-12.38	0.07	-0.14	--	--	--	-16.20	0.01	-0.19
Right precuneus cortical thickness	-27.92	0.003	-0.23	--	--	--	-14.16	0.12	-0.12
Right inferior temporal surface area	-0.01	0.09	-0.12	--	--	--	--	--	--
Right supramarginal surface area	-0.01	0.04	-0.14	--	--	--	-0.01	0.03	-0.14
Inferior parietal FDG PET	--	--	--	-0.002	0.13	-0.19	--	--	--
Precentral FDG PET	--	--	--	0.003	0.03	0.23	--	--	--
Precuneus FDG PET	--	--	--	-0.003	0.03	-0.30	-0.003	0.001	-0.25

Table 5.15. Models predicting baseline Trails B in MCI subjects. The MRI model accounted for 27% of the variance, FDG PET accounted for 17% of the variance, and combining modalities accounted for 30% of the variance.

	MRI MODEL			FDG PET MODEL			MULTIMODAL MODEL		
	Parameter Estimate	p-value	Standardized Estimate	Parameter Estimate	p-value	Standardized Estimate	Parameter Estimate	p-value	Standardized Estimate
Age	-0.29	0.63	-0.03	0.68	0.33	0.07	-0.58	0.36	-0.06
Gender	7.54	0.41	0.05	-1.03	0.92	-0.01	6.81	0.46	0.05
Education	-4.61	0.002	-0.19	-4.46	0.01	-0.18	-4.45	0.004	-0.18
Left isthmus of the cingulate cortical thickness	-81.26	<.0001	-0.28	--	--	--	-74.24	0.0002	-0.26
Left frontal pole cortical thickness	-29.55	0.04	-0.13	--	--	--	-23.77	0.11	-0.11
Left inferior parietal volume	-0.01	0.002	-0.20	--	--	--	-0.01	0.003	-0.19
Right cuneus surface area	-0.03	0.11	-0.10	--	--	--	-0.03	0.08	-0.11
Right superior frontal surface area	-0.02	0.00	-0.20	--	--	--	-0.02	0.001	-0.21
Banks STS FDG PET	--	--	--	-0.01	0.01	-0.37	--	--	--
Fusiform FDG PET	--	--	--	0.01	0.06	0.26	--	--	--
Inferior temporal FDG PET	--	--	--	-0.02	0.001	-0.42	--	--	--
Superior frontal FDG PET	--	--	--	0.01	0.03	0.25	--	--	--
Superior temporal FDG PET	--	--	--	0.03	0.001	0.57	--	--	--
Supramarginal FDG PET	--	--	--	-0.02	0.01	-0.47	-0.01	0.01	-0.18
Caudate FDG PET	--	--	--	-0.01	0.07	-0.17	--	--	--

Table 5.16. Models predicting baseline RAVLT 30 minute delayed recall in MCI subjects. The MRI model accounted for 31% of the variance, FDG PET accounted for 1% of the variance, and CSF accounted for 4% of the variance. Combining imaging modalities accounted for 30% of the variance, while combining all modaliites accounted for 23% of the variance. Param. Est. = Parameter Estimate, Std. Estimate = Standardized Estimate.

	MRI MODEL			FDG PET MODEL			CSF MODEL			MODEL			MULTIMODAL MODEL		
	Param. Est.	p-value	Std. Est.	Param. Est.	p-value	Std. Est.	Param. Est.	p-value	Std. Est.	Param. Est.	p-value	Std. Est.	Param. Est.	p-value	Std. Est.
Age	0.08	0.01	0.16	-0.01	0.83	-0.02	-0.002	0.96	-0.005	0.07	0.03	0.14	0.09	0.05	0.21
Gender	0.91	0.04	0.12	0.50	0.34	0.07	0.34	0.60	0.05	0.97	0.04	0.13	0.75	0.22	0.12
Education	0.12	0.11	0.10	0.08	0.37	0.07	0.01	0.94	0.01	0.09	0.23	0.08	-0.01	0.95	-0.01
Right superior parietal cortical thickness	5.08	0.001	0.28	--	--	--	--	--	--	5.06	0.001	0.28	4.17	0.04	0.27
Left entorhinal cortical thickness	0.75	0.15	0.12	--	--	--	--	--	--	0.83	0.12	0.13	0.96	0.15	0.17
Left pars orbitalis cortical thickness	1.47	0.11	0.11	--	--	--	--	--	--	1.52	0.11	0.12	1.26	0.32	0.11
Left insula cortical thickness	3.67	0.00	0.22	--	--	--	--	--	--	3.94	0.002	0.24	2.83	0.08	0.19
Right supramarginal cortical thickness	-5.39	0.002	-0.31	--	--	--	--	--	--	-5.87	0.001	-0.33	-4.65	0.05	-0.30
Left hippocampus volume	0.002	0.0001	0.32	--	--	--	--	--	--	0.002	0.0003	0.30	0.001	0.09	0.21
Left postcentral surface area	-0.001	0.04	-0.13	--	--	--	--	--	--	-0.001	0.03	-0.14	-0.001	0.34	-0.09
Left banks STS surface area	0.002	0.13	0.09	--	--	--	--	--	--	0.002	0.19	0.08	0.002	0.13	0.14
Isthmus of the cingulate FDG PET	--	--	--	0.0003	0.04	0.15	--	--	--	--	--	--			
Phosphorylated tau	--	--	--	--	--	--	-0.05	0.01	-0.28	--	--	--	-0.03	0.07	-0.18

Table 5.17. Models predicting APC of RAVLT 30 minute delayed recall in MCI subjects. The MRI model accounted for 26% of the variance, FDG PET accounted for 1% of the variance, and CSF accounted for 1% of the variance. Combining imaging modalities accounted for 26% of the variance, while combining all modaliites accounted for 12% of the variance. Param. Est. = Parameter Estimate, Std. Estimate = Standardied Estimate.

	MRI MODEL			FDG PET MODEL			CSF MODEL			MODEL			MULTIMODAL MODEL		
	Param. Est.	p-value	Std. Est.	Param. Est.	p-value	Std. Est.	Param. Est.	p-value	Std. Est.	Param. Est.	p-value	Std. Est.	Param. Est.	p-value	Std. Est.
Age	0.02	0.002	0.27	0.004	0.60	0.05	0.005	0.59	0.07	0.02	0.002	0.27	0.02	0.06	0.29
Gender	-0.09	0.36	-0.07	-0.14	0.25	-0.10	-0.08	0.58	-0.07	-0.08	0.42	-0.06	-0.09	0.54	-0.08
Education	-0.02	0.31	-0.08	-0.02	0.40	-0.07	0.01	0.58	0.07	-0.02	0.21	-0.10	0.01	0.50	0.08
Left superior parietal cortical thickness	0.60	0.02	0.19	--	--	--	--	--	--	0.55	0.04	0.17	0.29	0.39	0.12
Left entorhinal volume	0.0003	0.01	0.21	--	--	--	--	--	--	0.0003	0.01	0.22	0.0003	0.09	0.22
Left posterior cingulate volume	0.0003	0.02	0.19	--	--	--	--	--	--	0.0003	0.04	0.17	0.0003	0.07	0.24
Left caudate volume	0.0002	0.03	0.17	--	--	--	--	--	--	0.0002	0.03	0.18	0.0003	0.13	0.19
Right postcentral surface area	0.0004	0.0002	0.29	--	--	--	--	--	--	0.0004	0.0003	0.29	0.0001	0.48	0.09
Left pars opercularis surface area	0.0005	0.002	0.24	--	--	--	--	--	--	0.001	0.003	0.24	0.0005	0.07	0.24
Postcentral FDG PET	--	--	--	-0.0001	0.16	-0.13	--	--	--	--	--	--	--	--	--
Phosphorylated tau	--	--	--	--	--	--	-0.01	0.06	-0.24	--	--	--	-0.01	0.16	-0.18

Table 5.18. Model predicting baseline RAVLT 30 minute delayed recognition in MCI subjects. The MRI model accounted for 15% of the variance.

	MRI MODEL		
	Parameter Estimate	**p-value**	**Standardized Estimate**
Age	0.13	0.001	0.25
Gender	0.70	0.16	0.09
Education	0.11	0.21	0.08
Left pericalcarine cortical thickness	4.24	0.09	0.12
Right middle temporal cortical thickness	3.15	0.01	0.19
Left isthmus of the cingulate volume	0.002	0.06	0.13
Left hippocampus volume	0.001	0.01	0.18
Left postcentral surface area	-0.001	0.05	-0.14

Table 5.19. Models predicting baseline clock drawing in AD subjects. The MRI model accounted for 35% of the variance, FDG PET accounted for 6% of the variance, and CSF accounted for 1% of the variance. Combining imaging modalities accounted for 38% of the variance, while combining all modaliites accounted for 30% of the variance. Param. Est. = Parameter Estimate, Std. Est. = Standardized Estimate.

	MRI MODEL			FDG PET MODEL			CSF MODEL			MODEL			MULTIMODAL MODEL		
	Param. Est.	p-value	Std. Est.	Param. Est.	p-value	Std. Est.	Param. Est.	p-value	Std. Est.	Param. Est.	p-value	Std. Est.	Param. Est.	p-value	Std. Est.
Age	0.001	0.98	0.003	0.03	0.11	0.17	0.001	0.97	0.01	0.004	0.82	0.02	-0.01	0.62	-0.07
Gender	-0.20	0.40	-0.08	0.04	0.88	0.02	-0.05	0.88	-0.02	-0.25	0.31	-0.09	-0.28	0.41	-0.11
Education	-0.004	0.92	-0.01	-0.04	0.39	-0.09	-0.02	0.67	-0.06	-0.02	0.60	-0.05	-0.03	0.55	-0.08
Right superior parietal cortical thickness	1.33	0.08	0.23	--	--	--	--	--	--	1.24	0.10	0.21	-0.85	0.52	-0.15
Right temporal pole cortical thickness	0.65	0.01	0.24	--	--	--	--	--	--	0.67	0.01	0.26	0.69	0.05	0.30
Left pars orbitalis cortical thickness	0.84	0.04	0.20	--	--	--	--	--	--	0.77	0.07	0.18	0.48	0.44	0.12
Left parahippocampus cortical thickness	-1.14	0.001	-0.32	--	--	--	--	--	--	-1.24	0.0004	-0.34	-1.35	0.003	-0.44
Left inferior parietal cortical thickness	2.79	0.002	0.49	--	--	--	--	--	--	2.70	0.003	0.48	2.29	0.08	0.41
Left precuneus cortical thickness	-2.29	0.01	-0.38	--	--	--	--	--	--	-1.97	0.04	-0.33	-0.25	0.85	-0.05
Left pallidum volume	-0.002	0.01	-0.23	--	--	--	--	--	--	-0.001	0.09	-0.17	-0.001	0.52	-0.10
Left superior frontal surface area	0.0004	0.02	0.20	--	--	--	--	--	--	0.0004	0.02	0.20	0.0001	0.67	0.06
Cuneus FDG PET	--	--	--	-0.0001	0.02	-0.24	--	--	--	-0.0001	0.05	-0.19	-0.0001	0.41	-0.12
Total tau	--	--	--	--	--	--	-0.01	0.06	-0.29	--	--	--	-0.004	0.12	-0.23

Table 5.20. Model predicting APC of clock drawing in AD subjects. The MRI model accounted for 32% of the variance.

	MRI MODEL		
	Parameter Estimate	**p-value**	**Standardized Estimate**
Age	0.01	0.45	0.08
Gender	-0.08	0.60	-0.05
Education	-0.002	0.92	-0.01
Right pericalcarine cortical thickness	-2.26	0.01	-0.26
Right fusiform cortical thickness	0.75	0.04	0.21
Left paracentral volume	0.000	0.01	0.26
Left pars triangularis surface area	-0.001	0.01	-0.24
Left postcentral surface area	0.0004	0.07	0.17
Left entorhinal surface area	-0.002	0.02	-0.22
Right pars orbitalis surface area	0.001	0.17	0.12
Left lateral occipital surface area	0.0004	0.02	0.24
Right parahippocampus surface area	-0.004	0.001	-0.31

Table 5.21. Models predicting baseline digit span forward in AD subjects. The MRI model accounted for 35% of the variance, FDG PET accounted for <1% of the variance, and combining modalities accounted for 35% of the variance.

	MRI MODEL			FDG PET MODEL			MULTIMODAL MODEL		
	Parameter Estimate	p-value	Standardized Estimate	Parameter Estimate	p-value	Standardized Estimate	Parameter Estimate	p-value	Standardized Estimate
Age	0.02	0.38	0.09	0.02	0.44	0.08	0.02	0.52	0.06
Gender	-0.46	0.17	-0.12	-0.10	0.81	-0.03	-0.47	0.18	-0.12
Education	0.09	0.09	0.15	0.04	0.56	0.06	0.10	0.06	0.17
Left entorhinal volume	-0.001	0.01	-0.25	--	--	--	-0.001	0.01	-0.23
Left pars orbitalis volume	0.001	0.05	0.19	--	--	--	0.001	0.10	0.16
Right thalamus volume	-0.0004	0.17	-0.13	--	--	--	-0.0004	0.15	-0.13
Right pars triangularis surfrace area	-0.002	0.01	-0.23	--	--	--	-0.002	0.01	-0.24
Left postcentral surface area	-0.002	0.0004	-0.35	--	--	--	-0.002	0.0002	-0.39
Left superior temporal surface area	0.001	0.05	0.19	--	--	--	0.001	0.03	0.22
Right middle temporal surface area	0.002	0.002	0.33	--	--	--	0.002	0.003	0.32
Left inferior parietal surface area	0.001	0.09	0.17	--	--	--	0.001	0.08	0.18
Precuneus FDG PET	--	--	--	-0.0001	0.18	-0.15	--	--	--

Table 5.22. Models predicting APC of digit span forward in AD subjects. The MRI model accounted for 30% of the variance, CSF biomarkers accounted for 14% of the variance, and combining modalities accounted for 35% of the variance.

	MRI MODEL			CSF MODEL			MULTIMODAL MODEL		
	Parameter Estimate	p-value	Standardized Estimate	Parameter Estimate	p-value	Standardized Estimate	Parameter Estimate	p-value	Standardized Estimate
Age	0.01	0.27	0.11	0.04	0.03	0.32	0.04	0.02	0.31
Gender	0.16	0.38	0.08	-0.11	0.68	-0.06	0.07	0.79	0.03
Education	0.02	0.62	0.05	0.002	0.95	0.01	0.02	0.51	0.10
Right supramarginal volume	0.0003	0.0003	0.41	--	--	--	0.0001	0.46	0.14
Right pars opercularis volume	-0.001	0.001	-0.35	--	--	--	-0.00003	0.92	-0.02
Right accumbens volume	-0.002	0.07	-0.17	--	--	--	-0.001	0.59	-0.07
Left temporal pole surface area	-0.004	0.02	-0.23	--	--	--	-0.001	0.71	-0.05
Left frontal pole surface area	-0.01	0.02	-0.23	--	--	--	-0.002	0.52	-0.08
Left superior frontal surface area	0.0004	0.004	0.27	--	--	--	0.001	0.0002	0.50
ABETA142	--	--	--	0.01	0.06	0.26	0.01	0.05	0.27

Table 5.23. Models predicting baseline digit span backward in AD subjects. The MRI model accounted for 31% of the variance, FDG PET accounted for 6% of the variance, and CSF accounted for 5% of the variance. Combining imaging modalities accounted for 31% of the variance, while combining all modaliites accounted for 37% of the variance. Param. Est. = Parameter Estimate, Std. Est. = Standardized Estimate.

	MRI MODEL			FDG PET MODEL			CSF MODEL			IMAGING MODEL			MULTIMODAL MODEL		
	Param. Est.	p-value	Std. Est.	Param. Est.	p-value	Std. Est.	Param. Est.	p-value	Std. Est.	Param. Est.	p-value	Std. Est.	Param. Est.	p-value	Std. Est.
Age	-0.003	0.92	-0.01	0.07	0.03	0.24	0.04	0.28	0.16	0.01	0.79	0.03	0.01	0.85	0.03
Gender	-0.03	0.93	-0.01	0.18	0.67	0.04	0.28	0.60	0.08	-0.09	0.81	-0.02	-0.26	0.59	-0.07
Education	0.06	0.33	0.09	-0.03	0.71	-0.04	0.02	0.79	0.04	0.06	0.35	0.09	0.15	0.02	0.32
Left inferior parietal volume	0.0004	0.004	0.28	--	--	--	--	--	--	0.0003	0.01	0.27	0.0003	0.03	0.29
Left pallidum volume	-0.003	0.01	-0.26	--	--	--	--	--	--	-0.002	0.01	-0.25	-0.002	0.10	-0.23
Rught cuneus surface area	-0.003	0.01	-0.26	--	--	--	--	--	--	-0.002	0.02	-0.25	-0.003	0.01	-0.38
Left fusiform surface area	-0.002	0.002	-0.30	--	--	--	--	--	--	-0.001	0.01	-0.28	-0.002	0.01	-0.39
Left pars triangularis surface area	-0.002	0.06	-0.17	--	--	--	--	--	--	-0.002	0.07	-0.17	0.00004	0.97	0.005
Right rostral middle frontal surface area	0.001	0.001	0.32	--	--	--	--	--	--	0.001	0.003	0.31	0.002	0.002	0.48
Left precuneus surface area	0.001	0.17	0.14	--	--	--	--	--	--	0.001	0.13	0.16	0.001	0.05	0.31
Pericalcarine FDG PET	--	--	--	-0.0001	0.16	-0.16	--	--	--	--	--	--	--	--	--
Total tau	--	--	--	--	--	--	-0.01	0.06	-0.28	--	--	--	--	--	--

Table 5.24. Models predicting APC of digit span backward in AD subjects. The MRI model accounted for 23% of the variance, FDG PET accounted for 8% of the variance, and combining modalities accounted for 25% of the variance.

	MRI MODEL			FDG PET MODEL			MULTIMODAL MODEL		
	Parameter Estimate	p-value	Standardized Estimate	Parameter Estimate	p-value	Standardized Estimate	Parameter Estimate	p-value	Standardized Estimate
Age	0.04	0.01	0.27	0.01	0.33	0.10	0.03	0.08	0.18
Gender	0.44	0.03	0.23	0.32	0.12	0.16	0.44	0.03	0.22
Education	0.01	0.67	0.04	-0.03	0.41	-0.09	0.01	0.81	0.03
Right cuneus cortical thickness	-0.95	0.17	-0.14	--	--	--	--	--	--
Left frontal pole cortical thickness	-0.58	0.06	-0.19	--	--	--	-0.71	0.02	-0.23
Right parahippocampus volume	0.001	0.07	0.18	--	--	--	0.0005	0.13	0.15
Left isthmus of the cingulate surface area	0.002	0.04	0.20	--	--	--	0.002	0.03	0.21
Left caudal middle frontal surface area	0.001	0.04	0.21	--	--	--	0.001	0.04	0.21
Right pars triangularis surface area	-0.001	0.11	-0.16	--	--	--	-0.001	0.10	-0.16
Pericalcarine FDG PET	--	--	--	-0.0001	0.01	-0.28	-0.0001	0.16	-0.15

Table 5.25. Models predicting baseline Trails A in AD subjects. The MRI model accounted for 35% of the variance, FDG PET accounted for 3% of the variance, and CSF accounted for 17% of the variance. Combining imaging modalities accounted for 30% of the variance, while combining all modaliites accounted for 49% of the variance. Param. Est. = Parameter Estimate, Std. Est. = Standardized Estimate.

	MRI MODEL			FDG PET MODEL			CSF MODEL			IMAGING MODEL			MULTIMODAL MODEL		
	Param. Est.	p-value	Std. Est.	Param. Est.	p-value	Std. Est.	Param. Est.	p-value	Std. Est.	Param. Est.	p-value	Std. Est.	Param. Est.	p-value	Std. Est.
Age	-0.19	0.73	-0.04	-0.20	0.74	-0.04	-0.83	0.25	-0.16	-0.07	0.91	-0.01	-1.52	0.05	-0.30
Gender	2.42	0.74	0.03	8.88	0.30	0.12	-7.48	0.49	-0.09	4.25	0.56	0.06	-15.94	0.14	-0.20
Education	1.46	0.17	0.12	1.62	0.20	0.14	3.32	0.02	0.31	0.87	0.42	0.07	0.98	0.45	0.10
Right transverse temporal cortical thickness	-26.97	0.01	-0.24	--	--	--	--	--	--	-32.06	0.00	-0.28	-41.22	0.02	-0.35
Right entorhinal volume	0.01	0.09	0.16	--	--	--	--	--	--	0.02	0.01	0.26	0.04	0.003	0.42
Left inferior parietal volume	-0.01	0.01	-0.27	--	--	--	--	--	--	-0.01	0.002	-0.32	-0.003	0.47	-0.10
Brainstem volume	0.004	0.06	0.18	--	--	--	--	--	--	0.003	0.09	0.16	0.004	0.20	0.18
Right pars traingularis surface area	-0.03	0.04	-0.18	--	--	--	--	--	--	--	--	--	-0.004	0.85	-0.02
Right superior temporal surface area	0.02	0.09	0.16	--	--	--	--	--	--	--	--	--	0.003	0.87	0.02
Right inferior temporal surface area	-0.02	0.07	-0.17	--	--	--	--	--	--	-0.02	0.07	-0.17	-0.034	0.06	-0.33
Right parahippocampal surface area	0.07	0.14	0.13	--	--	--	--	--	--	--	--	--	-0.12	0.12	-0.23
Left lingual surface arrea	-0.01	0.18	-0.12	--	--	--	--	--	--	--	--	--	-0.01	0.58	-0.07
Inferior parietal FDG PET	--	--	--	-0.004	0.06	-0.21	--	--	--	--	--	--	0.001	0.79	0.03
Total tau	--	--	--	--	--	--	0.15	0.06	0.26	--	--	--	0.14	0.06	0.24

Table 5.26. Models predicting baseline Trails B in AD subjects. The MRI model accounted for 32% of the variance, FDG PET accounted for 12% of the variance, and CSF accounted for 10% of the variance. Combining imaging modalities accounted for 25% of the variance, while combining all modaliites accounted for 42% of the variance. Param. Est. = Parameter Estimate, Std. Est. = Standardized Estimate.

	MRI MODEL			FDG PET MODEL			CSF MODEL			IMAGING MODEL			MULTIMODAL MODEL		
	Param. Est.	p-value	Std. Est.	Param. Est.	p-value	Std. Est.	Param. Est.	p-value	Std. Est.	Param. Est.	p-value	Std. Est.	Param. Est.	p-value	Std. Est.
Age	-0.86	0.47	-0.07	-0.01	0.99	0.00	1.62	0.36	0.13	0.12	0.92	0.01	2.12	0.17	0.17
Gender	-8.50	0.62	-0.04	10.09	0.62	0.05	-25.05	0.35	-0.13	-10.58	0.54	-0.06	-27.57	0.22	-0.14
Education	-8.26	0.005	-0.28	-8.74	0.004	-0.30	-7.91	0.03	-0.32	-8.90	0.002	-0.31	-9.97	0.003	-0.40
Left precuneus cortical thickness	-64.36	0.14	-0.15	--	--	--	--	--	--	-75.69	0.08	-0.18	-120.56	0.02	-0.29
Left temporal pole volume	-0.06	0.01	-0.25	--	--	--	--	--	--	-0.05	0.04	-0.20	-0.07	0.03	-0.28
Right frontal pole volume	-0.12	0.04	-0.19	--	--	--	--	--	--	-0.12	0.04	-0.19	-0.11	0.13	-0.20
Right superior frontal volume	-0.01	0.16	-0.14	--	--	--	--	--	--	-0.01	0.19	-0.13	--	--	--
Right isthmus of the cingulate surface area	0.16	0.05	0.18	--	--	--	--	--	--	0.17	0.04	0.19	0.27	0.03	0.28
Left caudal middle frontal surface area	0.05	0.09	0.16	--	--	--	--	--	--	0.05	0.05	0.18	--	--	--
Right insula surface area	-0.14	0.01	-0.26	--	--	--	--	--	--	-0.15	0.004	-0.29	-0.14	0.04	-0.27
Right inferior parietal surface area	0.02	0.17	0.13	--	--	--	--	--	--	0.02	0.16	0.13	--	--	--
Temporal pole FDG PET	--	--	--	-0.02	0.01	-0.27	--	--	--	--	--	--	--	--	--
Total tau	--	--	--	--	--	--	0.40	0.05	0.28	--	--	--	0.36	0.05	0.25

Table 5.27. Models predicting APC of Trails B in AD subjects. The MRI model accounted for 24% of the variance, FDG PET accounted for 4% of the variance, and combining modalities accounted for 25% of the variance.

	MRI MODEL			FDG PET MODEL			MULTIMODAL MODEL		
	Parameter Estimate	p-value	Standardized Estimate	Parameter Estimate	p-value	Standardized Estimate	Parameter Estimate	p-value	Standardized Estimate
Age	0.02	0.25	0.13	-0.01	0.66	-0.05	0.02	0.31	0.12
Gender	0.21	0.38	0.08	0.23	0.40	0.09	0.19	0.44	0.08
Education	0.01	0.84	0.02	0.08	0.05	0.21	0.01	0.81	0.03
Right banks STS cortical thickness	-1.13	0.04	-0.23	--	--	--	-1.11	0.05	-0.22
Left rostral middle frontal volume	0.0001	0.06	0.22	--	--	--	0.0002	0.05	0.23
Right lateral orbitofrontal volume	-0.0004	0.02	-0.27	--	--	--	-0.0005	0.01	-0.31
Left hippocampus volume	0.001	0.03	0.24	--	--	--	0.001	0.02	0.26
Right postcentral surface area	-0.001	0.002	-0.33	--	--	--	-0.001	0.002	-0.33
Right entorhinal surface area	0.004	0.03	0.24	--	--	--	0.004	0.04	0.23
Left frontal pole surface area	0.01	0.03	0.22	--	--	--	0.01	0.03	0.22
Paracentral FDG PET	--	--	--	0.0001	0.11	0.17	--	--	--

Table 5.28. Models predicting baseline RAVLT 30 minute delayed recall in AD subjects. The MRI model accounted for 29% of the variance, FDG PET accounted for 7% of the variance, and combining modalities accounted for 34% of the variance.

	MRI MODEL			FDG PET MODEL			MULTIMODAL MODEL		
	Parameter Estimate	p-value	Standardized Estimate	Parameter Estimate	p-value	Standardized Estimate	Parameter Estimate	p-value	Standardized Estimate
Age	-0.01	0.77	-0.03	-0.02	0.44	-0.08	0.003	0.90	0.01
Gender	-0.28	0.27	-0.11	0.13	0.67	0.05	-0.23	0.39	-0.08
Education	-0.04	0.31	-0.10	0.01	0.90	0.01	-0.04	0.31	-0.10
Right superior temporal cortical thickness	2.06	0.001	0.35	--	--	--	1.92	0.005	0.33
Right lingual cortical thickness	-3.65	0.001	-0.34	--	--	--	-2.80	0.01	-0.26
Right superior parietal surface area	0.0004	0.11	0.15	--	--	--	0.0004	0.12	0.15
Right rostral middle frontal surface area	-0.001	0.01	-0.28	--	--	--	-0.001	0.003	-0.32
Left medial orbitofrontal surface area	0.002	0.07	0.20	--	--	--	0.002	0.08	0.20
Right lateral occipital surface area	-0.001	0.003	-0.28	--	--	--	-0.001	0.001	-0.30
Right paracentral surface area	0.002	0.02	0.23	--	--	--	0.002	0.03	0.20
Entorhinal FDG PET	--	--	--	0.0002	0.02	0.26	0.0002	0.10	0.17
Supramarginal FDG PET	--	--	--	-0.0002	0.01	-0.28	-0.0002	0.03	-0.22

Table 5.29. Models predicting APC of RAVLT 30 minute delayed recall in AD subjects. The MRI model accounted for 68% of the variance, FDG PET accounted for <1% of the variance, and combining modalities accounted for 78% of the variance.

	MRI MODEL			FDG PET MODEL			MULTIMODAL MODEL		
	Parameter Estimate	p-value	Standardized Estimate	Parameter Estimate	p-value	Standardized Estimate	Parameter Estimate	p-value	Standardized Estimate
Age	-0.01	0.30	-0.15	-0.01	0.58	-0.13	-0.004	0.52	-0.08
Gender	-0.04	0.73	-0.05	-0.10	0.57	-0.13	-0.15	0.13	-0.19
Education	-0.01	0.59	-0.07	0.01	0.70	0.08	-0.01	0.45	-0.10
Left parahippocamus cortical thickness	0.38	0.005	0.38	--	--	--	0.46	0.0003	0.48
Right superior parietal volume	-0.0001	0.01	-0.38	--	--	--	-0.0001	0.001	-0.41
Right frontal pole volume	-0.001	0.01	-0.36	--	--	--	-0.001	0.005	-0.33
Left pericalcarine surface area	0.001	0.01	0.40	--	--	--	0.001	0.03	0.32
Right posterior cingulate surface area	-0.001	0.08	-0.25	--	--	--	-0.0005	0.14	-0.18
Right inferior parietal surface area	-0.0003	0.01	-0.39	--	--	--	-0.0003	0.005	-0.35
Inferior parietal FDG PET	--	--	--	0.0001	0.12	0.39	0.00003	0.18	0.20

Table 5.30. Models predicting baseline RAVLT 30 minute delayed recognition in AD subjects. The MRI model accounted for 36% of the variance, FDG PET accounted for 11% of the variance, and combining modalities accounted for 35% of the variance.

	MRI MODEL			FDG PET MODEL			MULTIMODAL MODEL		
	Parameter Estimate	p-value	Standardized Estimate	Parameter Estimate	p-value	Standardized Estimate	Parameter Estimate	p-value	Standardized Estimate
Age	-0.14	0.01	-0.26	-0.08	0.16	-0.15	-0.13	0.02	-0.23
Gender	-0.92	0.20	-0.11	-1.37	0.11	-0.17	-0.89	0.23	-0.11
Education	-0.04	0.71	-0.03	-0.10	0.43	-0.08	-0.06	0.62	-0.05
Right transverse temporal cortical thickness	-3.50	0.002	-0.30	--	--	--	-3.54	0.003	-0.30
Left entorhinal cortical thickness	2.68	0.0001	0.36	--	--	--	2.71	0.0002	0.37
Left frontal pole volume	-0.01	0.01	-0.22	--	--	--	-0.01	0.02	-0.22
Brainstem volume	0.000	0.02	-0.20	--	--	--	-0.0004	0.02	-0.21
Right superior temporal surface area	0.002	0.04	0.19	--	--	--	0.002	0.06	0.17
Left lingual surface area	0.002	0.07	0.16	--	--	--	0.002	0.08	0.16
Entorhinal FDG PET	--	--	--	0.001	0.01	0.30	--	--	--
Superior temporal FDG PET	--	--	--	-0.001	0.01	-0.31	--	--	--

Table 5.31. Models predicting APC of RAVLT 30 minute delayed recognition in AD subjects. The MRI model accounted for 20% of the variance, FDG PET accounted for 4% of the variance, and combining modalities accounted for 23% of the variance.

	MRI MODEL			FDG PET MODEL			MULTIMODAL MODEL		
	Parameter Estimate	p-value	Standardized Estimate	Parameter Estimate	p-value	Standardized Estimate	Parameter Estimate	p-value	Standardized Estimate
Age	-0.01	0.30	-0.15	-0.01	0.58	-0.13	-0.004	0.52	-0.08
Gender	-0.04	0.73	-0.05	-0.10	0.57	-0.13	-0.15	0.13	-0.19
Education	-0.01	0.59	-0.07	0.01	0.70	0.08	-0.01	0.45	-0.10
Left parahippocamus cortical thickness	0.38	0.005	0.38	--	--	--	0.46	0.0003	0.48
Right superior parietal volume	-0.0001	0.01	-0.38	--	--	--	-0.0001	0.001	-0.41
Right frontal pole volume	-0.001	0.01	-0.36	--	--	--	-0.001	0.005	-0.33
Left pericalcarine surface area	0.001	0.01	0.40	--	--	--	0.001	0.03	0.32
Right posterior cingulate surface area	-0.001	0.08	-0.25	--	--	--	-0.0005	0.14	-0.18
Right inferior parietal surface area	-0.0003	0.01	-0.39	--	--	--	-0.0003	0.005	-0.35
Inferior parietal FDG PET	--	--	--	0.0001	0.12	0.39	0.00003	0.18	0.20

REFERENCES

Alexander, M.P., Stuss, D. & Gillingham, S., 2009. Impaired list learning is not a general property of frontal lesions. *Journal of cognitive neuroscience*, 21(7), pp.1422–1434.

Amici, S. et al., 2007. Anatomical correlates of sentence comprehension and verbal working memory in neurodegenerative disease. *The Journal of neuroscience: the official journal of the Society for Neuroscience*, 27(23), pp.6282–6290.

Black, F.W., 1986. NEUROANATOMIC AND NEUROPSYCHOLOGIC CORRELATES OF DIGIT SPAN PERFORMANCE BY BRAIN-DAMAGED ADULTS. *Perceptual and Motor Skills*, 63(2), pp.815–822.

Blanke, O. et al., 2000. Location of the human frontal eye field as defined by electrical cortical stimulation: anatomical, functional and electrophysiological characteristics. *Neuroreport*, 11(9), pp.1907–1913.

Blumenfeld, R.S. & Ranganath, C., 2007. Prefrontal cortex and long-term memory encoding: an integrative review of findings from neuropsychology and neuroimaging. *The Neuroscientist: a review journal bringing neurobiology, neurology and psychiatry*, 13(3), pp.280–291.

Bohbot, V.D. et al., 1998. Spatial memory deficits in patients with lesions to the right hippocampus and to the right parahippocampal cortex. *Neuropsychologia*, 36(11), pp.1217–1238.

Bohbot, V.D., Allen, J.J. & Nadel, L, 2000. Memory deficits characterized by patterns of lesions to the hippocampus and parahippocampal cortex. *Annals of the New York Academy of Sciences*, 911, pp.355–368.

Browndyke, J.N. et al., 2012. Phenotypic regional functional imaging patterns during memory encoding in mild cognitive impairment and Alzheimer's disease. *Alzheimer's & dementia: the journal of the Alzheimer's Association*.

Cabeza, R. & Nyberg, L., 2000. Imaging Cognition II: An Empirical Review of 275 PET and fMRI Studies. *Journal of Cognitive Neuroscience*, 12(1), pp.1–47.

Caroli, A. et al., 2010. Functional compensation in incipient Alzheimer's disease. *Neurobiology of aging*, 31(3), pp.387–397.

Caselli, R.J. et al., 2008. Correlating cerebral hypometabolism with future memory decline in subsequent converters to amnestic pre-mild cognitive impairment. *Archives of Neurology*, 65(9), pp.1231–1236.

Champod, A.S. & Petrides, Michael, 2007. Dissociable roles of the posterior parietal and the prefrontal cortex in manipulation and monitoring processes. *Proceedings of the National Academy of Sciences of the United States of America*, 104(37), pp.14837–14842.

Chang, Y.-L. et al., 2010. Brain substrates of learning and retention in mild cognitive impairment diagnosis and progression to Alzheimerâs disease. *Neuropsychologia*, 48(5), pp.1237–1247.

Clément, F. & Belleville, S., 2010. Compensation and disease severity on the memory-related activations in mild cognitive impairment. *Biological psychiatry*, 68(10), pp.894–902.

Clément, F. & Belleville, S., 2012. Effect of disease severity on neural compensation of item and associative recognition in mild cognitive impairment. *Journal of Alzheimer's disease: JAD*, 29(1), pp.109–123.

Clément, F., Gauthier, S. & Belleville, S., 2012. Executive functions in mild cognitive impairment: Emergence and breakdown of neural plasticity. *Cortex; a journal devoted to the study of the nervous system and behavior*.

Cohen, R.H. & Jr, C.J.V., 1993. Population estimates for responses of cutaneous mechanoreceptors to a vertically indenting probe on the glabrous skin of monkeys. *Experimental Brain Research*, 94(1), pp.105–119.

Dale A.M., Fischl B. & Sereno M.I., 1999. Cortical Surface-Based Analysis I. Segmentation and Surface Reconstruction. *NeuroImage*, 9(2), pp.179–194.

Desikan, R.S. et al., 2006. An automated labeling system for subdividing the human cerebral cortex on MRI scans into gyral based regions of interest. *NeuroImage*, 31(3), pp.968–980.

Fischl, B., Sereno, M.I. & Dale, A. M., 1999. Cortical surface-based analysis - II: Inflation, flattening, and a surface-based coordinate system. Available at: http://discovery.ucl.ac.uk/145122/ [Accessed September 21, 2011].

Fischl, Bruce, Van der Kouwe, André, et al., 2004. Automatically Parcellating the Human Cerebral Cortex. *Cerebral Cortex*, 14(1), pp.11 –22.

Fischl, Bruce, Salat, David H, et al., 2004. Sequence-independent segmentation of magnetic resonance images. *NeuroImage*, 23 Suppl 1, pp.S69–84.

Fischl, Bruce et al., 2002. Whole Brain Segmentation. *Neuron*, 33(3), pp.341–355.

Fischl, Bruce & Dale, Anders M., 2000. Measuring the thickness of the human cerebral cortex from magnetic resonance images. *Proceedings of the National Academy of Sciences*, 97(20), pp.11050 –11055.

Förstl, H. et al., 1993. Neuropathological basis for drawing disability (constructional apraxia) in Alzheimer's disease. *Psychological medicine*, 23(3), pp.623–629.

Geva, S. et al., 2012. The Effect of Aging on the Neural Correlates of Phonological Word Retrieval. *Journal of cognitive neuroscience*, 24(11), pp.2135–2146.

Gómez-Isla, T. et al., 1997. Neuronal loss correlates with but exceeds neurofibrillary tangles in Alzheimer's disease. *Annals of Neurology*, 41(1), pp.17–24.

Greve, Douglas N & Fischl, Bruce, 2009. Accurate and robust brain image alignment using boundary-based registration. *NeuroImage*, 48(1), pp.63–72.

Guedj, E. et al., 2009. Effects of medial temporal lobe degeneration on brain perfusion in amnestic MCI of AD type: deafferentation and functional compensation? *European journal of nuclear medicine and molecular imaging*, 36(7), pp.1101–1112.

Happaney, K., Zelazo, P.D. & Stuss, D.T., 2004. Development of orbitofrontal function: current themes and future directions. *Brain and cognition*, 55(1), pp.1–10.

Hou, Y. & Liu, T., 2012. Neural correlates of object-based attentional selection in human cortex. *Neuropsychologia*, 50(12), pp.2916–2925.

Johnsrude, I.S. et al., 1999. A cognitive activation study of memory for spatial relationships. *Neuropsychologia*, 37(7), pp.829–841.

Kerchner, G.A. et al., 2012. Hippocampal CA1 apical neuropil atrophy and memory performance in Alzheimer's disease. *NeuroImage*, 63(1), pp.194–202.

Leyhe, T. et al., 2009. Changes in Cortical Activation during Retrieval of Clock Time Representations in Patients with Mild Cognitive Impairment and Early Alzheimer’s Disease. *Dementia and Geriatric Cognitive Disorders*, 27(2), pp.117–132.

Li, R. et al., 2012. The Neuronal Correlates of Digits Backward Are Revealed by Voxel-Based Morphometry and Resting-State Functional Connectivity Analyses. *PLoS ONE*, 7(2), p.e31877.

Libon, D.J. et al., 1996. Further analyses of clock drawings among demented and nondemented older subjects. *Archives of clinical neuropsychology: the official journal of the National Academy of Neuropsychologists*, 11(3), pp.193–205.

Logan, J.M. et al., 2002. Under-recruitment and nonselective recruitment: dissociable neural mechanisms associated with aging. *Neuron*, 33(5), pp.827–840.

Mendez, M.F., Ala, T. & Underwood, K.L., 1992. Development of scoring criteria for the clock drawing task in Alzheimer's disease. *Journal of the American Geriatrics Society*, 40(11), pp.1095–1099.

Moscovitch, M. et al., 2005. Functional neuroanatomy of remote episodic, semantic and spatial memory: a unified account based on multiple trace theory. *Journal of Anatomy*, 207(1), pp.35–66.

Mufson, E.J. et al., 2012. Mild Cognitive Impairment: Pathology and mechanisms. *Acta Neuropathologica*, 123(1), pp.13–30.

Oosterman, J.M. et al., 2010. Assessing mental flexibility: neuroanatomical and neuropsychological correlates of the Trail Making Test in elderly people. *The Clinical neuropsychologist*, 24(2), pp.203–219.

Otten, L.J., Henson, R.N. & Rugg, M.D., 2001. Depth of processing effects on neural correlates of memory encoding: relationship between findings from across- and within-task comparisons. *Brain: a journal of neurology*, 124(Pt 2), pp.399–412.

Owen, A.M. et al., 1996. Memory for object features versus memory for object location: a positron-emission tomography study of encoding and retrieval processes. *Proceedings of the National Academy of Sciences*, 93(17), pp.9212–9217.

PA, J. et al., 2010. Gray matter correlates of set-shifting among neurodegenerative disease, mild cognitive impairment, and healthy older adults. *Journal of the International Neuropsychological Society□: JINS*, 16(4), pp.640–650.

Perry, R.J. & Hodges, J.R., 1999. Attention and executive deficits in Alzheimer's disease A critical review. *Brain*, 122(3), pp.383–404.

Petersen, Steven E & Posner, Michael I, 2012. The attention system of the human brain: 20 years after. *Annual review of neuroscience*, 35, pp.73–89.

Poirel, N. et al., 2012. Number conservation is related to children's prefrontal inhibitory control: an fMRI study of a piagetian task. *PloS one*, 7(7), p.e40802.

Posner, M I & Petersen, S E, 1990. The attention system of the human brain. *Annual review of neuroscience*, 13, pp.25–42.

Qi, Z. et al., 2010. Impairment and compensation coexist in amnestic MCI default mode network. *NeuroImage*, 50(1), pp.48–55.

Rouleau, I. et al., 1992. Quantitative and qualitative analyses of clock drawings in Alzheimer's and Huntington's disease. *Brain and Cognition*, 18(1), pp.70–87.

Royall, D.R., Cordes, J.A. & Polk, M., 1998. CLOX: an executive clock drawing task. *Journal of Neurology, Neurosurgery & Psychiatry*, 64(5), pp.588–594.

Salat, D H et al., 2009. Age-associated alterations in cortical gray and white matter signal intensity and gray to white matter contrast. *NeuroImage*, 48(1), pp.21–28.

Salat, D.H. et al., 2011. Hippocampal degeneration is associated with temporal and limbic gray matter/white matter tissue contrast in Alzheimer's disease. *NeuroImage*, 54(3), pp.1795–1802.

Shaw, L.M. et al., 2011. Qualification of the analytical and clinical performance of CSF biomarker analyses in ADNI. *Acta Neuropathologica*, 121(5), pp.597–609.

Shulman, K.I., 2000. Clock-drawing: is it the ideal cognitive screening test? *International Journal of Geriatric Psychiatry*, 15(6), pp.548–561.

Stuss, D.T. & Alexander, M.P., 2007. Is there a dysexecutive syndrome? *Philosophical Transactions of the Royal Society B: Biological Sciences*, 362(1481), pp.901–915.

Sunderland, T. et al., 1989. Clock drawing in Alzheimer's disease. A novel measure of dementia severity. *Journal of the American Geriatrics Society*, 37(8), pp.725–729.

Takahashi, M. et al., 2008. Poor performance in Clock-Drawing Test associated with visual memory deficit and reduced bilateral hippocampal and left temporoparietal regional blood flows in Alzheimer's disease patients. *Psychiatry and Clinical Neurosciences*, 62(2), pp.167–173.

Tuokko, H. et al., 1992. The Clock Test: a sensitive measure to differentiate normal elderly from those with Alzheimer disease. *Journal of the American Geriatrics Society*, 40(6), pp.579–584.

Ungerleider, L.G. & Haxby, J.V., 1994. "What" and "where" in the human brain. *Current opinion in neurobiology*, 4(2), pp.157–165.

Walhovd, K.B. et al., 2010. Multi-modal imaging predicts memory performance in normal aging and cognitive decline. *Neurobiology of Aging*, 31(7), pp.1107–1121.

Wechsler, D., 1987. *WMS-R: Wechsler Memory Scale--Revised manual*, Psychological Corp., Harcourt Brace Jovanovich.

Wolk, D.A. & Dickerson, B.C., 2011. Fractionating Verbal Episodic Memory in Alzheimer's Disease. *NeuroImage*, 54(2), pp.1530–1539.

Yakushev, I. et al., 2008. Choice of reference area in studies of Alzheimer's disease using positron emission tomography with fluorodeoxyglucose-F18. *Psychiatry Research*, 164(2), pp.143–153.

Yanase, D. et al., 2005. Brain FDG PET study of normal aging in Japanese: effect of atrophy correction. *European Journal of Nuclear Medicine and Molecular Imaging*, 32(7), pp.794–805.

Zakzanis, K.K., Mraz, R. & Graham, S.J., 2005. An fMRI study of the Trail Making Test. *Neuropsychologia*, 43(13), pp.1878–1886.

Chapter 6 - Overall discussion

OVERALL DISCUSSION

The overall goal of this study was to utilize a data-driven multimodal approach to examine structural, functional, neuropsychological, and pathological markers of MCI and AD. The specific aims of this study were examined in four studies. The first of these compared partial volume correction techniques and appropriate normalization reference regions for FDG PET post processing. In this study, the effects of two partial volume correction methods were compared, namely using a gray matter mask and taking residuals of cortical thickness and subcortical volume. In addition, this study examined which reference region for normalization provided the best discrimination between normal aging, MCI, and AD. The brainstem, cerebellum, precentral gyrus, postcentral gyrus, and thalamus were the candidate regions assessed. FDG metabolism in the brain was normalized using statistical residuals, effectively removing the individual variation in uptake from the PET scans. In both parts of this study, stepwise logistic regression was used to establish the discriminability of FDG PET metabolism under the various partial volume correction and normalization region conditions. Based on the c-statistic, a measure of discriminability, normalization to the cerebellum with gray matter mask partial volume correction provided the most meaningful means for FDG PET post-processing.

The second study's aim addressed changes in gray/white matter intensity ratio (GWIR) and its use as a correction factor for cortical thickness in normal aging, MCI, and AD. Recent studies have suggested that brain changes that

occur in normal aging and as a result of accumulation of pathology in MCI and AD may result in blurring of the gray/white matter boundary. Because this boundary is used to calculate cortical thickness values, it is possible that the potential age- and/or disease-related changes in the gray/white matter intensity ratio may influence the cortical thickness measurements. This chapter addressed four hypotheses: 1) GWIR correlates positively with age in normal aging subjects, 2) GWIR decreases progressively between normal aging, MCI, and AD subject groups, 3) adjusting cortical thickness measurements for GWIR improves the ability to differentiate between normal aging, MCI, and AD subjects using statistical models, and 4) the effect size of cortical thickness increases after adjusting for GWIR. The results show that there were no significant correlations between GWIR and age in the normal aging population we studied. We did not observe any significant differences in GWIR between the disease groups, nor was GWIR able to differentiate between the groups in a meaningful way, though adjusting cortical thickness for GWIR did slightly improve the ability to differentiate between groups. The effect size of cortical thickness increased after correcting for GWIR, though it is not certain if this increase represents a real phenomenon or merely provides a means for reducing the variance in the data. The results of this study provide support for adjusting cortical thickness for variations in GWIR, although it does not support the use of GWIR on its own for discriminating between normal aging, MCI, and AD, nor does this study provide evidence in favor of age-related changes in the elderly.

The third study examined which combination of FDG metabolism, MRI morphometry, neuropsychological, and CSF biomarker concentration data best discriminated between normal aging, MCI, and AD. We used stepwise logistic regression to determine which variables contributed unique variance to the model with each modality individually and then in combination. MRI morphometric measures and neuropsychological test scores produced better discriminated than FDG PET or CSF biomarker concentration measures. Combining modalities increased the c-statistic in all instances. These findings provide support for the use of multiple modalities in comparing groups.

The fourth study identified the baseline CSF biomarker concentration, FDG metabolic, and MRI morphometric variables that predict baseline neuropsychological test scores and future cognitive decline in normal aging, MCI, and AD subject groups. We used stepwise linear regression to determine which imaging and CSF biomarker concentration variables contribute variance to the models predicting clock drawing, Trails A, Trails B, digit span forward, digit span backward, and RAVLT 30 minute delayed recall and recognition baseline score and subsequent decline. MRI measures predicted both baseline and decline for all tests better than FDG metabolism or CSF biomarker concentration measures. Normal aging subjects declined only on Trails A, while MCI subjects declined only on delayed recall. AD subjects showed decline across all tests with the exception of Trails A.

The first two studies were more technical in nature and were used to determine how to best treat the data from two of the modalities (FDG PET and cortical thickness) in the third and fourth studies. The results of the third and fourth studies provide insight into the current models of disease progression and the modalities that best distinguish between disease stages and predict cognitive decline. Recent hypothetical models suggest that there is an order in which different modalities are most telling of AD pathology. In this model CSF variables are thought to change first, followed by FDG metabolism measures, MRI morphometric measures, and then neuropsychological test scores. According to the model postulated by Jack et al (Jack Jr et al. 2010), CSF concentrations of aBeta or PET amyloid imaging provide the earliest indicators of incipient AD, followed by CSF tau concentrations and FDG PET, which target Tau-mediated neuronal injury and dysfunction. As pathology continues to build up in the brain, neuronal integrity begins to change, resulting in atrophy, which is detectable with MRI morphometry. Eventually the neuronal loss and changes in glucose metabolism result in cognitive impairment, which may be the last modality to detect AD. Unfortunately for most individuals, it isn't until memory or other cognitive domains show deficits that they present to clinics for further study, by which point many underlying brain changes have likely occurred. The results of our study do not fully support this dynamic biomarkers model, as it was MRI and neuropsychological tests, rather than the purported more sensitive FDG PET and CSF biomarkers concentrations, that best differentiated between groups. It may

be that in our subjects, FDG PET and CSF biomarker concentrations change prior to a definitive diagnosis of MCI or AD. We do not think that this is the case because if FDG PET and CSF biomarkers changed prior to MCI (e.g. in normal aging), we might expect these two markers to be more sensitive to future cognitive decline in our fourth study. This was not what we observed, suggesting that perhaps this dynamic biomarker model cannot be applied to all subject groups. There is great debate in the literature as to which imaging modality (FDG PET or MRI morphometry) provides the best index for determining current disease state and potential to decline in the future. There are studies supporting both sides of the debate, with MRI outperforming FDG PET (K B Walhovd et al. 2009) and conversely, FDG PET outperforming MRI (De Santi S. et al. 2001; Matsunari et al. 2007; Kawachi et al. 2006). Our results provide support for MRI.

Another aspect of the dynamic biomarker model of AD is that within each modality, different features within that modality (e.g. brain regions for imaging, CSF biomarker types, etc) contribute to differentiating between disease stages earlier than others. In MRI, medial temporal atrophy is followed by lateral temporal and finally frontal atrophy, whereas in FDG PET, metabolism decreases initially in the posterior cingulate cortex, followed by the lateral temporal and frontal lobes (Jack Jr et al. 2010). Based on this model, we would expect medial and lateral temporal atrophy and posterior cingulate hypometabolism to discriminate normal aging from MCI and frontal atrophy and hypometabolism to discriminate MCI from AD. Our models suggest that the brain regions that best

discriminate groups are not necessarily in the order that we would expect. The variables that contributed the highest variance for differentiating MCI from normal aging tended to be localized to the medial temporal lobes, cingulate cortex, and frontal lobes. Because the frontal lobes are hypothesized to be affected later in the disease progression, it is possible that our MCI subjects have progressed further along the AD spectrum than initially anticipated. The regions that best differentiated between MCI and AD were localized to the medial temporal, lateral temporal, insula, and occipital regions. The occipital lobe is not involved in AD pathology until late in the disease, thus it is surprising that this region may be useful in differentiating MCI from early AD. So far as the progression of CSF variables from aBeta to tau, our CSF biomarker concentration models suggest that both types of pathology are useful for discriminating normal aging, MCI, and AD when using CSF alone. When CSF markers were combined with the other modalities, however, aBeta was more sensitive than tau at differentiating MCI and normal aging, while both aBeta and pTau were useful for differentiating MCI and AD. This suggests that there may be an earlier build up of aBeta in the CSF than there is a decrease in tau.

The results from the fourth study, determining which imaging variables are most highly associated with baseline neuropsychological function and best predict future cognitive decline, indicate that MRI outperformed FDG PET again. The brain regions that were associated with each tasks highlighted the types of cognitive skills required for successful completion of the test and also highlighted

that these regions, when damaged, can result in poor memory, executive function, and visuospatial abilities.

The findings of this study can be applied to future research in MCI and AD in a number of ways. The first two chapters outline important post-processing steps in both MRI and FDG PET data that may improve the accuracy of the measures, which may in turn increase the likelihood of detecting changes due to treatment effects or disease progression. The third chapter highlights which brain regions, neuropsychological tests, and CSF biomarker concentrations should be targeted as biomarkers, which may be useful indicators of disease staging in clinical trials. The fourth chapter highlights which brain regions are associated with various types of cognitive impairments and those that are indicative of future cognitive decline. Morphometric features and metabolism characteristics in these areas may be useful endpoints for clinical trials for MCI to slow down the rate of disease progression and cognitive decline.

This study did not examine longitudinal change in MRI morphometry or FDG metabolism. These two areas may add insight into the prediction of future decline and underlying brain changes. Our results showed a number of unexpected brain regions associated with discriminating disease groups, baseline neuropsychological tests, or predicting future cognitive decline. Future studies ought to look into these regions further and identify whether their involvement is due to true disease effects or is a by-product of the statistical methods employed. In regression models, the variables that change most with

the disease may not contribute enough independent variance to enter into the model, or stay in it once other variables are entered.

There is still so much about MCI and AD that is unknown. Each piece of information that is gained through studies such as this one may hopefully one day culminate in the development of an effective prevention regimen and treatment plan that can limit the huge impact of AD and MCI on our society.

REFERENCES

Jack Jr, C.R. et al., 2010. Hypothetical model of dynamic biomarkers of the Alzheimer's pathological cascade. *The Lancet Neurology*, 9(1), pp.119–128.

Kawachi, T. et al., 2006. Comparison of the diagnostic performance of FDG-PET and VBM-MRI in very mild Alzheimer's disease. *European Journal of Nuclear Medicine and Molecular Imaging*, 33(7), pp.801–809.

Matsunari, I. et al., 2007. Comparison of 18F-FDG PET and optimized voxel-based morphometry for detection of Alzheimer's disease: aging effect on diagnostic performance. *Journal of Nuclear Medicine: Official Publication, Society of Nuclear Medicine*, 48(12), pp.1961–1970.

De Santi S. et al., 2001. Hippocampal formation glucose metabolism and volume losses in MCI and AD. *Neurobiology of Aging*, 22(4), pp.529–539.

Walhovd, K.B. et al., 2009. Multimodal imaging in mild cognitive impairment: Metabolism, morphometry and diffusion of the temporal-parietal memory network. *NeuroImage*, 45(1), pp.215–223.

Cumulative Bibliography

Alexander, M.P., Stuss, D. & Gillingham, S., 2009. Impaired list learning is not a general property of frontal lesions. *Journal of cognitive neuroscience*, 21(7), pp.1422–1434.

Amici, S. et al., 2007. Anatomical correlates of sentence comprehension and verbal working memory in neurodegenerative disease. *The Journal of neuroscience: the official journal of the Society for Neuroscience*, 27(23), pp.6282–6290.

Anon, 2012. 2012 Alzheimer's disease facts and figures. *Alzheimer's and Dementia*, 8(2), pp.131–168.

Auer, S. & Reisberg, B, 1997. The GDS/FAST staging system. *International Psychogeriatrics / IPA*, 9 Suppl 1, pp.167–171.

Black, F.W., 1986. NEUROANATOMIC AND NEUROPSYCHOLOGIC CORRELATES OF DIGIT SPAN PERFORMANCE BY BRAIN-DAMAGED ADULTS. *Perceptual and Motor Skills*, 63(2), pp.815–822.

Blanke, O. et al., 2000. Location of the human frontal eye field as defined by electrical cortical stimulation: anatomical, functional and electrophysiological characteristics. *Neuroreport*, 11(9), pp.1907–1913.

Blennow, K et al., 1995. Tau protein in cerebrospinal fluid: a biochemical marker for axonal degeneration in Alzheimer disease? *Molecular and chemical neuropathology / sponsored by the International Society for Neurochemistry and the World Federation of Neurology and research groups on neurochemistry and cerebrospinal fluid*, 26(3), pp.231–245.

Blumenfeld, R.S. & Ranganath, C., 2007. Prefrontal cortex and long-term memory encoding: an integrative review of findings from neuropsychology and neuroimaging. *The Neuroscientist: a review journal bringing neurobiology, neurology and psychiatry*, 13(3), pp.280–291.

Bohbot, V.D. et al., 1998. Spatial memory deficits in patients with lesions to the right hippocampus and to the right parahippocampal cortex. *Neuropsychologia*, 36(11), pp.1217–1238.

Bohbot, V.D., Allen, J.J. & Nadel, L, 2000. Memory deficits characterized by patterns of lesions to the hippocampus and parahippocampal cortex. *Annals of the New York Academy of Sciences*, 911, pp.355–368.

Braak, H & Braak, E., 1991. Neuropathological stageing of Alzheimer-related changes. *Acta neuropathologica*, 82(4), pp.239–259.

Braak, H & Braak, E., 1995. Staging of Alzheimer's disease-related neurofibrillary changes. *Neurobiology of aging*, 16(3), pp.271–278; discussion 278–284.

Braak, Heiko & Del Tredici, K., 2011a. Alzheimer's pathogenesis: is there neuron-to-neuron propagation? *Acta Neuropathologica*, 121(5), pp.589–595.

Braak, Heiko & Del Tredici, K., 2011b. The pathological process underlying Alzheimer's disease in individuals under thirty. *Acta neuropathologica*, 121(2), pp.171–181.

Browndyke, J.N. et al., 2012. Phenotypic regional functional imaging patterns during memory encoding in mild cognitive impairment and Alzheimer's disease. *Alzheimer's & dementia: the journal of the Alzheimer's Association*.

Cabeza, R. & Nyberg, L., 2000. Imaging Cognition II: An Empirical Review of 275 PET and fMRI Studies. *Journal of Cognitive Neuroscience*, 12(1), pp.1–47.

Caroli, A. et al., 2010. Functional compensation in incipient Alzheimer's disease. *Neurobiology of aging*, 31(3), pp.387–397.

Caselli, R.J. et al., 2008. Correlating cerebral hypometabolism with future memory decline in subsequent converters to amnestic pre-mild cognitive impairment. *Archives of Neurology*, 65(9), pp.1231–1236.

Cedazo-Minguez, A. & Winblad, B., 2010. Biomarkers for Alzheimer's disease and other forms of dementia: Clinical needs, limitations and future aspects. *Experimental Gerontology*, 45(1), pp.5–14.

Champod, A.S. & Petrides, Michael, 2007. Dissociable roles of the posterior parietal and the prefrontal cortex in manipulation and monitoring processes. *Proceedings of the National Academy of Sciences of the United States of America*, 104(37), pp.14837–14842.

Chang, Y.-L. et al., 2010. Brain substrates of learning and retention in mild cognitive impairment diagnosis and progression to Alzheimerâs disease. *Neuropsychologia*, 48(5), pp.1237–1247.

Cidis Meltzer, C. et al., 2000. Does Cerebral Blood Flow Decline in Healthy Aging? A PET Study with Partial-Volume Correction. *Journal of Nuclear Medicine*, 41(11), pp.1842 –1848.

Clément, F. & Belleville, S., 2010. Compensation and disease severity on the memory-related activations in mild cognitive impairment. *Biological psychiatry*, 68(10), pp.894–902.

Clément, F. & Belleville, S., 2012. Effect of disease severity on neural compensation of item and associative recognition in mild cognitive impairment. *Journal of Alzheimer's disease: JAD*, 29(1), pp.109–123.

Clément, F., Gauthier, S. & Belleville, S., 2012. Executive functions in mild cognitive impairment: Emergence and breakdown of neural plasticity. *Cortex; a journal devoted to the study of the nervous system and behavior*.

Cohen, R.H. & Jr, C.J.V., 1993. Population estimates for responses of cutaneous mechanoreceptors to a vertically indenting probe on the glabrous skin of monkeys. *Experimental Brain Research*, 94(1), pp.105–119.

Courchesne, E. et al., 2000. Normal brain development and aging: quantitative analysis at in vivo MR imaging in healthy volunteers. *Radiology*, 216(3), pp.672–682.

Dale A.M., Fischl B. & Sereno M.I., 1999. Cortical Surface-Based Analysis I. Segmentation and Surface Reconstruction. *NeuroImage*, 9(2), pp.179–194.

DeLong, E.R., DeLong, D.M. & Clarke-Pearson, D.L., 1988. Comparing the Areas under Two or More Correlated Receiver Operating Characteristic Curves: A Nonparametric Approach. *Biometrics*, 44(3), pp.837–845.

Desgranges, B. et al., 2002. The neural substrates of episodic memory impairment in Alzheimer's disease as revealed by FDG–PET: relationship to degree of deterioration. *Brain*, 125(5), pp.1116–1124.

Desikan, R.S. et al., 2006. An automated labeling system for subdividing the human cerebral cortex on MRI scans into gyral based regions of interest. *NeuroImage*, 31(3), pp.968–980.

Devanand, D.P. et al., 1997. Questionable dementia: clinical course and predictors of outcome. *Journal of the American Geriatrics Society*, 45(3), pp.321–328.

Dickerson, B.C., Feczko, E., et al., 2009. Differential effects of aging and Alzheimer's disease on medial temporal lobe cortical thickness and surface area. *Neurobiology of Aging*, 30(3), pp.432–440.

Dickerson, B.C., Bakkour, A., et al., 2009. The Cortical Signature of Alzheimer's Disease: Regionally Specific Cortical Thinning Relates to Symptom Severity in

Very Mild to Mild AD Dementia and Is Detectable in Asymptomatic Amyloid-Positive Individuals. *Cerebral Cortex*, 19(3), pp.497–510.

Dukart, J. et al., 2010. Differential effects of global and cerebellar normalization on detection and differentiation of dementia in FDG-PET studies. *NeuroImage*, 49(2), pp.1490–1495.

Ewers, M. et al., 2007. Multicenter assessment of CSF-phosphorylated tau for the prediction of conversion of MCI. *Neurology*, 69(24), pp.2205–2212.

Ewers, Michael et al., 2011. Staging Alzheimer's disease progression with multimodality neuroimaging. *Progress in Neurobiology*, 95(4), pp.535–546.

Eyler, L.T. et al., 2011. Genetic and Environmental Contributions to Regional Cortical Surface Area in Humans: A Magnetic Resonance Imaging Twin Study. *Cerebral Cortex*, 21(10), pp.2313–2321.

Fischl, B., Sereno, M.I. & Dale, A. M., 1999. Cortical surface-based analysis - II: Inflation, flattening, and a surface-based coordinate system. Available at: http://discovery.ucl.ac.uk/145122/ [Accessed September 21, 2011].

Fischl, Bruce, Van der Kouwe, André, et al., 2004. Automatically Parcellating the Human Cerebral Cortex. *Cerebral Cortex*, 14(1), pp.11 –22.

Fischl, Bruce, Salat, David H, et al., 2004. Sequence-independent segmentation of magnetic resonance images. *NeuroImage*, 23 Suppl 1, pp.S69–84.

Fischl, Bruce et al., 2002. Whole Brain Segmentation. *Neuron*, 33(3), pp.341–355.

Fischl, Bruce & Dale, Anders M., 2000. Measuring the thickness of the human cerebral cortex from magnetic resonance images. *Proceedings of the National Academy of Sciences*, 97(20), pp.11050 –11055.

Folstein, M.F., Folstein, S.E. & McHugh, P.R., 1975. "Mini-mental state". *Journal of Psychiatric Research*, 12(3), pp.189–198.

Förstl, H. et al., 1993. Neuropathological basis for drawing disability (constructional apraxia) in Alzheimer's disease. *Psychological medicine*, 23(3), pp.623–629.

Galasko, D. et al., 1990. The Mini-Mental State Examination in the early diagnosis of Alzheimer's disease. *Archives of neurology*, 47(1), pp.49–52.

Geva, S. et al., 2012. The Effect of Aging on the Neural Correlates of Phonological Word Retrieval. *Journal of cognitive neuroscience*, 24(11), pp.2135–2146.

Gómez-Isla, T. et al., 1997. Neuronal loss correlates with but exceeds neurofibrillary tangles in Alzheimer's disease. *Annals of Neurology*, 41(1), pp.17–24.

Greve, Douglas N & Fischl, Bruce, 2009. Accurate and robust brain image alignment using boundary-based registration. *NeuroImage*, 48(1), pp.63–72.

Grignon, Y. et al., 1998. Cytoarchitectonic alterations in the supramarginal gyrus of late onset Alzheimer's disease. *Acta Neuropathologica*, 95(4), pp.395–406.

Grydeland, H. et al., 2012. Improved prediction of Alzheimer's disease with longitudinal white matter/gray matter contrast changes. *Human brain mapping*. Available at: http://www.ncbi.nlm.nih.gov/pubmed/22674625 [Accessed August 2, 2012].

Guedj, E. et al., 2009. Effects of medial temporal lobe degeneration on brain perfusion in amnestic MCI of AD type: deafferentation and functional compensation? *European journal of nuclear medicine and molecular imaging*, 36(7), pp.1101–1112.

Hansson, O. et al., 2006. Association between CSF biomarkers and incipient Alzheimer's disease in patients with mild cognitive impairment: a follow-up study. *Lancet neurology*, 5(3), pp.228–234.

Happaney, K., Zelazo, P.D. & Stuss, D.T., 2004. Development of orbitofrontal function: current themes and future directions. *Brain and cognition*, 55(1), pp.1–10.

Herlitz, A. et al., 1997. Detection of mild dementia in community surveys. Is it possible to increase the accuracy of our diagnostic instruments? *Archives of neurology*, 54(3), pp.319–324.

Hou, Y. & Liu, T., 2012. Neural correlates of object-based attentional selection in human cortex. *Neuropsychologia*, 50(12), pp.2916–2925.

Hulette, C.M. et al., 1998. Neuropathological and neuropsychological changes in "normal" aging: evidence for preclinical Alzheimer disease in cognitively normal individuals. *Journal of neuropathology and experimental neurology*, 57(12), pp.1168–1174.

Ishii, K. et al., 2005. Comparison of gray matter and metabolic reduction in mild Alzheimer's disease using FDG-PET and voxel-based morphometric MR studies. *European Journal of Nuclear Medicine and Molecular Imaging*, 32(8), pp.959–963.

Jack Jr, C.R. et al., 2010. Hypothetical model of dynamic biomarkers of the Alzheimer's pathological cascade. *The Lancet Neurology*, 9(1), pp.119–128.

Jack Jr., C.R. et al., 2008. The Alzheimer's disease neuroimaging initiative (ADNI): MRI methods. *Journal of Magnetic Resonance Imaging*, 27(4), pp.685–691.

Johnsrude, I.S. et al., 1999. A cognitive activation study of memory for spatial relationships. *Neuropsychologia*, 37(7), pp.829–841.

Kawachi, T. et al., 2006. Comparison of the diagnostic performance of FDG-PET and VBM-MRI in very mild Alzheimer's disease. *European Journal of Nuclear Medicine and Molecular Imaging*, 33(7), pp.801–809.

Kerchner, G.A. et al., 2012. Hippocampal CA1 apical neuropil atrophy and memory performance in Alzheimer's disease. *NeuroImage*, 63(1), pp.194–202.

Killiany, R J et al., 2002. MRI measures of entorhinal cortex vs hippocampus in preclinical AD. *Neurology*, 58(8), pp.1188–1196.

Kuhl, D.E. et al., 1982. Effects of human aging on patterns of local cerebral glucose utilization determined by the [18F]fluorodeoxyglucose method. *Journal of Cerebral Blood Flow and Metabolism: Official Journal of the International Society of Cerebral Blood Flow and Metabolism*, 2(2), pp.163–171.

De Leon, M J, Ferris, S.H., George, A.E., Reisberg, B, et al., 1983. Computed tomography and positron emission transaxial tomography evaluations of normal aging and Alzheimer's disease. *Journal of Cerebral Blood Flow and Metabolism: Official Journal of the International Society of Cerebral Blood Flow and Metabolism*, 3(3), pp.391–394.

De Leon, M J, Ferris, S.H., George, A.E., Christman, D.R., et al., 1983. Positron emission tomographic studies of aging and Alzheimer disease. *AJNR. American Journal of Neuroradiology*, 4(3), pp.568–571.

De Leon, M J et al., 1984. Positron emission tomography and computed tomography assessments of the aging human brain. *Journal of Computer Assisted Tomography*, 8(1), pp.88–94.

Leyhe, T. et al., 2009. Changes in Cortical Activation during Retrieval of Clock Time Representations in Patients with Mild Cognitive Impairment and Early Alzheimer’s Disease. *Dementia and Geriatric Cognitive Disorders*, 27(2), pp.117–132.

Li, R. et al., 2012. The Neuronal Correlates of Digits Backward Are Revealed by Voxel-Based Morphometry and Resting-State Functional Connectivity Analyses. *PLoS ONE*, 7(2), p.e31877.

Li, Y. et al., 2008. Regional analysis of FDG and PIB-PET images in normal aging, mild cognitive impairment, and Alzheimer's disease. *European Journal of Nuclear Medicine and Molecular Imaging*, 35(12), pp.2169–2181.

Libon, D.J. et al., 1996. Further analyses of clock drawings among demented and nondemented older subjects. *Archives of clinical neuropsychology: the official journal of the National Academy of Neuropsychologists*, 11(3), pp.193–205.

Logan, J.M. et al., 2002. Under-recruitment and nonselective recruitment: dissociable neural mechanisms associated with aging. *Neuron*, 33(5), pp.827–840.

Martin, A.J. et al., 1991. Decreases in regional cerebral blood flow with normal aging. *Journal of Cerebral Blood Flow and Metabolism: Official Journal of the International Society of Cerebral Blood Flow and Metabolism*, 11(4), pp.684–689.

Matsuda, H. et al., 2003. Correction for partial-volume effects on brain perfusion SPECT in healthy men. *Journal of Nuclear Medicine: Official Publication, Society of Nuclear Medicine*, 44(8), pp.1243–1252.

Matsunari, I. et al., 2007. Comparison of 18F-FDG PET and optimized voxel-based morphometry for detection of Alzheimer's disease: aging effect on diagnostic performance. *Journal of Nuclear Medicine: Official Publication, Society of Nuclear Medicine*, 48(12), pp.1961–1970.

Meltzer, C.C. et al., 1999. Comparative evaluation of MR-based partial-volume correction schemes for PET. *Journal of Nuclear Medicine: Official Publication, Society of Nuclear Medicine*, 40(12), pp.2053–2065.

Meltzer, C.C. et al., 1996. Regional hypometabolism in Alzheimer's disease as measured by positron emission tomography after correction for effects of partial volume averaging. *Neurology*, 47(2), pp.454–461.

Mendez, M.F., Ala, T. & Underwood, K.L., 1992. Development of scoring criteria for the clock drawing task in Alzheimer's disease. *Journal of the American Geriatrics Society*, 40(11), pp.1095–1099.

Minoshima, S. et al., 1995. Preserved pontine glucose metabolism in Alzheimer disease: a reference region for functional brain image (PET) analysis. *Journal of Computer Assisted Tomography*, 19(4), pp.541–547.

Morris, J C, 1993. The Clinical Dementia Rating (CDR): current version and scoring rules. *Neurology*, 43(11), pp.2412–2414.

Mosconi, L., 2005. Brain glucose metabolism in the early and specific diagnosis of Alzheimer's disease. *European Journal of Nuclear Medicine and Molecular Imaging*, 32(4), pp.486–510.

Mosconi, L. et al., 2009. FDG-PET changes in brain glucose metabolism from normal cognition to pathologically verified Alzheimer's disease. *European Journal of Nuclear Medicine and Molecular Imaging*, 36(5), pp.811–822.

Mosconi, L., Pupi, A. & De Leon, Mony J, 2008. Brain glucose hypometabolism and oxidative stress in preclinical Alzheimer's disease. *Annals of the New York Academy of Sciences*, 1147, pp.180–195.

Moscovitch, M. et al., 2005. Functional neuroanatomy of remote episodic, semantic and spatial memory: a unified account based on multiple trace theory. *Journal of Anatomy*, 207(1), pp.35–66.

Mufson, E.J. et al., 2012. Mild Cognitive Impairment: Pathology and mechanisms. *Acta Neuropathologica*, 123(1), pp.13–30.

Oosterman, J.M. et al., 2010. Assessing mental flexibility: neuroanatomical and neuropsychological correlates of the Trail Making Test in elderly people. *The Clinical neuropsychologist*, 24(2), pp.203–219.

Otten, L.J., Henson, R.N. & Rugg, M.D., 2001. Depth of processing effects on neural correlates of memory encoding: relationship between findings from across- and within-task comparisons. *Brain: a journal of neurology*, 124(Pt 2), pp.399–412.

Owen, A.M. et al., 1996. Memory for object features versus memory for object location: a positron-emission tomography study of encoding and retrieval processes. *Proceedings of the National Academy of Sciences*, 93(17), pp.9212–9217.

PA, J. et al., 2010. Gray matter correlates of set-shifting among neurodegenerative disease, mild cognitive impairment, and healthy older adults. *Journal of the International Neuropsychological Society□: JINS*, 16(4), pp.640–650.

Park, H.-J. et al., 2006. Cortical surface-based analysis of 18F-FDG PET: measured metabolic abnormalities in schizophrenia are affected by cortical structural abnormalities. *NeuroImage*, 31(4), pp.1434–1444.

Perry, R.J. & Hodges, J.R., 1999. Attention and executive deficits in Alzheimer's disease A critical review. *Brain*, 122(3), pp.383–404.

Petersen, R. C., 2001. Current Concepts in Mild Cognitive Impairment. *Archives of Neurology*, 58(12), pp.1985–1992.

Petersen, Steven E & Posner, Michael I, 2012. The attention system of the human brain: 20 years after. *Annual review of neuroscience*, 35, pp.73–89.

Poirel, N. et al., 2012. Number conservation is related to children's prefrontal inhibitory control: an fMRI study of a piagetian task. *PloS one*, 7(7), p.e40802.

Posner, M I & Petersen, S E, 1990. The attention system of the human brain. *Annual review of neuroscience*, 13, pp.25–42.

Qi, Z. et al., 2010. Impairment and compensation coexist in amnestic MCI default mode network. *NeuroImage*, 50(1), pp.48–55.

Rakic, P., 1988. Specification of cerebral cortical areas. *Science (New York, N.Y.)*, 241(4862), pp.170–176.

Rapoport, S.I., 1986. Positron emission tomography in normal aging and Alzheimer's disease. *Gerontology*, 32 Suppl 1, pp.6–13.

Reiber, H. & Peter, J.B., 2001. Cerebrospinal fluid analysis: disease-related data patterns and evaluation programs. *Journal of the neurological sciences*, 184(2), pp.101–122.

Reisberg, B et al., 1988. Global Deterioration Scale (GDS). *Psychopharmacology Bulletin*, 24(4), pp.661–663.

Rouleau, I. et al., 1992. Quantitative and qualitative analyses of clock drawings in Alzheimer's and Huntington's disease. *Brain and Cognition*, 18(1), pp.70–87.

Rousset, O.G., Ma, Y. & Evans, A.C., 1998. Correction for partial volume effects in PET: principle and validation. *Journal of Nuclear Medicine: Official Publication, Society of Nuclear Medicine*, 39(5), pp.904–911.

Rousset, O.G. & Zaidi, H., 2006. Correction for Partial Volume Effects in Emission Tomography. In Habib Zaidi, ed. *Quantitative Analysis in Nuclear Medicine Imaging*. Boston: Kluwer Academic Publishers, pp. 236–271. Available

at: http://www.springerlink.com/content/t250737450351613/ [Accessed August 31, 2011].

Royall, D.R., Cordes, J.A. & Polk, M., 1998. CLOX: an executive clock drawing task. *Journal of Neurology, Neurosurgery & Psychiatry*, 64(5), pp.588–594.

Salat, D H et al., 2009. Age-associated alterations in cortical gray and white matter signal intensity and gray to white matter contrast. *NeuroImage*, 48(1), pp.21–28.

Salat, D.H. et al., 2011. Hippocampal degeneration is associated with temporal and limbic gray matter/white matter tissue contrast in Alzheimer's disease. *NeuroImage*, 54(3), pp.1795–1802.

Samuraki, M. et al., 2007. Partial volume effect-corrected FDG PET and grey matter volume loss in patients with mild Alzheimer's disease. *European Journal of Nuclear Medicine and Molecular Imaging*, 34(10), pp.1658–1669.

De Santi, S et al., 1995. Age-related changes in brain: II. Positron emission tomography of frontal and temporal lobe glucose metabolism in normal subjects. *The Psychiatric Quarterly*, 66(4), pp.357–370.

De Santi S. et al., 2001. Hippocampal formation glucose metabolism and volume losses in MCI and AD. *Neurobiology of Aging*, 22(4), pp.529–539.

Schmand, B. et al., 2011. Value of Neuropsychological Tests, Neuroimaging, and Biomarkers for Diagnosing Alzheimer's Disease in Younger and Older Age Cohorts. *Journal of the American Geriatrics Society*, 59(9), pp.1705–1710.

Shaw, L.M. et al., 2011. Qualification of the analytical and clinical performance of CSF biomarker analyses in ADNI. *Acta Neuropathologica*, 121(5), pp.597–609.

Shulman, K.I., 2000. Clock-drawing: is it the ideal cognitive screening test? *International Journal of Geriatric Psychiatry*, 15(6), pp.548–561.

St George-Hyslop, P.H., 2000. Molecular genetics of Alzheimer's disease. *Biological psychiatry*, 47(3), pp.183–199.

Stuss, D.T. & Alexander, M.P., 2007. Is there a dysexecutive syndrome? *Philosophical Transactions of the Royal Society B: Biological Sciences*, 362(1481), pp.901–915.

Sunderland, T. et al., 1989. Clock drawing in Alzheimer's disease. A novel measure of dementia severity. *Journal of the American Geriatrics Society*, 37(8), pp.725–729.

Takahashi, M. et al., 2008. Poor performance in Clock-Drawing Test associated with visual memory deficit and reduced bilateral hippocampal and left temporoparietal regional blood flows in Alzheimer's disease patients. *Psychiatry and Clinical Neurosciences*, 62(2), pp.167–173.

Thal, D.R. et al., 2002. Phases of Aβ-deposition in the human brain and its relevance for the development of AD. *Neurology*, 58(12), pp.1791–1800.

Thompson, P.M. et al., 2003. Dynamics of Gray Matter Loss in Alzheimer's Disease. *The Journal of Neuroscience*, 23(3), pp.994–1005.

Trojanowski, J.Q. et al., 1993. Altered Tau and Neurofilament Proteins in Neuro-Degenerative Diseases: Diagnostic Implications for Alzheimer's Disease and Lewy Body Dementias. *Brain Pathology*, 3(1), pp.45–54.

Tuokko, H. et al., 1992. The Clock Test: a sensitive measure to differentiate normal elderly from those with Alzheimer disease. *Journal of the American Geriatrics Society*, 40(6), pp.579–584.

Ungerleider, L.G. & Haxby, J.V., 1994. "What" and "where" in the human brain. *Current opinion in neurobiology*, 4(2), pp.157–165.

Walhovd, K B, Fjell, A M, Brewer, J., et al., 2010. Combining MR imaging, positron-emission tomography, and CSF biomarkers in the diagnosis and prognosis of Alzheimer disease. *AJNR. American Journal of Neuroradiology*, 31(2), pp.347–354.

Walhovd, K B, Fjell, A M, Dale, A M, et al., 2010. Multi-modal imaging predicts memory performance in normal aging and cognitive decline. *Neurobiology of Aging*, 31(7), pp.1107–1121.

Walhovd, K B et al., 2009. Multimodal imaging in mild cognitive impairment: Metabolism, morphometry and diffusion of the temporal-parietal memory network. *NeuroImage*, 45(1), pp.215–223.

Wechsler, D., 1987. *WMS-R: Wechsler Memory Scale--Revised manual*, Psychological Corp., Harcourt Brace Jovanovich.

Westlye, L.T. et al., 2009. Increased sensitivity to effects of normal aging and Alzheimer's disease on cortical thickness by adjustment for local variability in gray/white contrast: a multi-sample MRI study. *NeuroImage*, 47(4), pp.1545–1557.

Wolk, D.A. & Dickerson, B.C., 2011. Fractionating Verbal Episodic Memory in Alzheimer's Disease. *NeuroImage*, 54(2), pp.1530–1539.

Yakushev, I. et al., 2008. Choice of reference area in studies of Alzheimer's disease using positron emission tomography with fluorodeoxyglucose-F18. *Psychiatry Research*, 164(2), pp.143–153.

Yanase, Daisuke et al., 2005. Brain FDG PET study of normal aging in Japanese: effect of atrophy correction. *European Journal of Nuclear Medicine and Molecular Imaging*, 32(7), pp.794–805.

Zakzanis, K.K., Mraz, R. & Graham, S.J., 2005. An fMRI study of the Trail Making Test. *Neuropsychologia*, 43(13), pp.1878–1886.

Zetterberg, H., Wahlund, L.-O. & Blennow, Kaj, 2003. Cerebrospinal fluid markers for prediction of Alzheimer's disease. *Neuroscience letters*, 352(1), pp.67–69.

Zhang, D. et al., 2011. Multimodal classification of Alzheimer's disease and mild cognitive impairment. *NeuroImage*, 55(3), pp.856–867.

VITA: Corinna Mae Bauer, Ph.D., M.A.

[redacted]

Laboratory for Visual Neuroplasticity, Massachusetts Eye and Ear Infirmary

[redacted]

[redacted]

Education:

Ph.D., Anatomy and Neurobiology — May 2013

M.A., Bioimaging — September 2008

Boston University School of Medicine, Boston, MA U.S.A.

B.Sc., Honors Physiology and Psychology; B.Mus.A., Musical Arts — April 2007

The University of Western Ontario, London, ON Canada

Postdoctoral Training:

Senior Research Fellow, Laboratory for Visual Neuroplasticity, — January 2013

Massachusetts Eye and Ear Infirmary, Boston, MA, U.S.A.

Peer-Reviewed Publications:

N. Saito, C. Bauer, H. Jara, A. Norbash, and O. Sakai. Age-related relaxo-volumetric quantitative MRI of the major salivary glands. *Journal of Computer Assisted Tomography*. (In press).

C. Bauer, H. Jara, and R. Killiany. Whole brain quantitative T2 MRI across multiple scanners with dual echo FSE: applications to normal aging, MCI, and AD. *NeuroImage*, 2010, 52:508-514.

Abstracts presented at scientific meetings:

C. Bauer, H. Cabral, and R. Killiany. Brain regions associated with baseline cognitive function and subsequent decline in normal aging and mild cognitive impairment as measured with MRI and FDG-PET. *Alzheimer's Association International Conference*, 2012

C. Bauer, H. Cabral, and R. Killiany. A multimodal statistical model for predicting future decline in memory and executive function amongst subjects from the ADNI. *American Academy of Neurology*, 2012

C. Bauer, H. Cabral, and R. Killiany. A multimodal statistical model for discriminating between cognitively normal aged subjects and those with mild cognitive impairment. *Society for Neuroscience*, 2011.

C. Bauer and R. Killiany. Regional FDG uptake in AD, MCI, and normal aging. *Society for Neuroscience*, 2010.

C. Bauer, R. Killiany, and H. Jara. T2 quantitative MRI histogram signature in AD and MCI. *6th Annual Alzheimer's Disease Research Day, Boston University School of Medicine*, 2008

N. Saito, C. Bauer, H. Jara, and O. Sakai. Early maturation and temporal evolution of the human salivary glands: A T2 and secular-T2 multispectral quantitative-MRI analysis. *Radiological Society of North America,* 2008.

Seminars and Talks:

C. Bauer. Multi-modal imaging in normal aging and mild cognitive impairment. *Russek Day for Student Achievement*, 2012.

C. Bauer. Building a multi-modal statistical model for differentiating between normal aging and MCI: Combining MRI morphometry, FDG PET, and neuropsychological testing. *Department of Anatomy and Neurobiology Seminar Series*, 2011.

C. Bauer, R. Killiany, and H. Jara. T2 quantitative MRI: A multi-modal scanner brand calibration study using ADNI data. *Alzheimer's Disease Neuroimaging Initiative Data Presentations Meeting*, 2009.

C. Bauer, N. Saito, R. Killiany, O. Sakai, and H. Jara. T2 quantitative MRI of the brain with the dual-echo fast spin-echo (DE-FSE) pulse sequence at 1.5T: A multi-MRI scanner brand calibration study on 55 subjects. *Radiological Society of North America*, 2008.

Professional Memberships:

2012 The Alzheimer's Association International Society

2010 Society for Neuroscience

2009 American Academy of Neurology

2008 Association for Women in Science

Honors and Awards:

2012 Henry I. Russek Student Achievement Award

2012 Boston University Graduate Medical Sciences Travel Award

2012 Boston University GMSSO Professional Development Award

2004 University of Western Ontario Dean's Honor List

2002-2006 The Wyeth Pharmaceuticals Canada Scholarship